11182

INTERACTION OF MAGNETIZED PLASMA WITH NEUTRAL GAS

BY

N. VENKATARAMANI

A THESIS

SUBMITTED FOR THE DEGREE OF

DOCTOR OF PHILOSOPHY

OF THE

GUJARAT UNIVERSITY

MAY 1981

043

B11182

PHYSICAL RESEARCH LABORATORY
AHMEDABAD
INDIA

DEDICATED

TO MY PARENTS

CONTENTS

	CERTIFICATE	5
	ACKNOWLEDGEMENTS	6
	LIST OF PUBLICATIONS	9
	ABSTRACT OF THE THESIS	11
Chapter 1	INTRODUCTION	13-30
	1.1 Alfvén's critical velocity hypothesis	14
	1.2 Varma's threshold velocity concept	14
	1.3 Experiments on critical velocity	15
	1.4 Important aspects of plasma-neutral gas interaction	18
	1.4.1 Heating of electrons	18
	1.4.2 Braking of plasma motion	25
	1.4.3 Role of transverse magnetic field	27
	1.4.4 Boundary effects	28
	1.5 Scope of the thesis	29
Chapter 2	EXPERIMENTAL APPARATUS AND DIAGNOSTICS	31-59
	2.1 The Device	33
	2.1.1 Coaxial plasma gun	33
	2.1.2 Electromagnetic valves	34
	2.1.3 Interaction region	36
	2.1.4 Magnetic fields	37
	2.2 Operation scheme	38

2.3 Diagnostics 40

2.3.1 Plasma velocity 41

2.3.2 Plasma density and temperature 44

2.3.3 High voltage probe 49

2.3.4 Reflex discharge probe 51

2.3.5 Potential fluctuations 51

2.3.6 Neutral flux probe 53

2.3.7 Current probes 53

2.4 Relevant condition for impact experiment 58

Chapter 3 CHARACTERISTIC VELOCITIES IN PLASMA-NEUTRAL GAS INTERACTION 60-85

3.1 Alfvén's critical velocity 62

3.2 Varma's threshold velocity 66

3.3 Interaction of plasma stream with diffused gas clouds 72

3.4 Discussion 74

3.4.1 Non-existence of Varma's threshold velocity 74

3.4.2 Validity of observations of plasma deceleration in diffused gas clouds 75

3.4.3 Interaction at low neutral gas cloud density 83

Chapter 4 PLASMA RETARDATION 86-114

4.1 Experimental set-up 87

4.2 Scale lengths of plasma deceleration 88

4.3 Discussion 98

4.3.1 Role of various atomic processes 98

4.3.2 Wall losses 111

4.3.3 Deceleration by electrostatic fields 112

Chapter 5 SHEATH AND CURRENT STRUCTURE 115-154

5.1 Experimental set-up 116

5.2 Observations on space charge sheath 118

5.2.1 Detection of sheath 119

5.2.2 Sheath velocity 124

5.2.3 Sheath potential 126

5.2.4 Effect of gas density 130

5.2.5 Role of atomic processes 130

5.3 Interaction at low magnetic fields 136

5.4 Currents in sheath 136

5.5 Discussion 140

5.5.1 Formation and characteristics of sheath structure 140

5.5.2 Role of sheath in excitation of modified two-stream instability 150

5.5.3 Role of currents in plasma retardation 152

Chapter 6 CONCLUSION 155-165

6.1 Summary of the experimental results 155

6.2 Model for plasma-neutral gas interaction 158

6.3 Scope for future work 160

6.3.1 Momentum/energy sharing between the original and newly produced ions 161

6.3.2 Instabilities 162

6.3.3 Space charge 163

6.3.4 Currents 164

6.3.5 Minimum critical density 164

6.3.6 Alfven's cosmogonic theory 165

Appendix 'A' SYSTEM OPERATION 166-181

A.1 Condenser banks 169

A.2 Triggering system 172

A.2.1 Master trigger 172

A.2.2 Pulse generators 172

A.2.3 SCR trigger generators 172

A.2.4 Thyratron trigger circuit 176

A.3 Synchronisation 178

A.4 Summary 178

Appendix 'B' SHEATH POTENTIAL MEASUREMENT USING FLOATING LANGMUIR PROBE 182-185

REFERENCES 186-189

C E R T I F I C A T E

I hereby declare that the work presented in this thesis is original and has not formed the basis for the award of any degree or diploma by any University or Institution.

N. VENKATARAMANI
(AUTHOR)

Certified by:

R.K.VARMA
Professor-in-charge

May 2, 1981

ACKNOWLEDGEMENTS

I wish to express my deep sense of gratitude to Dr. S.K. Mattoo whose constant encouragement contributed immensely to the development of the work presented in the thesis. It has been a pleasure and privilege to work with him. I sincerely thank him for the keen interest and enthusiasm throughout my Ph.D. period.

I am grateful to my Thesis supervisor Prof. R.K.Varma for his interest in the work and exposing me to the various theoretical aspects of the thesis problem. I have been greatly benefitted by the numerous discussions with him.

It is a pleasure to thank Professors Y.C.Saxena and P.I.John for many useful discussions and suggestions at

various stages of my work. I am thankful to Prof. Sheorey, Prof. Vijaykumar and Mr. Krishnakumar for the help given by them in collecting necessary data on various atomic and molecular processes. I also thank Professors Buti and Abhijit Sen for useful discussions on a few selected parts of my thesis work.

I express my heartfelt thanks to my colleagues Kamlesh, Dhiraj, Sekar and Veena for friendly advice and frank comments and suggestions during the discussions on various technical aspects and results of the experiment. Their readiness to cooperate and bubbling enthusiasm made the period of my thesis work lively and pleasant.

My special thanks are due to Mr. S.B. Bhatt and Mr. A.H. Shaikh for the technical assistance in setting up the system for various experiments. I also thank Messrs. Pujara, Lali, Pathak, Vijayan, Choksi and Vinchi for providing me technical help at necessary times.

I am grateful to Drs. A.K. Jain, H.S.S. Sinha, S.M. Bhandari, Vaman Kulkarni, Muralikrishna and Harish Chandra for their friendly advice especially during my initial days in PRL. Dialogues with Rajesh, Mohan, Nagesh, Mukul, Velu, Sharma and Pradeep have always been informative. The helpful attitude and lively company

of my other friends are gratefully acknowledged.

I thank the staff of Library, Workshop, Drafting and Photography sections for the help throughout the course of this work. I thank Mr. Bhupendra for neatly cyclostyling the thesis.

Lastly, words fail me when I wish to express my feelings of gratitude to Kamales Kar, Patro, Chandrasekar, Sahu, Ashok and Chandramohan. The moral boost they gave me while typing out the thesis and the help given by them enabled me to complete the final stage of thesis work in a remarkably short time.

LIST OF PUBLICATIONS

1. On the threshold velocity in the interaction between a magnetised plasma and a neutral gas.

   Mattoo S.K. and Venkataramani N., Phys.Letters A76(1980)257

2. Plasma retardation in Alfvén's critical velocity phenomenon.

   Venkataramani N. and Mattoo S.K., Phys.Letters A79(1980)393

3. On plasma-neutral gas interaction.

   Venkataramani N. and Mattoo S.K., Pramana 15(1980)117

4. Use of Reflex discharge probes for evaluating the dynamics of neutral gas clouds.

   Venkataramani N. and Mattoo S.K., Proceedings of the Indian Academy of Sciences, EPS 89(1980)431

5. Springless fast opening electromagnetic valve.

Venkataramani N. and Mattoo S.K., Indian Journal of Pure and Applied Physics, 19 (1981) 56

6. A coaxial plasma gun with a controllable streaming velocity in the range of 3-100 km/sec.

Venkataramani N. and Mattoo S.K., Indian Journal of Pure and Applied Physics (in press).

7. A pyroelectric crystal detector for measurement of neutral flux.

Venkataramani N. and Mattoo S.K., sent for publication.

8. Effect of pre-ionisation by UV photons in plasma-neutral gas interaction.

Venkataramani N. and Mattoo S.K., sent for publication.

9. Formation of space charge sheath in plasma-gas interaction.

Venkataramani N. and Mattoo S.K., sent for publication.

10. Excitation of currents at the plasma-neutral gas interface and its role in the braking of plasma motion.

Venkataramani N. and Mattoo S.K., Paper to be presented at the Symposium on Plasma Research, Theory and Experiment, Spring College on Fusion Physics, May 1981, Trieste, Italy.

11. Multipole plasma source.

Venkataramani N., PRL Technical Note (1978).

12. System operation for plasma-neutral gas interaction experiment.

Pujara H.D., Lali K.S., Mattoo S.K., Saxena Y.C. and Venkataramani N., PRL Technical Note (1981).

ABSTRACT OF THE THESIS

This thesis describes an experimental study of the interaction between a moving plasma and stationary neutral gas cloud in perpendicular magnetic field. While the experimental results clearly show that the only characteristic velocity in the plasma-neutral gas interaction is Alfvén's critical velocity, the predicted threshold velocity of Varma is not observed.

The detailed study of plasma stream retardation in gas clouds of densities in the range 10^{17} - 10^{21} m^{-3} revealed that occurrence of Alfvén's critical velocity phenomenon does not depend on the absolute gas density value in the above range. However, for retarding plasma stream to a value close to Alfvén's critical velocity, the integrated neutral gas density has to exceed a minimum value $\sim 10^{18}$ m^{-2}. More significant results of these studies is that the plasma stream retards far more rapidly than what can be expected from the theories which relate the retardation mechanism to processes of ionisation or any other simple atomic process. At high gas densities ($N_g > 10^{19}$ m^{-3}), the plasma momentum/ energy loss is

partially explained by the combination of all atomic processes. At low gas densities, we have shown that presently available theories including those which invoke collective processes are not able to explain our results.

The most important causal link between the braking of plasma motion and heating of the electrons seems to be the formation of sheath. The sheaths have been observed. The characteristics of the sheath have been delineated at various gas densities and in various symmetric and asymmetric interactions. The sheath electric field is sufficient enough to give rise to drift of electrons for satisfying the threshold conditions for the excitation of modified two-stream instability. Further, an indirect evidence of modified two-stream instability during the interaction is found from the observations of lower limit on the magnetic field for Alfvén's critical velocity phenomenon to occur. The implications of the observed current structures accompanying the sheaths are further examined in the light of plasma retardation.

The thesis ends with suggestions for further work that needs to be done in order to understand the various facets of the interaction.

Chapter 1

INTRODUCTION

An enhanced ionisation interaction at the critical velocity between a magnetised plasma and a gas was postulated by Alfvén in 1954 in connection with his theory on the origin of the solar system. Since then numerous experimental results have put this hypothesis on a firm foundation. While there are many astrophysical phenomena (Danielsson and Kasai, 1968; Wurm, 1963; Beard, 1966; Wallis, 1972; Burlaga et al., 1973; Mendis and Ip, 1977; Lehnert, 1978; Petelski et al., 1979), which can be explained by invoking the Alfvén's hypothesis, most of the laboratory experiments have demonstrated the phenomenon of the critical velocity

through an associated voltage limitation effect in rotating plasma devices. Only in the recent past, experiments were specifically designed to study the plasma-neutral gas interaction. Meanwhile, the theories that followed are basically attempts to provide the justification for the Alfvén's hypothesis.

1.1 Alfvén's critical velocity hypothesis

Basically, the hypothesis is that a rapid ionisation of the neutral gas occurs when the relative motion between a plasma and a neutral gas in perpendicular magnetic field exceeds a critical value V_{cr}, given by the relation

$$\tfrac{1}{2} M_n V_{cr}^2 = e \phi_{ion} \qquad .. \quad (1.1)$$

where M_n is the atomic mass of the neutral gas and ϕ_{ion} is its ionisation potential (Alfvén, 1954).

1.2 Varma's threshold velocity concept

For the critical velocity phenomenon to be initiated Varma's theory predicts a threshold velocity different from Alfvén's critical velocity. Assuming that an ion, on the average, transfers whole of its energy to an electron, the theory predicts that the ionising interaction between a plasma and a neutral gas will not ensue unless the relative velocity exceeds the threshold velocity V_{th} given by

$$\tfrac{1}{2} M_i V_{th}^2 = e \phi_{ion} \quad .. \quad (1.2)$$

where M_i is the mass of plasma stream ion (Varma, 1978). Further, this theory envisages that, after initiation of the ionisation interaction, the plasma velocity is decelerated till it reaches a terminal velocity where the interaction ceases to occur. This terminal velocity is identified with the Alfvén's critical velocity. A comparison between equations (1.1) and (1.2) immediately tells us that the critical velocity is less than the threshold velocity in case of the interactions where $M_i < M_n$, and therefore, in such interactions Alfvén's critical velocity phenomenon must begin to occur only when the relative velocity is greater than the Varma's threshold velocity.

1.3 Experiments on critical velocity

Ever since the hypothesis of critical velocity was proposed, several laboratory experiments with different sets of magnetohydrodynamic parameters have been performed to test it. A review of these experiments can be found in Danielsson (1973). In electric discharges of rotating plasma devices where the discharge voltage and currents are applied across an axial magnetic field, the observed voltage limitation effect is likened to the phenomenon of the critical velocity (Fahleson, 1961; Angerth et al.; 1962; Lehnert et al., 1966; Himmel et al., 1976). These experiments, performed in a

coaxial cylindrical geometry with a magnetic field aligned along the axis, were carried out with discharge currents of 10 A to 10 kA and initial gas pressure ranging from 10^{-4} to 10^{-1} Torr. No significant variation of the burning voltage could be detected by varying the discharge current. Similarly, critical velocity was observed over the neutral gas pressure range of 3 orders of magnitude. In the recent experiment of Himmel et al. (1976), it was demonstrated that the occurrence of the critical velocity is causally connected with the formation of a spoke structure in the rotating plasma.

The phenomenon of the critical velocity is also found to occur in coaxial plasma guns (Eninger, 1965; Axnäs, 1972). In these experiments, it is found that the maximum drift velocity attained by the plasma is limited to the critical velocity as long as the gas in the coaxial gun is not completely ionised. The experiments on rotating devices and coaxial guns, however, suffered from a disadvantage of interpreting data in view of the fact that the discharge within the device is solely controlled by the circuit parameters external to the device. The difficulty arose in calculating the details of momentum/energy transfer from ions to the neutral gas atoms. In an attempt to overcome these difficulties, Danielsson (1970) performed an experiment wherein a plasma stream detached from its source

was allowed to penetrate through a gas cloud and thus any connection to the external circuitory was avoided. A remarkable result of this experiment was that the plasma stream approaching the gas cloud with super-critical velocity was found to retard in a short distance of 2 cm of penetration through the gas cloud. This experiment also demonstrated the collisionless nature of the critical velocity phenomenon.

What has been established by the above mentioned experiments is the occurrence of the critical velocity as predicted by Alfvén. None of these experiments could have detected Varma's threshold because of peculiar reasons with each device. For verification of this hypothesis, the essential requirement would be to adjust the discharge voltage in rotating devices, such that it gives rise to rotating velocity less than the Varma's threshold but greater than the Alfvén's critical velocity. However, in rotating devices, the problem presented was that for initiating the discharge, the applied voltage has to be much higher than the value corresponding to the Varma's threshold. The same kind of problem was faced with the coaxial guns. In the experiment of Danielsson (1970), apparently the velocity of the plasma stream was not controllable to detect Varma's threshold. Thus, to look for Varma's threshold, the requirement is that the plasma

velocity should be independently controllable over a wide range from below Alfvén's critical to well above Varma's threshold velocity.

1.4 Important aspects of plasma-neutral gas interaction

Besides the observation of the criticality in the relative velocity between the plasma and neutral gas for ionisation interaction to occur, these experiments have unambiguously established the following: (i) The fast ionisation of the gas cannot be explained by electron and ion impact ionisation of the gas atoms at original plasma temperature. This would mean that electrons have to be energised. The energy for heating electrons has to come from ions; (ii) the plasma ion also has to transfer a part of the momentum/energy to the ionised gas and (iii) the presence of the transverse magnetic field is essential for the critical velocity phenomenon to occur.

1.4.1 Heating of electrons

That the electron acceleration is the key intermediate process for the ionising interaction has been clearly demonstrated by the experiments of Danielsson (1970) and Danielsson and Brenning (1975). They found that during the plasma stream retardation to the critical velocity, electrons were heated to about 80 - 100 eV temperature. Also, Möbius et al. (1979b) have spectroscopically observed the presence of low and high frequency microfields created by the

electrostatic instabilities, indicating a strong electron heating. The present understanding of these experiments is that neither ions nor electrons, at their initial energies, have reasonable ionisation cross section to explain the observed ionisation. However, if the ion drift energy is transformed into electron energy, an explanation for the observed rapid ionisation can be provided in terms of electron impact ionisation. In order to make ionisation collision mean free path considerably smaller than the dimension of the gas cloud, the electron heating from an initial temperature of about 5 eV to about 100 eV is required. Thus, an essential feature of the plasma-neutral gas interaction is electron heating.

There are a number of theories providing a causal connection between braking of the plasma motion and electron heating. The theories which prescribe some kind of collective interaction for rapid heating of electrons are the most successful. Extensive reviews of these models are given by Sherman (1973) and Raadu (1979, 1980). Most of these models deal with a homogeneous plasma. Only in the models of Colgate (1961, 1962), Lehnert (1967), Varma (1978) and Piel et al. (1978) density gradients are taken into account.

Generation of a relative motion between electrons and ions, exceeding ion sound velocity is the basic aim of some of the models. Sherman's model (Sherman, 1969; 1972) invokes modified two-stream instability for heating of electrons and

Raadu (1975; 1978) has shown that those modes which saturate at high energies, mainly energise the electrons rather than ions, which is necessary for explaining the observed rapid ionisation of gas atoms. The above model considers two typical cases: In the first case, the relative motion is established through the establishment of a relative drift of electrons with respect to newly produced ions. In the situation where ions are unmagnetised and electrons are magnetised, Sherman (1970) has shown that relative velocity between electrons and ions can become as high as 90% of the initial drift velocity in a restricted range of parameters. However, as this model fails to establish a high relative velocity in a wide parameter range, it cannot explain the observation of critical velocity phenomenon in gases with density ranging over 3-4 orders of magnitude (Himmel et al., 1976; Venkataramani and Mattoo, 1980b). In the other situation where both electrons and ions are magnetised (Sherman, 1972), a relative drift is assumed to occur between the drifting plasma and the secondary ions, which are produced by ionising neutrals at rest. This mechanism works over a time scale less than the acceleration time for secondary ions. The difficulty with this mechanism is that only a small fraction of ions takes part in the excitation of instability. This makes the growth rate of two-stream instability and heating

efficiency of electrons very small. Thus, the primary drift between electrons and secondary ions also may not explain rapid rapid heating of electrons.

A different scenario can be fixed if the plasma is assumed to be inhomogeneous and to contain non-thermal ions. The source of non-thermal ions can be secondary ions produced initially by a few charge transfer and other ionising collisions which occur between the plasma and gas atoms. In Lehnert's model (Lehnert, 1967), a space charge is established over a gyroradius of the non-thermal ions. In this potential structure, electrons get energised. For electrons to reach atleast the ionisation energy collisions of electrons with gas atoms are required. Piel et al. (1978) use a similar space charge field to generate a secondary drift of electrons and invoke modifed two-stream instability to efficiently heat electrons and ions. Another space charge model is given by Varma (1978). In his model, however, no instabilities are invoked to heat electrons. Instead, electrons are energised along the magnetic field by the electric field in that direction. The electric field arises due to spatial variation of density of plasma stream and gas cloud. Colgate's model (Colgate, 1962) is ruled out because the plasma-neutral gas interaction experiment presents a low-β situation.

An attractive feature of space charge models is that secondary ions have been used to build up the space charge sheath. Once the sheath is established the whole electron gas is rapidly energised either through electrostatic acceleration as in Varma's model or through the secondary electron current which is unstable (Piel et al., 1978). The time scale for heating of electrons is much less than the plasma-neutral gas interaction time. Further, these models are provided with a positive feed-back mechanism. New ions created within the sheath by the ionisation of the neutrals become a source to reinforce the space charge sheath.

The notable predictions of the space charge theories are: (i) Sheaths may attain maximum potential equivalent to the initial kinetic energy of the plasma ion. (ii) The thickness of the sheath should be greater than the electron gyroradius but less than the ion gyroradius. The former limit is to prevent short-circuiting of the sheath through electrons and latter so as not to reduce the sheath potential by space charge neutralisation. Following Piel et al. (1978), expressions for dimension and electric fields of sheath can be derived as below:

The number density of non-thermal ions formed is given by

$$N_{nt} = N_g N_p \langle \sigma V \rangle \tau_{fsh} \quad .. \quad (1.3)$$

where

N_{nt} is the density of non-thermal ions;

N_g is the neutral gas cloud density;

N_p is the plasma stream density;

$\langle \sigma V \rangle$ is the total reaction rate for production of non-thermal ions by charge transfer and electron impact ionisation collisions and

τ_{fsh} is the formation time of sheath.

The sheath formation time can approximately be evaluated from

$$\tau_{fsh} = D/V_o \qquad .. \quad (1.4)$$

where

D is the sheath length and

V_o is the initial plasma stream velocity.

The electric field inside the sheath is given by Poisson's equation

$$\phi_o/D^2 = N_{nt}\, e / \epsilon_o \qquad .. \quad (1.5)$$

where

ϕ_o is the maximum potential of sheath;

ϵ_o is the permittivity of the medium and

N_{nt} is the average non-thermal ion density in the sheath region derived from equation (1.3).

We emphasise that these calculations presume that the density

of non-thermal ions in the sheath region is constant and later we show that this assumption is incompatible with the observed profile of the potential in the sheath region.

The maximum potential of sheath is obtained by equating the potential energy of sheath to the kinetic energy of non-thermal ions

$$\tfrac{1}{2} M_i V_o^2 = e \phi_o \qquad .. \quad (1.6)$$

where

M_i is the mass of non-thermal ion.

Making use of equations (1.3) - (1.6), the sheath dimension can be easily derived as

$$D = 3.81 \times 10^2 \left[\tfrac{1}{2} M_i V_o^2 / N_g N_p \sigma \right]^{1/3} \qquad .. \quad (1.7)$$

where

$\tfrac{1}{2} M_i V_o^2$ is expressed in eV;

N_g & N_p are expressed in m^{-3};

σ is expressed in m^2 and

D is obtained in m.

The average electric field inside sheath is then given by

$$E = \phi_o / D$$

$$= 2.61 \times 10^{-3} \left[\tfrac{1}{2} M_i V_o^2 \right]^{2/3} \left[N_g N_p \sigma \right]^{1/3} \qquad .. \quad (1.8)$$

where E is obtained in V/m.

Experimentally, sheaths have been observed in rotating plasma experiment of Piel et al. (1978). In direct collision experiment no such observations have been made reported so far. Keeping in view that space charge formation may be the most important causal link between braking of the plasma motion and heating of electrons even in direct collision experiments, it is imperative that their existence and characteristics are investigated.

1.4.2 Braking of plasma motion

The experimental results on plasma retardation are available only in limited parameter ranges of the plasma and the gas. Thus, the role of the atomic processes in the retardation of the plasma stream has not been clearly delineated. Though the theories have successfully explained the onset of rapid ionisation, they only broadly describe braking of plasma motion as due to sharing of momentum between original plasma ions in the stream (momentum residing with electrons is negligible) and newly produced ionised atoms. Two mechanisms considered for sharing momentum between original plasma ions and newly created ions are : (i) various atomic collisions and (ii) acceleration of newly created ions by electrostatic space charge formed at the interface where Alfvén's critical velocity phenomenon is taking place. In

the second mechanism the energy/momentum residing with ions is first transferred to the electrostatic field as a result of collisions. Hence for braking of plasma motion, atomic processes is considered to play a significant role.

Very few calculations exist which attempt to derive an expression for the length over which the plasma stream loses its momentum. A simple calculation by Danielsson and Brenning (1975) assumes that (i) the plasma retardation scale length is determined mainly by the ionisation process; (ii) they invoke collective interaction to heat the electrons so that the ionisation time, τ, becomes comparable to the transit time of the plasma through the gas. The plasma retardation scale length L is related to τ by

$$L = V_o \tau = \frac{V_o}{N_g \chi(E)} \left[M_i/M_n\right] \quad .. \quad (1.9)$$

where

V_o is the initial plasma stream velocity;

N_g is the gas density;

$\chi(E)$ is the ionisation function dependent upon the electron energy E and

$\left[M_i/M_n\right]$ is the mass ratio of the plasma ion to the neutral gas atom.

This expression directly gives deceleration scale length of plasma stream.

1.4.3 Role of transverse magnetic field

The role of the magnetic field has been assessed differently by different models. In Lehnert's and Varma's models (Lehnert, 1967; Varma, 1978), the magnetic field is necessary for the creation of the space charge. In the theories of Sherman (1969), Raadu (1975) and Piel et al. (1978), the magnetic field is also found necessary for generating the relative drift between electrons and ions. While it would not be possible to establish the role of the magnetic field in rotating devices, the experiment of Danielsson and Brenning (1975) has clearly demonstrated that the enhanced ionisation interaction is observed only when the transverse magnetic field is present.

Whether or not electron heating is due to excitation of instabilities or through simple electrostatic acceleration is difficult to infer directly from the observations. The difficulty stems from the lack of appropriate non-disturbing diagnostics. However, indirect inferences can be drawn from the observation of the critical velocity at varying magnetic fields. For example, it is well known that electron heating occurs mainly parallel to the magnetic field by the modified two-stream instability when $f_{ce} > f_{pe}$, where f_{ce} and f_{pe} are the electron-cyclotron and electron plasma frequencies

respectively. An experimental proof of it is seen in the results of Danielsson and Brenning (1975). They found that their polarisation data of emission lines of Helium is compatible with only if the electrons are preferentially accelerated along the magnetic field. Until recently, there were no experimental results available in the parameter range of $f_{ce} \ll f_{pe}$. Such results would throw light on whether or not electron heating parallel to the magnetic field is linked with the occurrence of critical velocity phenomenon. We must mention that after this thesis was written, we came to know of Brenning's results (Brenning, 1980). He has observed the non-occurrence of the critical velocity at magnetic field which correspond to the condition of $f_{ce} \ll f_{pe}$.

1.4.4 Boundary effects

Lastly, the boundaries in interaction region can seriously influence the characteristics of plasma-neutral gas interaction. The efflux of particles from wall due to plasma particle bombardment, flow of currents from interaction region to conducting walls, establishment of sheath in insulating boundaries are some of the factors which can change the features of plasma-neutral gas interaction. These effects, to some extent, can be avoided by keeping the walls far away from interaction region. Of course,

the ideal condition would be to perform the experiment in an open space laboratory as proposed by Möbius et al. (1979d).

An important factor to be considered in connection with the boundary effects is the gyroradius effect. In many of the laboratory experiments, the ion gyroradius is much larger than the dimension of the device. Also, in the proposed space lab experiment the gyroradius of xenon is of the order of gas cloud dimension. Experiments have indicated that this effect plays insignificant role in plasma-neutral gas interaction (Fiel & Möbius, 1978; Venkataramani and Mattoo, 1980b).

1.5 Scope of the thesis

The experimental study presented in this thesis is directed towards understanding some of the characteristics of critical velocity interaction between a plasma and neutral gas. The work aims (i) to determine parameters of the neutral gas cloud upon which depends the retardation of the plasma stream to Alfvén's critical velocity. (ii) to identify and verify the characteristic velocities in the interaction between moving magnetised plasma and neutral gas cloud, (iii) to measure plasma retardation scale length and to specify the role of atomic interactions in plasma retardation; (iv) to study the formation and role of sheath at the head of the plasma stream as it penetrates the neutral

gas cloud and (v) to identify the mechanism of plasma retardation.

The experimental device, its performance characteristics and the description of various diagnostics deployed are given in Chapter 2. The experiments on the observation of characteristic velocities and the role of neutral gas cloud parameters are described in Chapter 3. The measurements of scale lengths for the plasma retardation in neutral gas clouds of densities in the range of 10^{17} - 10^{21} m^{-3} are presented in Chapter 4. This Chapter also includes a discussion on the role of atomic processes in plasma retardation. Chapter 5 presents and discusses the characteristics and role of sheath structure that gets formed when the plasma stream meets neutral gas cloud in presence of transverse magnetic field. Also, the current structure accompanying the sheath and the role of magnetic field are discussed from the point of view of our experimental observations. Chapter 6 summarises our conclusions. A model for the plasma-neutral gas interaction is presented at the end of this chapter.

Chapter 2

EXPERIMENTAL APPARATUS AND DIAGNOSTICS

A schematic of the experimental set-up is shown in figure 2-1. It essentially consists of a device, various diagnostics and different electronic circuitry. The device consists of a plasma gun which produces a plasma stream and an interaction region where the plasma stream penetrates a neutral gas cloud. Initially the whole system is kept at a pressure of 10^{-6} Torr. A number of diagnostics have been deployed at the interaction region for measuring plasma and neutral gas cloud parameters. The various operations in the procedure of making a plasma stream encounter a neutral gas cloud and subsequently the acquisition of data are sequenced and started by a command signal. Following sections give

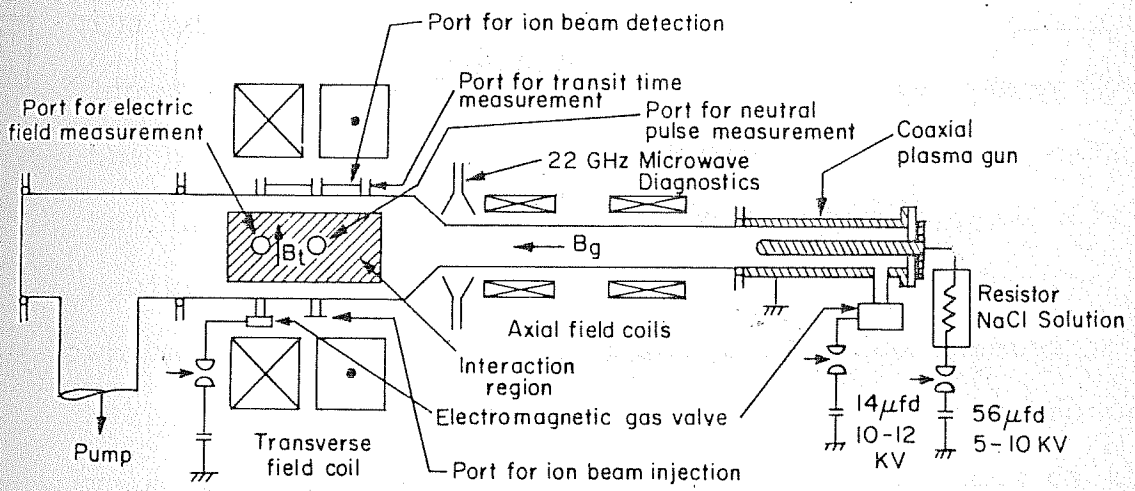


Figure 2-1. A schematic of the set-up.

the details of various aspects of the experimental set-up.

2.1 The Device

2.1.1 Coaxial plasma gun

The plasma gun is of coaxial type (Marshall, 1958). The length of brass plasma gun is 51 cm and the diameters of inner and outer cylinders are 4 and 11 cm respectively. At the breech end, a pyrex glass jacket on the inner cylinder terminates into a flange which holds the two cylinders in position and insulates them from each other. The desired gas, which is to be ionised and subsequently accelerated in the plasma gun, is injected by a fast opening electromagnetic valve into the annular region through a port hole on the outer cylinder at 4 cm from the glass breech end.

The energy storage connected to the plasma gun is a capacitor bank capable of delivering a maximum of 15 kJ. The bank consists of 4 capacitors of 14 μfd each and chargeable upto 20 kV. The gun is connected across the capacitor bank by 32 low inductance, 1.2 m long coaxial cables in parallel. This is done so as to reduce the energy transmission loss between the storage and the gun.

Initially, the inner electrode of the gun is kept at a negative voltage of 5 - 10 kV, the outer electrode remaining grounded. The neutral gas which is to be ionised and

accelerated is injected through the valve. When the local gas pressure in the region between two coaxial conductors near the breech end reaches a value of about 1 Torr, the gas breaks down and an arc is formed. The magnetic field resulting from the current carried by the inner conductor behind the arc along with radial current generates an accelerating force on the plasma which propels it down the system towards the open end of the gun where plasma attains its final velocity.

A 0.2 - 25 Ω variable NaCl electrolytic resistor is included in the discharge path of the condenser bank to control the discharge current. By varying discharge current the stream velocity can be varied which for atomic hydrogen ranges between 2 - 100 km s^{-1} (Venkataramani and Mattoo, 1981b). In the interaction region, 1.6 m away from the plasma gun, the typical plasma parameters are : plasma density $\sim 10^{18} - 10^{19}$ m^{-3} and electron temperature $\sim$ 5 eV.

2.1.2 Electromagnetic valves

In our device two valves are deployed, one for admitting gas into the plasma gun for ionisation and acceleration purposes and other for injecting neutral gas into the interaction region for the studies on plasma-neutral gas interaction. The essential feature of this

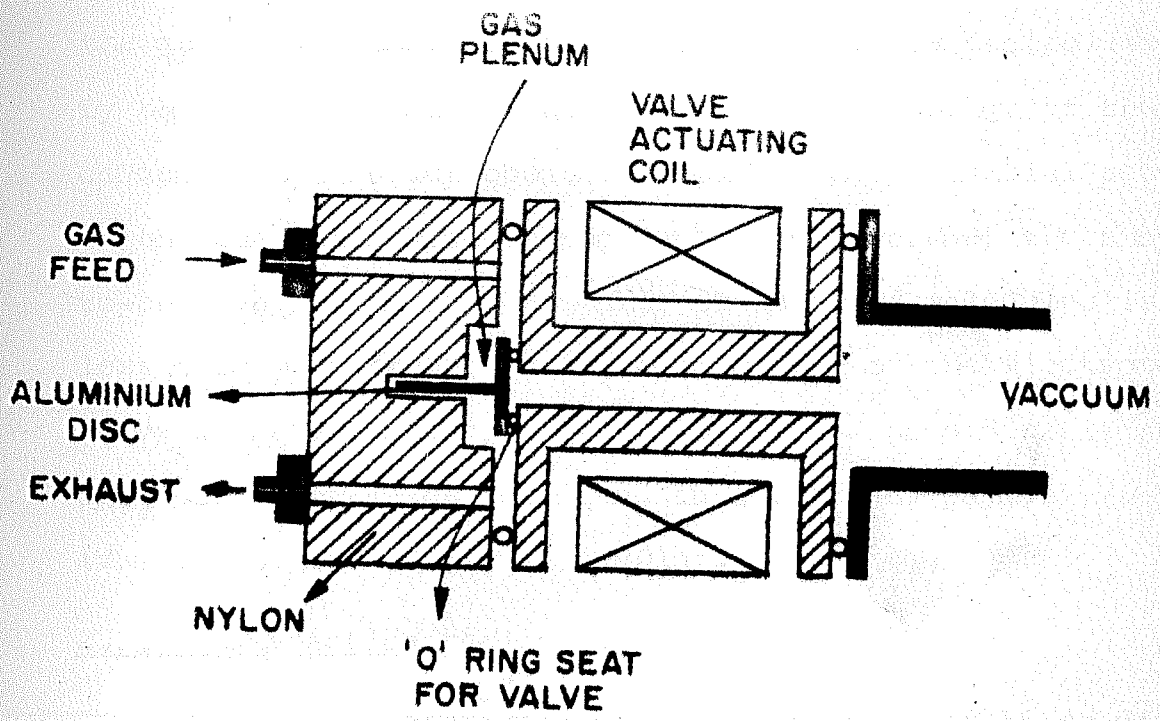


Figure 2-2. Schematic diagram of the cross-section of springless electromagnetic valve.

The interaction region is accessible to the plasma stream from plasma gun by a drift tube of 1.6 m long. A guide magnetic field of upto 2.5 kG is provided along the axis of the drift tube so as to minimise diffusion losses to its walls while plasma transits from gun to the interaction region.

2.1.4 Magnetic fields

The guide magnetic field along the drift tube is obtained by discharging a 20 μfd, 5 kV capacitor bank through a pair of solenoids. The solenoids of 40 cm length and 16 cm inner diameter are placed 15 cm apart end to end. With this configuration, we get a magnetic field of about 20 G at the half length of drift tube for each ampere of discharge current passing through coils. The capacitor bank can supply a current of 25 A for each kV of its charging and hence maximum magnetic field of 2.5 kG along the axis of drift tube can be produced. The ringing period of pulsed magnetic field is about 3.7 ms which is much larger than transit time of 10 μs of plasma through the drift tube. We synchronise our operation such that plasma transits through the drift tube at the first peak of ringing guide magnetic field.

In the interaction region, we have provided coils for producing a d.c. magnetic field upto 1 kG and coils for

producing a pulsed magnetic field for values greater than 1 kG and upto 5 kG. The d.c. transverse field of 1 kG is obtained by a pair of pancake coils fed by a d.c. source of 300 A. The Helmholtz configuration in which two coils are connected provides a uniform magnetic field over radial distance of 30 cm. Each coil consists of 42 turns of water cooled copper tube. Its inner and outer diameters are 44 and 51 cms respectively.

Another pair of rectangular coils of 25 cm x 15 cm is placed for providing a pulsed high magnetic field upto 5 kG. Each coil has 50 turns. The current is supplied by discharging a 5 kV, 20 μfd condenser bank and the duration of a pulse is $\sim$ 1 ms. When this pulsed magnetic field is used, the uniformity of transverse magnetic field is reduced to a length of 10 cm axially and 3 cm radially from the axis of the plasma stream.

2.2 Operation scheme

The sequence of operation begins with the discharge of capacitor bank feeding the guide magnetic field coils. After about 500 μs, the electromagnetic valve at the breech end feeds the desired gas into the annular region of plasma gun for the production of plasma stream. The gun discharges as soon as the pressure in the annular region reaches about

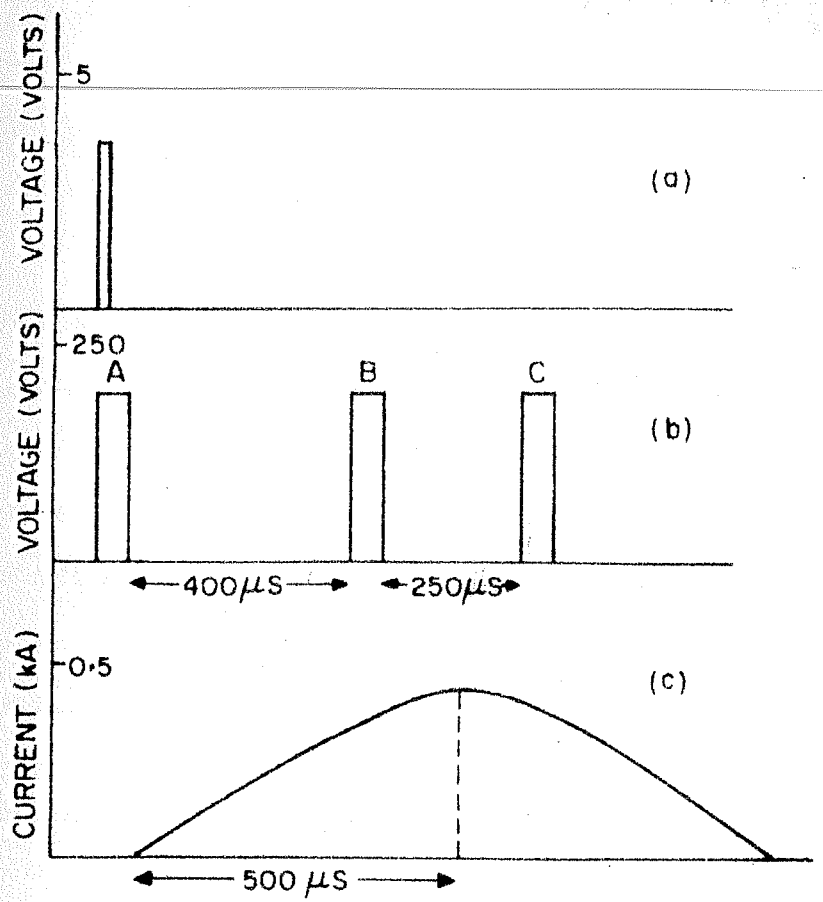


Figure 2-3. Operation scheme for a typical plasma-neutral gas interaction experiment. (a) master trigger; (b) pulse A triggers the discharge circuit to set up the guide magnetic field. B & C open two electromagnetic valves to admit neutral gas in coaxial gun and interaction region respectively; (c) the time profile of current producing the magnetic field for guiding plasma from coaxial gun to interaction region.

1 Torr. In this way, the discharge of the capacitor bank connected to the plasma gun is synchronised so that the plasma stream passes through the drift tube just when the magnetic field along the drift axis reaches to first maximum value.

During this time, another switching pulse opens the other electromagnetic gas valve placed at the interaction region to inject the desired gas cloud. The opening of this valve is so adjusted that when the plasma stream meets the neutral gas cloud, the gas cloud is of required density and dimension. In our experiment, the neutral gas cloud density was varied in the range of 10^{17} - 10^{21} m^{-3} and correspondingly the dimension varied from 40 to 2 cm. The three discharges are sequentially obtained with definite controllable delays between them as shown in figure 2-3.

The discharging of various condenser banks is done by triggering spark gaps through thyratron switches. Appendix 'A' discusses various electronic circuits used to provide trigger pulses for spark gaps and characteristics of various condenser banks used to discharge plasma gun, produce pulsed magnetic fields and open electromagnetic valves.

2.3 Diagnostics

A host of diagnostics are deployed to measure various

plasma and neutral gas parameters needed for understanding plasma-neutral gas interaction. Also several diagnostics were built to analyse the circuit performance of various discharge circuits, utilised. A detailed account of diagnostics of various parameters is given as follows.

2.3.1 Plasma velocity

The plasma stream velocity was measured by two methods: (i) by measuring the transit of plasma between two spaced probes and (ii) by measuring the polarisation electric field that a plasma stream develops while traversing the transverse magnetic field region, $\underline{E} = - \underline{V} \times \underline{B}$ (Lindberg and Kristofferson, 1970). Figure 2-4 gives the typical polarisation electric field profile obtained with a V x B - probe. The electric field so obtained is related to velocity of the plasma stream and for the profile in this figure, the peak velocity corresponded to 50 km s^{-1}.

We have placed six V x B - probes along the axis of the interaction region. The minimum seperation is 8 mm and maximum seperation is 16 cm between two spaced probes. These are used to measure the axial profile of plasma velocity. In presence of the gas cloud, these probes allow us to measure the retardation of plasma stream.

The plasma velocity is also determined by time-of-flight method. Typical oscilloscope traces obtained through

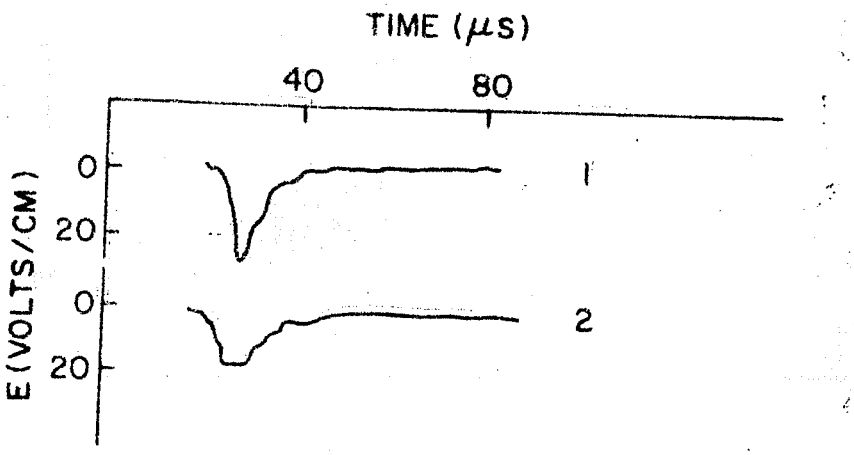


Figure 2-4. Typical signals of the polarisation electric field measured by the V x B - probe in the interaction region. Traces 1 & 2 represent observations without and with interaction, while argon plasma was traversing through hydrogen neutral gas respectively.

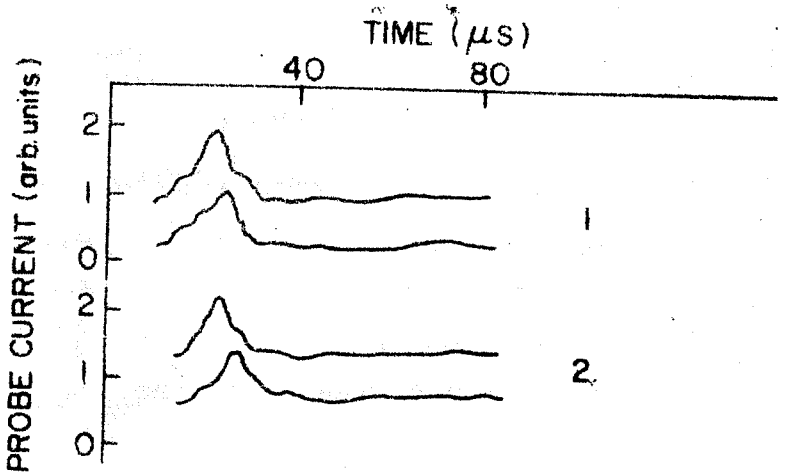


Figure 2-5. Typical signals from probes seperated by 8 cm in the line of plasma stream. Traces 1 & 2 represent observations without and with interaction while argon plasma was traversing through hydrogen neutral gas.

Langmuir probes for velocity measurement by time-of-flight is shown in figure 2-5.

A comparison of two methods of measuring plasma velocity indicated that there is a good agreement between the values of velocity obtained by two methods. This point is illustrated in Chapter 3 (see figures 3-2 & 3-3). The shot-to-shot variation of plasma velocity under identical conditions of the discharge circuit parameters and gas feed to the gun was not more than 20%.

2.3.2 Plasma density and temperature

An interferometer at 22 GHz measures plasma density. A typical record is shown in figure 2-6. The interferometer signal shows a shift of 3 well resolved fringes before cut-off occurs. This means that the peak plasma density produced by the plasma gun is greater than 5×10^{18} m^{-3}. It is to be noted that the cut-off is dependent on the peak plasma density and the phase shift on integrated plasma density. Figure 2-7 shows the expected phase shift for different radial density profiles at a given plasma density at the centre of the plasma column. The effect of varying central plasma density from below to above critical density is also plotted in this figure. From this figure, it is obvious that when peak density of plasma column is the critical density value for cut-off

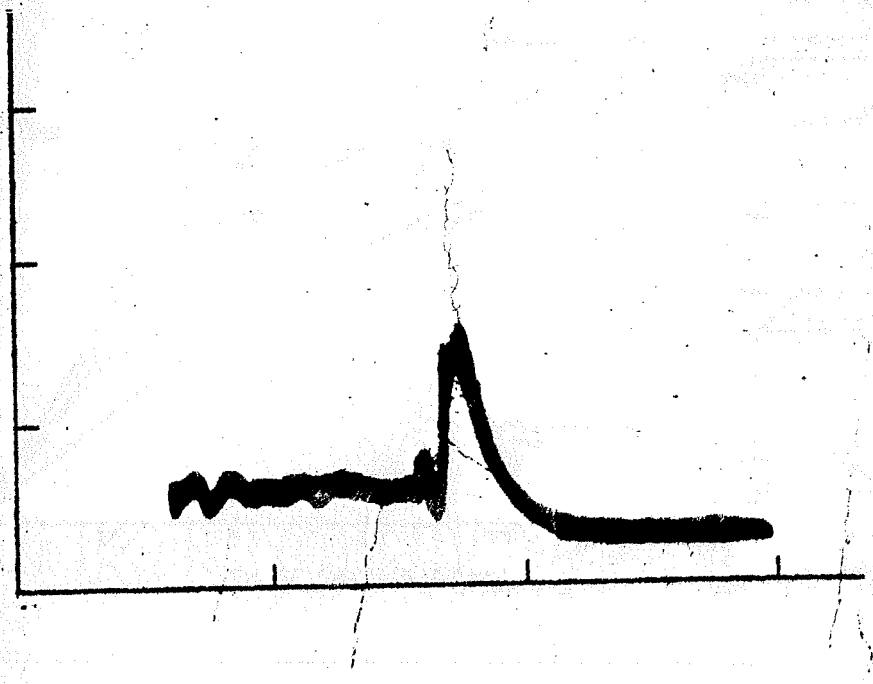


Figure 2-6. Typical oscilloscope trace of microwave interferometer signal. Scale:- X-axis : 75 μs/div., Y-axis: 40 mv/div. and one fringe = 2×10^{18} m^{-3}.

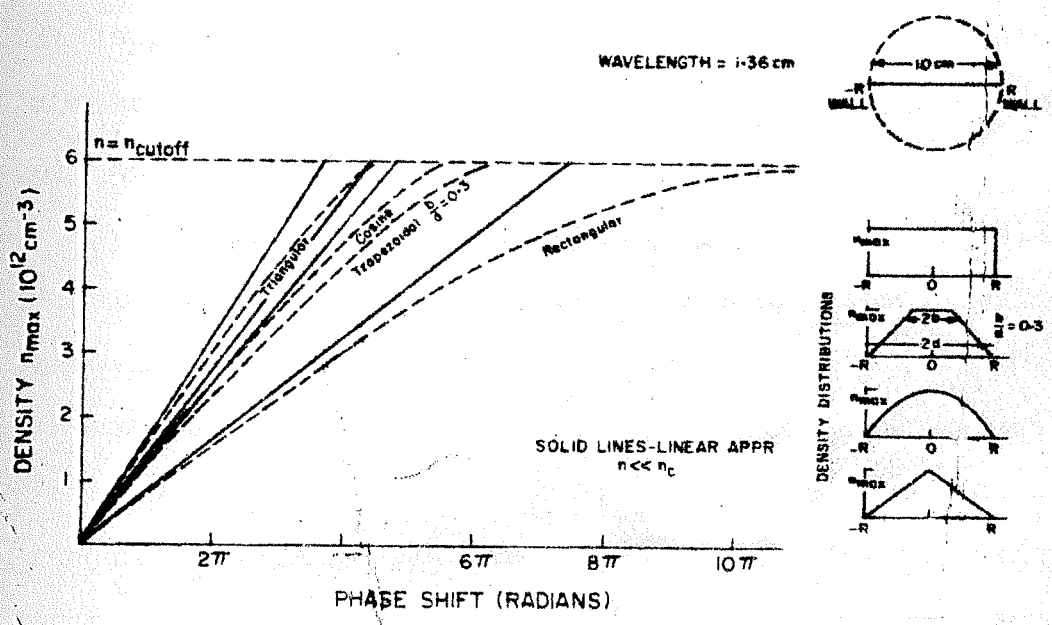


Figure 2-7. Plot of phase shift of microwave signal passing through plasma column with the peak plasma density value for a few typical density distributions. Solid and dotted lines correspond to the linear and second order approximations respectively.

to occur, the phase shift tends to infinity. However, for a peak density value slightly less than the cut-off value, the phase shift or the number of fringes is somewhat uniquely defined by the plasma density profile. Thus using figure 2-7, it is possible to say approximately the plasma density profile. In our case, the distribution is half-sine with the peak value at the centre.

To obtain the complete temporal profile of plasma density we made use of a pulsed Langmuir probe. Using microwave interferometer, the pulsed Langmuir probe was calibrated. It was then used to measure the peak electron density. Triangular pulse of fixed frequency in the range of 1-20 MHz ranging in voltage between - 40 and + 40 V was applied to the probe to bias it and probe current was measured through a high frequency pulse transformer. When the period of this pulse is much smaller than the plasma pulse period, the assumption of stationarity of the plasma parameters during the bias pulse period is fairly valid.

The interpretation of the probe signals from pulsed high density flowing plasmas have been discussed by Chung et al. (1975), Kanal (1964) and Tan (1973). The analysis of the obtained probe characteristics to calculate the electron density have been carried out assuming conventional 'thin' sheath model. Cylindrical probe oriented such that its long

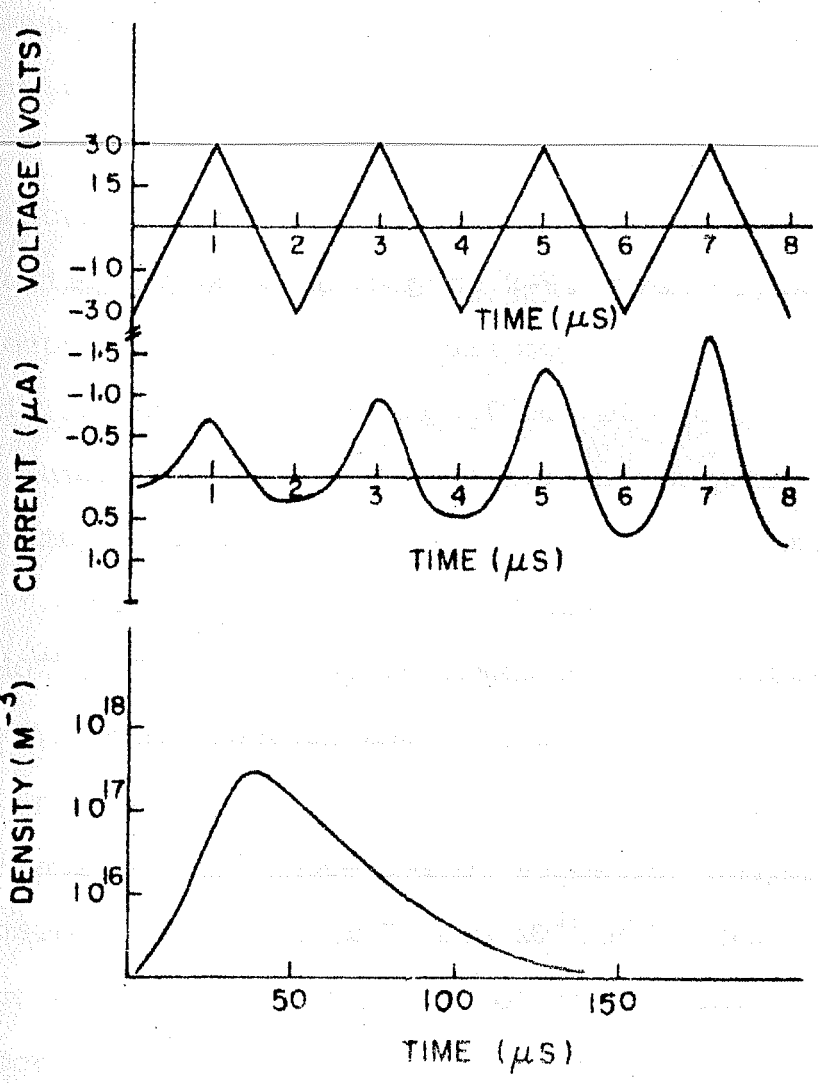


Figure 2-8. (a) The bias signal applied to the Langmuir probe. (b) Current signal from the probe. (c) The evaluated plasma electron density.

side is perpendicular to the flow direction gives value for temperature higher than its true value. For this reason, we have oriented long side of our probe in the direction of flow.

The bias signal applied to the probe, the current signal from the probe and the evaluated density profile are shown in figure 2-8. This figure shows that electron saturation does not occur in the probe characteristics. This is because shielding effect of the probe is destroyed by the high speed ion flow (Segall and Koopman, 1973). The plasma density is found from the ion saturation current.

The peak value of the plasma density was found to be $\sim 10^{19}$ m^{-3} and the upper limit on the electron temperature 10 eV. The electron temperature remained constant throughout the plasma pulse period and showed very little shot-to-shot variation. The shot-to-shot variation ranged the plasma density between 5×10^{18} and 10^{19} m^{-3}. The probe did not give any reliable estimate of high energy tail of electrons, possibly it was less than 20 eV.

2.3.3 High voltage probe

A high voltage capacitor probe was constructed with a view to measure the voltage on gun during the period of discharge. A cross-sectional view of the probe is given in figure 2-9. The design considerations of this voltage

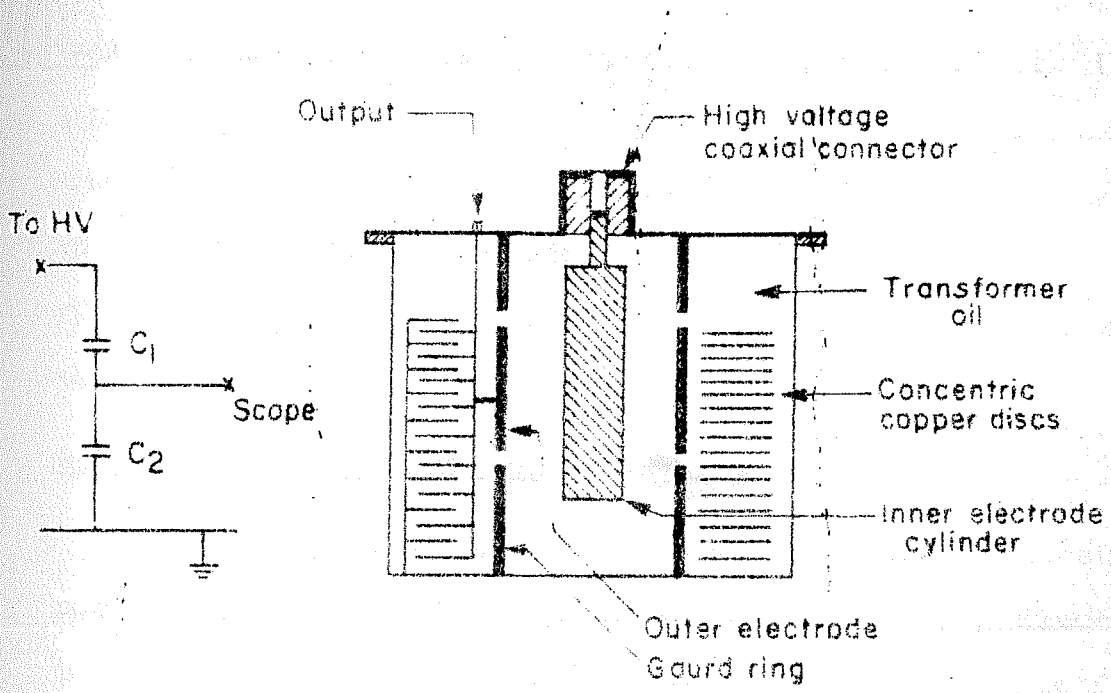


Figure 2-9. Cross-sectional view of capacitive voltage divider and its equivalent circuit.

divider and observations on coaxial plasma gun parameters and its efficiency are described elsewhere (Venkataramani and Mattoo, 1981b).

2.3.4 Reflex discharge probe

The neutral gas cloud injected by the electromagnetic valve is monitored using a specially designed relfex discharge probe. A schematic of the probe and the associated electronic circuit is given in figure 2-10. The design and characteristics of this probe and the delineation of the evolution of gas cloud injected by the electromagnetic gas valve are described elsewhere (Venkataramani and Mattoo, 1980c).

2.3.5 Potential fluctuations

Floating Langmuir probes have been used to measure the spatial and temporal characteristics of potential fluctuations in the frequency range 0.1 - 1 MHz during the interaction of plasma with neutral gas cloud. Probes with good shielding and high-frequency sensitivity have been used. The probe tip is a cylindrical wire made of stainless steel. The length of probe tip is 2 mm and its diameter is 0.2 mm. This probe is kept aligned parallel to the magnetic field direction and perpendicular to the plasma stream flow. Appendix 'B' lists the considerations for the application of such a probe for measuring plasma potential in the plasma-

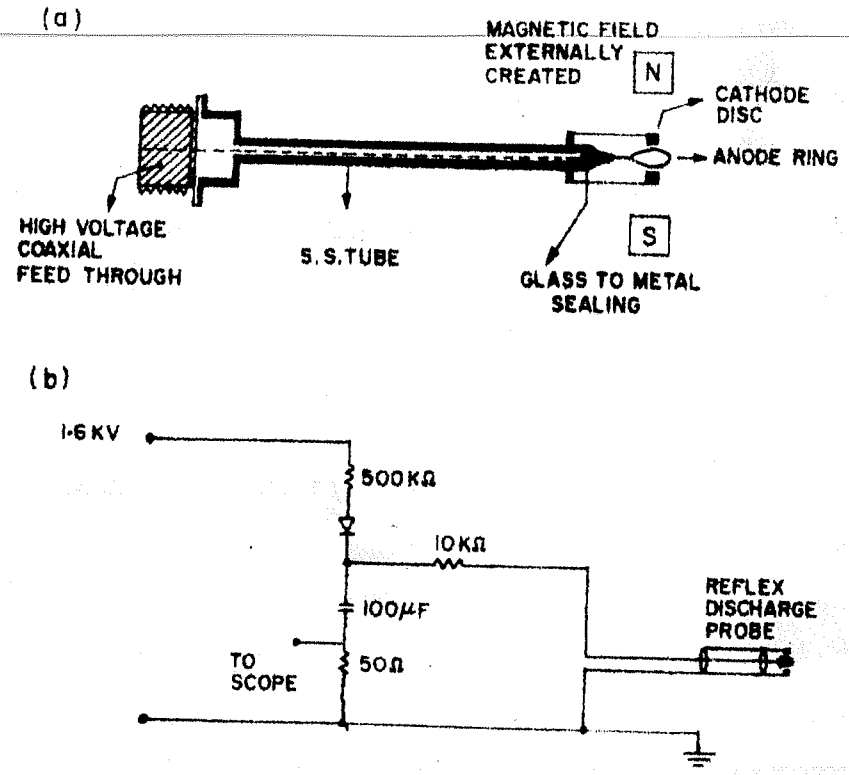


Figure 2-10. (a) A schematic of the reflex discharge probe. (b) The circuit for measuring probe discharge current.

neutral gas interface.

2.3.6 Neutral flux probe

During the penetration of plasma stream through neutral gas, fast neutral particles are generated by charge transfer collisions. These particles escape out of interaction region in the plasma stream direction. The measurement of this neutral flux has been done using a pyroelectric crystal detector. A schematic of the detector assembly is shown in figure 2-11. The design and characteristics of this detector have been presented elsewhere (Venkataramani and Mattoo, 1981d).

2.3.7 Current probes

Rogowski coils and magnetic probes have been used to measure the currents excited during plasma-neutral gas interaction. A schematic of Rogowski loop used in our experiment is shown in figure 2-12. It consists of a 1 mm copper enamelled wire wound over a mild steel torus whose major radius is 2 cm and the radius of circular cross section is 3 mm. The total number of turns is 20. One end of the coil is wound back inside the toroidal coil to compensate the induced voltages due to any azimuthal current. The two ends of the coil are connected by a copper wire of negligible resistance. A current probe (standard Pearson current probe) is used to measure the current induced in the Rogowski coil. By this,

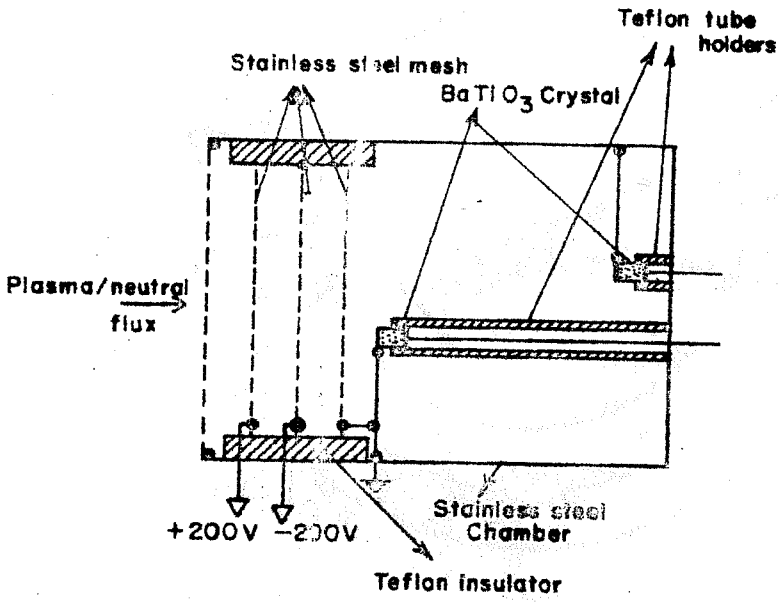


Figure 2-11. Cross-sectional view of the detector assembly housing two pyroelectric crystals.

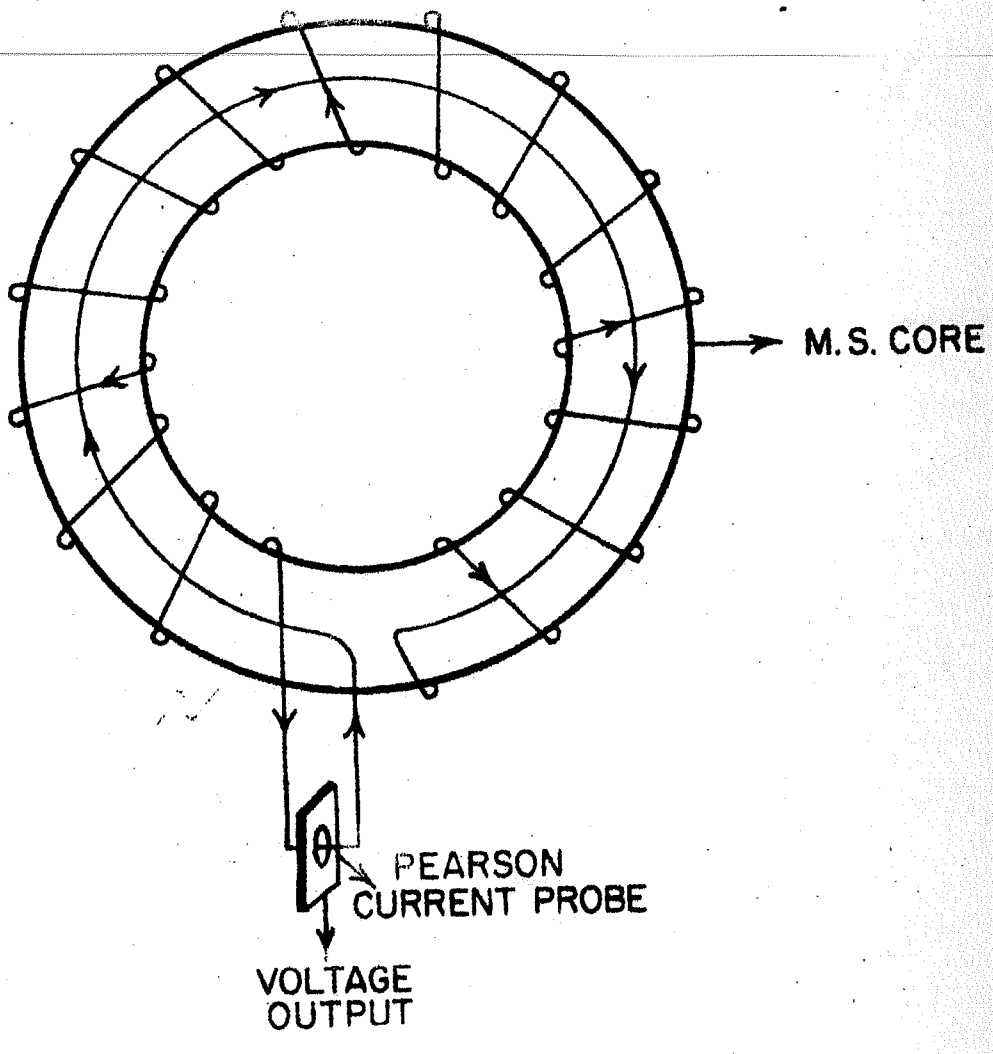


Figure 2-12. A schematic of Rogowski loop. The current flowing through Rogowski coil is measured by a standard pearson current probe.

we ensured a total elimination of pick-up in the signal. A calibration of the whole set-up was performed by passing a known current through the axis of the Rogowski loop. A number of such coils are used to delineate the profiles of current structure in interaction region.

The magnetic probe consists of 3 coils fixed at right angles to each other to sense the change in magnetic field in all the three coordinate directions. The coils are made of 0.2 mm enamelled copper wire. Each coil has 10 turns and has a diameter of 2 mm. To increase the sensitivity and get rid of electrostatic pick-ups, the centre of each coil is grounded and the differential output between the ends of each coil is measured. The construction details are shown in figure 2-13. Whole structure containing the three coils is enclosed in a pyrex glass tube of 12 mm diameter with a semi-spherical end. The inner surface of glass tube is coated with a 5 micron silver layer to avoid any electrostatic coupling between the coil and plasma. The penetration time of magnetic field is 0.1 μs which is much less than duration of current loop. The whole structure is mounted on a movable probe and the electrical connections are taken through shielded copper wires. The voltage output of coil is given by

$$V = n A \left[dB/dt \right] \qquad .. \quad (2.1)$$

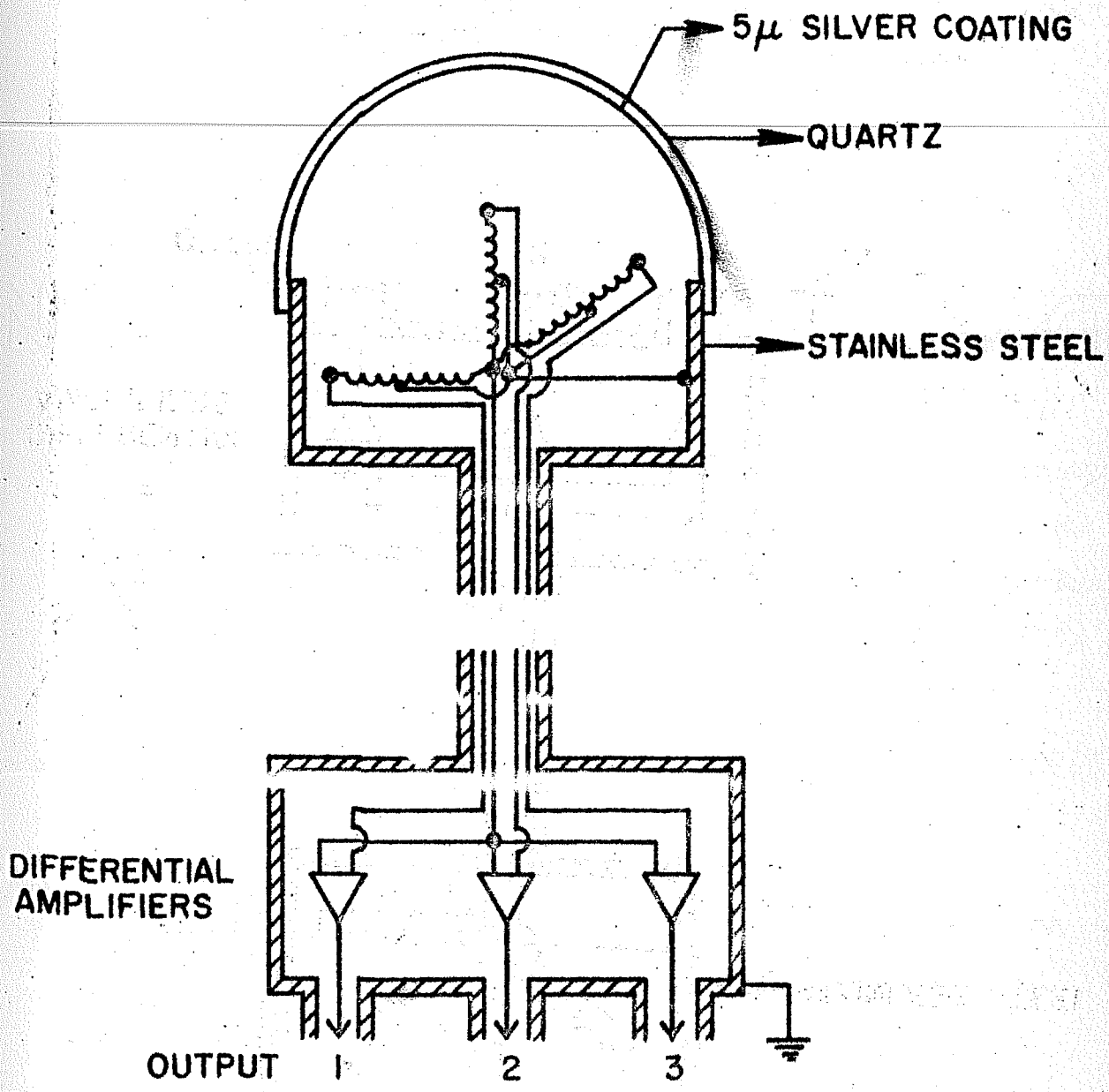


Figure 2-13. A schematic of the three-axis magnetic probe for measuring (dB/dt). B(t) is obtained by graphical integration.

where

n is the number of turns;

A is the area per turn in m^2 and

$\left[dB/dt\right]$ is rate of field change in $W/m^2 s$.

2.4 Relevant condition for impact experiment

In our experiment, plasma pulse width is ~ 30 μs at the mouth of the coaxial gun. The transit time of plasma through the drift tube at the highest plasma stream velocity is 16 μs. Thus the plasma pulse width is greater than the transit time of plasma through the drift tube for velocities greater than 50 km s^{-1}. At velocities less than 50 km s^{-1}, the plasma pulse width is less than the transit time of plasma. From this, it appears that the high velocity plasma stream (> 50 km s^{-1}) connects the central cathode of the coaxial gun with the interaction region. However, the following observations indicate that the situation may not be similar to plasma-neutral gas interaction experiments performed within the coaxial gun itself.(Axnäs, 1972; Fahleson, 1961): (a) The plasma potential is low, ~ 30 V. (b) Rogowski coils do not indicate any current flow between gun and body of plasma in interaction region. (c) The boundary of the interaction region is made of an insulator so that if there were any currents flowing from the electrodes of gun to the plasma at the interaction region, the return

current path is not set up through the body of the device.

(d) No characteristics of discharge circuit are carried over to the plasma as indicated by plasma potential etc. So, we opine that atleast in the velocity range of 2 - 50 km s^{-1}, there is no power supplied to the gun when plasma reaches to the interaction region.

Chapter 3

CHARACTERISTIC VELOCITIES IN PLASMA-NEUTRAL GAS INTERACTION

In this Chapter, the results on characteristic velocities in the plasma-neutral gas interaction are presented. The main emphasis is on Varma's threshold velocity.

Before discussing the experiments on characteristic velocities in plasma-neutral gas interaction, it is necessary to consider the binary atomic collisions between plasma stream and neutral gas particles, as this would be of decisive importance in interpreting the experimental observations. Table 3-1 gives the relevant experimental parameters related to interaction region, plasma stream

Table 3-1

PARAMETERS OF PLASMA AND NEUTRAL GAS IN THE EXPERIMENT

Plasma density	m^{-3}	$10^{17} - 10^{18}$
Plasma temperature	eV	5 - 10
Plasma velocity	km s^{-1}	3 - 100
Neutral gas density (dense)	m^{-3}	$10^{19} - 10^{21}$
Interaction scale length (dense)	m	$10^{-3} - 5\times10^{-2}$
Expansion velocity of the gas blob	m s^{-1}	10^{2}
Neutral gas density (diffused)	m^{-3}	$10^{16} - 10^{17}$
Interaction scale length (diffused)	m	0.5 - 10

and neutral gas cloud for our experiment. Table 3-2 presents the collision times and electron and ion Hall parameters. All possible combinations of interactions of plasma and neutral gas formed out of hydrogen, nitrogen, oxygen, neon and argon have been taken into account in forming the above table. It is clear from the table that the strong ionisation of neutral gas cloud and plasma momentum loss cannot occur by simple binary collisions without invoking plasma collective processes. The interaction, thus, is collisionless to begin with.

3.1 Alfvén's critical velocity

In the experiment to observe Alfvén's critical velocity for nitrogen, the interaction region was evacuated to its base pressure of 10^{-6} Torr, initially. A d.c. magnetic field of 1 kG was applied in the interaction region. In the first shot, nitrogen plasma stream generated by coaxial plasma gun was allowed to penetrate the interaction region. The velocity of plasma stream was recorded by a V x B - probe in the interaction region. In the next shot, an electromagnetic valve was opened to let in a small cloud of nitrogen gas which developed into an axial depth of 20 cm and an average density of 10^{20} m^{-3} by the time plasma penetrated it in the interaction region. The velocity of plasma stream was recorded

Table 3-2

RELEVANT SPATIAL AND TIME SCALES FOR VARIOUS BINARY COLLISIONS IN THE EXPERIMENT

τ_{en}	Ionisation (10 ev maxwellian)	μs	30 - 60
τ_{en}	Ionisation (100 eV)	μs	0.25 - 0.4
τ_{pn}	Ionisation	μs	100 - 250
τ_{pn}	Charge transfer	μs	150 - 250
τ_{en}	Elastic scattering (10 eV)	μs	0.1
τ_{en}	Elastic scattering (100 eV)	μs	0.4
τ_{in}	Charge transfer	μs	1 - 3
ρ_e	(10 eV)	cm	7×10^{-3}
ρ_p	($V = V_o$)	cm	0.7 - 30
ρ_i	($V = V_{cr}$)	cm	0.3 - 2.6
$(\omega\tau)_e$			10^5
$(\omega\tau)_p$			50 - 10^3
$(\omega\tau)_i$			2 - 10

Symbols : ω - gyrofrequency; τ - collision time; ρ - gyroradius.

Indices: n - neutral atom; p - plasma ion; i - ion of neutral atom; e - electron.

after it had traversed atleast 20 cm of the gas cloud. The obtained signals by V x B - probe are shown in figure 3-1.

In this figure, trace 1 gives velocity of the plasma stream passing through the interaction region without neutral gas; the velocity at the head of the stream is 200 km s^{-1} and goes down to 3 km s^{-1} at the rear. The total plasma pulse period is about 50 μs. Trace 2 gives velocity of nitrogen plasma stream after it has penetrated through nitrogen gas cloud of 20 cm length and 10^{20} m^{-3} density. A constant plateau of this trace, which corresponds to the Alfvén's critical velocity of 14 km s^{-1} for nitrogen (N) gives an unambiguous demonstration of the critical velocity phenomenon. It is clear that front part of the plasma stream, which had velocity greater than 14 km s^{-1} before its interaction with neutral nitrogen gas, was decelerated to the Alfvén's critical velocity for nitrogen. On the other hand, the rear part of the stream which had velocity less than the Alfvén's critical velocity remained unaffected by its penetration through the neutral gas. A delay of 10 μs between the beginnings of traces 1 and 2 is another indication that the plasma stream was decelerated while it penetrated through the neutral gas cloud.

The experiment was repeated with plasma streams made out of hydrogen, oxygen, neon and argon. The results indicated

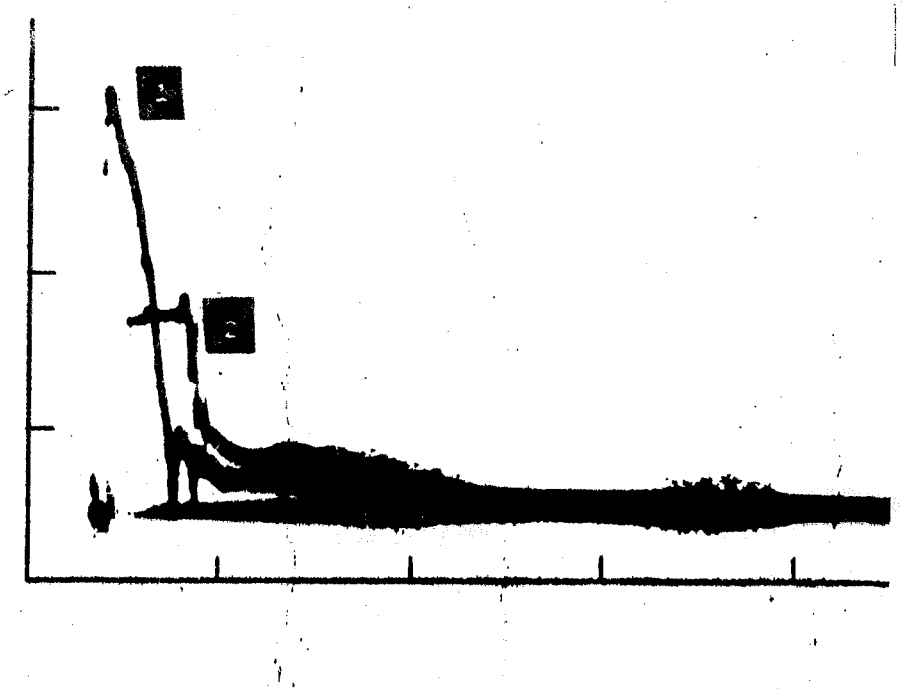


Figure 3-1. The polarisation electric field measurements with a V x B - probe placed in the interaction region. Trace 1 corresponds to the measurement without the neutral gas cloud and trace 2 with. Scale:- X-axis: 100 μs/div., Y-axis: 30 v cm^{-1}/div. for trace 1 and 4.0 v cm^{-1}/div. for trace 2. The traces were obtained for nitrogen plasma interaction with nitrogen gas cloud. The peak of trace 1 corresponds to a velocity of 2×10^5 m s^{-1}.

that the final velocity of plasma stream always corresponded to a value very close to Alfvén's critical velocity for nitrogen. Similar experiments with hydrogen, oxygen, neon and argon gas clouds confirmed the existence of the Alfvén's critical velocity corresponding to each gas as listed in Table 3-3. This table also lists the ionisation potentials of different gases.

3.2 Varma's threshold velocity

It is seen from equations (1.1) and (1.2) that in the experimental situations where plasma ion mass is smaller than the atomic mass of neutral gas, V_{th} is greater than V_{cr}. Table 3-4 gives Alfvén's critical and Varma's threshold velocities for hydrogen, helium, nitrogen, oxygen, neon, argon and xenon using atomic hydrogen plasma as the moving magnetised plasma for neutral gas-plasma interaction to occur. The large difference between the two velocities in case of argon, neon and xenon and their monoatomic nature make them best suited for the experiment to test the existence of Varma's threshold velocity. In our experiment, we have chosen combination of hydrogen and argon.

The initial plasma stream velocity was varied in the range of 2-100 km s^{-1}. It was then allowed to penetrate the neutral gas cloud of 15 cms with average density of

Table 3-3

IONISATION POTENTIAL AND ALFVÉN'S CRITICAL VELOCITIES FOR VARIOUS NEUTRAL GASES

Gas	Ionised mass	Ionisation potential	Critical Velocity
	a.m.u.	volts	km s^{-1}
H	1	13.6	51.0
He	4	24.5	34.4
N	14	14.6	14.2
O	16	13.7	12.7
Ne	20.2	21.6	14.4
Ar	39.9	15.6	8.7
X_2	131.3	12.13	4.2

Table 3-4

THRESHOLD AND CRITICAL VELOCITIES FOR HYDROGEN PLASMA PENETRATING THROUGH VARIOUS NEUTRAL GAS CLOUDS

Neutral gas	Threshold velocity	Critical velocity
	km s^{-1}	km s^{-1}
Hydrogen	51.0	51.0
Helium	68.8	34.4
Neon	64.72	14.4
Nitrogen	53.13	14.2
Oxygen	50.8	12.7
Argon	54.96	8.7
Xenon	48.25	4.21

10^{20} m^{-3} in the presence of transverse magnetic field.

In this investigation, the plasma velocity was measured by V x B - probe and by time-of-flight method. While shot-to-shot variation of the plasma velocity as measured with V x B - probe during the interaction is quite large, ~ 20%, the variation in time-of-flight method is less than 2%. We explain the discrepancy between the two methods as due to the fact that our V x B - probe is placed in the cloud region close to where plasma is decelerated and that time-of-flight gives a velocity averaged over a spatial distance of 16 cm between the two spaced probes. For reasons of shot-to-shot variation the points represented in figures 3-2 and 3-3 are an average of atleast 4 shots.

Figure 3-2 shows a plot between the velocity of argon plasma before it interacts with neutral hydrogen gas cloud and its velocity 2 cm behind the centre of gas cloud. For very low velocity, plasma penetrates the neutral gas cloud without suffering any deceleration. At velocities greater than 51 km s^{-1}, the Alfvén's critical velocity for hydrogen, plasma velocity is reduced to a value close to V_{cr}. This figure clearly demonstrates the Alfvén's critical velocity phenomenon in the ionising interaction between argon plasma and hydrogen neutral gas.

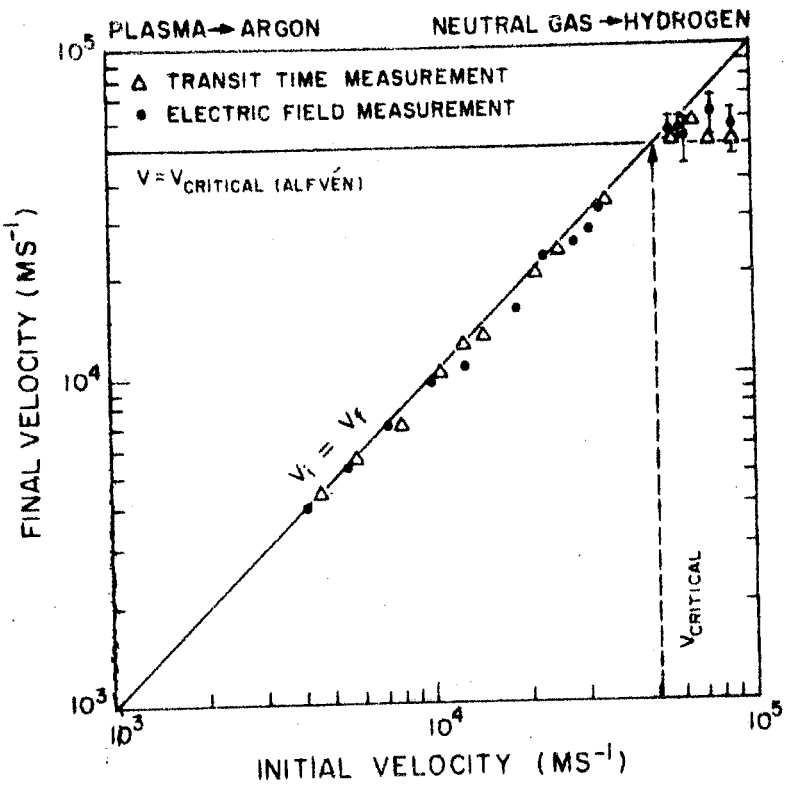


Figure 3-2. Plot of argon plasma velocity 2 cm behind the centre of the hydrogen gas cloud against its initial velocity. The solid horizontal line represents Alfvén's critical velocity for hydrogen.

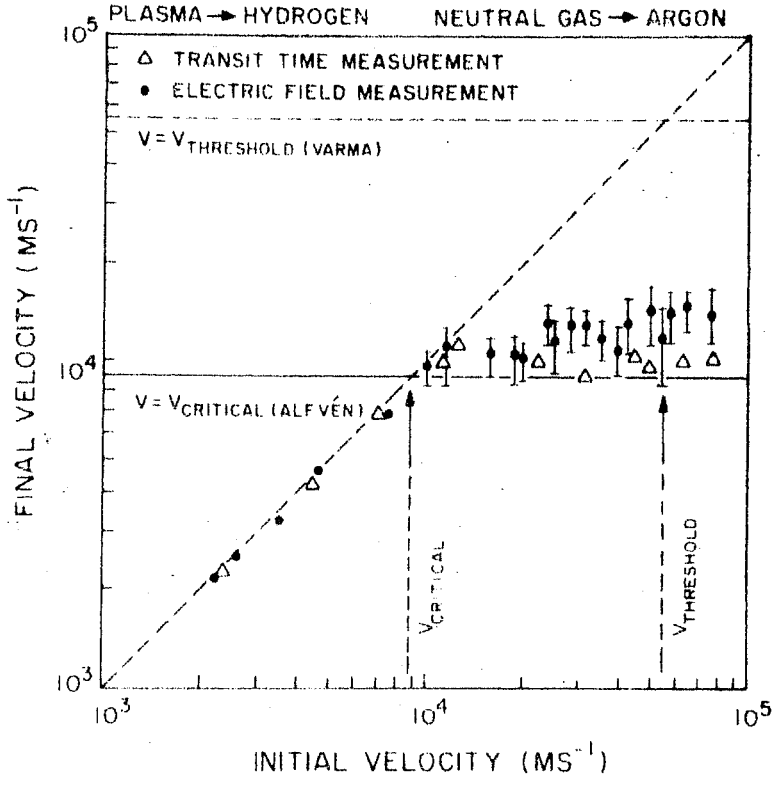


Figure 3-3. Plot of the hydrogen plasma velocity 2 cm behind the centre of the argon gas cloud against its initial velocity. The horizontal solid line represents Alfvén's critical velocity for argon and the dashed line represents Varma's threshold velocity for hydrogen plasma in argon.

Figure 3-3 is a similar plot for hydrogen plasma and argon neutral gas. The Alfvén's critical and Varma's threshold velocity for argon are 8.7 and 54.96 km s^{-1} respectively. These are represented in figure 3-3 by two lines parallel to initial plasma velocity axis. The figure clearly shows that hydrogen plasma after its penetration through the neutral gas cloud has its velocity reduced to a value close to Alfvén's critical velocity of 8.7 km s^{-1} even when the initial plasma velocity is less than the Varma's threshold velocity of 54.96 km s^{-1}. Thus our investigations clearly point out the non-existence of Varma's threshold on the relative velocity in the ionising interaction between a plasma and a neutral gas. These results remained unaltered by varying the neutral gas density between 10^{19} - 10^{20} m^{-3} and transverse magnetic field in the range of 600 - 1000 G.

3.3 Interaction of plasma stream with diffused gas clouds

While testing the performance of the plasma gun, at the background pressure of 10^{-5} Torr in the system, our observations indicated that the velocity of plasma stream made out of air, as measured with V x B - probe, was always very close to the critical velocity of nitrogen. On the contrary, the velocity determined by the time-of-flight method, with no magnetic field in the interaction region, was about

100 km s^{-1}. This is an order of magnitude greater than that obtained with V x B - probe which requires magnetic field for its measurements. These results suggest that plasma stream suffered plasma-neutral gas interaction with diffused low density neutral gas of the background.

That we were not able to produce high velocity plasma streams in the presence of transverse magnetic field in the interaction region was indeed due to a limitation imposed by Alfvén's critical velocity phenomenon. This was further evidenced by experiments wherein the base pressure of the device was maintained at 10^{-5} Torr, but plasma gun was injected with different gases. It was found that the stream velocity for hydrogen plasma was well above its critical velocity whereas it remained close to Alfvén's critical velocity for argon, in case of the plasma formed out of argon. This increase or decrease in plasma velocity was observed only after several plasma gun discharges, suggesting that the gas injected into the plasma gun used to form the background in the interaction region. Furthermore, the plasma velocity increased as V x B - probe was moved towards the plasma gun; a reduction of 20 cm in interaction length increased the plasma velocity by a factor of 2. At improved base pressure of the device to 10^{-6} Torr, plasma was found to travel with almost the initial velocity.

This implies that the plasma retardation in the experimentally available interaction length at the background pressure of 10^{-6} Torr was not appreciable enough to be detected by our probes.

3.4 Discussion

3.4.1 Non-existence of Varma's threshold velocity

The non-existence of threshold velocity can be explained by examining the assumptions of acceleration of electrons in Varma's model. In this model, it is assumed that the entire kinetic energy in a plasma ion is taken up by a plasma electron on the average. This assumption is too restrictive in light of recent experiments (Danielsson, 1970; Danielsson and Brenning, 1975; Himmel et al. 1976). These experiments have established that plasma-neutral gas interaction involve collective processes such as two-stream instability (Sherman, 1969; Raadu, 1975) or Lehnert's space charge model (Lehnert, 1967). Further, electrons created during the ionisation of the neutral gas in the initiation period of the interaction also could take up a part of the energy contained in plasma ion. If only the first assumption is relaxed to that a (M_i/M_n) fractionof the ionisation energy of the neutral gas is transferred from plasma ion kinetic energy to the heat content of the plasma electrons, Varma's threshold velocity

becomes equal to Alfvén's critical velocity in case of $M_i < M_n$. But there is no valid reason, a priori, to make such an assumption as the plasma-neutral gas interaction in the initiation period of the interaction is much more complex than suggested by above simple assumption.

We also wish to emphasize that in Varma's model $V_{th} < V_{cr}$ in case of $M_i > M_n$, and thus this part of his model for plasma-neutral gas interaction is already too restrictive in its application. Results of section 3.1 show that Alfvén's critical velocity for the interaction of neutral gas with plasma is independent of the mass of the plasma ion. This implies that it is the relative velocity which is important in the plasma-neutral gas interaction and not whether the kinetic energy resides with plasma ion or neutral gas.

3.4.2 Validity of observations of plasma deceleration in diffused gas clouds

Following Danielsson and Brenning (1975), a scale length for electron impact ionisation can be defined by

$$L = V_o / \nu_{en} \qquad .. \quad (3.1)$$

where

V_o is the initial plasma velocity and

ν_{en} is the ionisation frequency.

The ionisation frequency can be written as

$$\nu_{en} = N_g \chi(E) \qquad .. \quad (3.2)$$

where

N_g is the gas density;

$\chi(E)$ is the ionisation function and

E is the electron energy.

Thus equations (3.1) and (3.2) relate the gas density with its scale length for appreciable ionisation to occur. This relation is :

$$L = V_o / N_g \chi(E) \qquad .. \quad (3.3)$$

Table 3-5 shows the ionisation function $\chi(E)$ and the scale length L calculated for the plasma stream deceleration in the neutral gas of the same species of which plasma is formed. In these calculations, value of the gas density N_g is 3×10^{17} m^{-3}, a value corresponding to the background pressure of 10^{-5} Torr and the initial plasma velocity of 100 km s^{-1}. The electron energy is assumed to be 100 eV. This table shows that at the device background pressure of 10^{-5} Torr, the scale length for plasma deceleration ranges between 25 - 70 cm for xenon, argon and nitrogen. In our experimental device the maximum available interaction

Table 3-5

IONISATION FUNCTION AT ELECTRON ENERGY OF 100 eV AND DECELERATION SCALE LENGTHS AT NEUTRAL GAS DENSITY OF 3×10^{17} m^{-3} FOR PLASMA INTERACTING WITH THE SAME GAS AT A VELOCTY OF 100 km s^{-1}.

Gas	Ionisation function	Deceleration scale length
	m^3 s^{-1}	m
Hydrogen	3.4×10^{-14}	3.0
Helium	2.0×10^{-14}	5.0
Nitrogen	1.4×10^{-13}	0.7
Oxygen	8.5×10^{-15}	13.0
Neon	3.9×10^{-14}	2.7
Argon	1.8×10^{-13}	0.5
Xenon	4.0×10^{-13}	0.25

length for appreciable deceleration of the plasma stream is about 60 cm.

It is obvious from Table 3-5 that hydrogen plasma stream velocity could not have been limited to Alfvén's critical velocity as it requires a long deceleration length of 3 m at 10^{17} m^{-3} which is greater than the total length of device. Further, this table makes amply clear that argon and nitrogen plasma streams were suffering deceleration due to their interaction with the diffused background gas. These results together with the results obtained from interactions in dense clouds (Danielsson and Brenning, 1975; Sections 3.1 and 3.2) lead to a significant conclusion that it is the integrated column neutral gas density and not the absolute value of density of the gas cloud which is important for retarding plasma streams to a value close to Alfvén's critical velocity. However, for establishing this result, it is imperative that we examine whether the observed limitation of plasma stream velocity to Alfvén's critical velocity at the device base pressure of 10^{-5} Torr can be accounted for by invoking some of the processes which might lead to the increased neutral gas density in the interaction region at the time of electric discharge of the injected gas in the plasma gun. It is also important to assess whether pre-ionisation of the background gas by ultraviolet

photon flux emanating at the time of electrical discharge in the plasma gun could lead to a precursory process by which plasma collective processes can be initiated at lower neutral gas density than suggested by calculations (Sherman, 1969; Raadu, 1977; Lehnert, 1967). We discuss these possibilities one by one.

It may be argued that the outgasing from the electrodes of plasma gun or perspex breech end at the time of electrical breakdown of the gas in plasma gun results in a dense gas cloud at the interaction region. To have an interaction taking place in the interaction region, the arrival of the outgased gas in the interaction region must precede that of the plasma stream. For this, the velocity of the outgased gas should be much greater than that of the plasma stream. There is no process which could have accelerated the outgased gas to a velocity greater than 100 km s^{-1} in our device. Also, there is no reason why the gas should escape unionised through the gun region.

From observational point of view, the reflex discharge probe did not show any neutral gas pulse with density greater than the background gas density before the arrival of the plasma stream in the interaction region. Further, when perspex breech end was replaced by glass jacket (see section 2.1.1) the results remained unaltered.

To make sure that some unionised gas from the plasma gun region did not escape to form a dense cloud in the interaction region when neutral gas was injected into the plasma gun for the formation and acceleration of plasma stream, the capacitor bank connected across the gun was not charged and the neutral gas parameters were measured at the interaction region. It was found that the velocity of the gas arriving at the interaction region was 3 orders of magnitude less than the plasma stream velocity and the peak gas density was not more than 10^{16} m^{-3}. Considering that electrical discharge in the plasma gun occurs within the first 100 μs of the injected gas pulse width of 600 μs, it is impossible for the interaction region to have received a dense gas cloud before arrival of the plasma stream.

At first glance, it might seem that due to the high neutral gas density localised in the plasma gun region, the charge exchange type of collisions between ionised and unionised components in the gun region can give rise to a neutral gas cloud moving with a high velocity into the interaction region. The velocity of this cloud would be comparable to that of the plasma stream. However, in that case, the plasma-neutral gas interaction would not occur since the relative velocity between the unionised gas and plasma stream would have been much less than the Alfvén's

critical velocity. Knowing that plasma production in the plasma gun region is nearly 100% efficient, not much unionised gas is expected to have been left behind to give rise to charge exchange produced high velocity neutrals. Also by reducing the amount of gas injected into the gun by an order of magnitude, the velocity of plasma stream did not increase beyond the Alfvén's critical velocity whenever interaction region was pervaded by magnetic field.

Thus, it does not seem possible that a dense neutral gas cloud could have formed in the interaction region by processes such as outgasing at the electrodes at the breech end, direct escape of the gas from the gun region and charge exchange collisions between the unionised and the ionised components of the gas in the gun region. We have also examined the effect of pre-ionisation of the background neutral gas in the interaction region by the ultraviolet photons emitted at the time of the electrical discharge on the Alfvén's critical velocity phenomenon. The point we have specifically examined is whether the pre-ionisation can lower the threshold of collective processes which lead to the phenomenon of Alfvén's critical velocity at the background gas densities. The suggested collective processes in the literature are the two-stream instability

mechanism (Sherman, 1969; Raadu, 1977) and the space charge formation (Lehnert, 1967). Lack of evidences from different experimental results (Danielsson, 1970; Danielsson and Brenning, 1975; Piel et al., 1978; Mattoo and Venkataramani, 1980) makes it difficult to decide which of the proposed collective processes can explain the plasma-neutral gas interaction. Further Piel et al. (1978) have suggested that the space charge is formed in the initial period of the ionising interaction subsequently followed by modified two-stream instability to heat the plasma electron to about 100 eV. These hot electrons then ionise the neutral gas rapidly and thus cause plama deceleration. In view of their suggestion, it is not clear whether or not both the suggested collective processes are operating in the Alfvén's critical velocity phenomenon. Because of this uncertainty, we have examined the effect of pre-ionisation on both the plasma collective processes that is, the two-stream instability and the space charge formation.

Considering discharge current of ~ 1 kA in the plasma gun for injected gas of hydrogen, our calculations (Venkataramani and Mattoo, 1981c) indicate that the total number of ultraviolet photons reaching the interaction region is 10^{13} in a plasma pulse of period of 20 μs. With photo-ionisation cross section of 10^{-23} m^2, neutral gas density

of 10^{17} m^{-3} and time of 20 μs available for recombination before plasma stream penetrates the diffused gas cloud, the number density of photoionised ions is $\sim 10^{10}$ m^{-3} (Venkataramani and Mattoo, 1981c).

In Sherman's model (Sherman, 1969), the minimum density of charge exchange produced ions which can trigger the instability is atleast 4 orders of magnitude greater than the density of photoionisation produced ions just estimated. Thus photoionisation could not have acted as a precursory process for initiating two-stream instability. In Lehnert's space charge model (Lehnert, 1967), the essential requirement is that plasma contains a group of particles with non-maxwellian distribution and having varying density distribution. Thus even this interaction also could not have been switched on since the photo-ionisation produced plasma is neither non-maxwellian in velocity distribution nor can have density gradients in the background neutral gas cloud.

3.4.3 Interaction at low neutral gas cloud density

The essential point that emerges from the above discussions of the result reported here is that it is the integrated column neutral gas density which is important in retarding a plasma stream to a value close to Alfvén's

critical velocity during plasma-neutral gas interaction and not the absolute value of the neutral gas density. However, a restraint should be exercised in extending this line of arguments to very low neutral gas density limit. It does not seem appropriate to say that as along as the integrated column neutral gas density in the effective interaction region corresponds to a given required value, it does not matter whether neutral gas is of low density, large extent or high density, short length. For example, consider that modified two-stream instability explains the Alfvén's critical velocity phenomenon. Now the electrons can attain needed drift velocity for this instability to be excited under the assumption that the ions remain unmagnetised while electrons are magnetised and move freely along the magnetic field lines. Such a drift can occur only when the potential sheath formed by the non-thermal ions arising out of charge-exchange collisions is not short-circuited by the gyrating motion of the electrons. This gives the upper limit on the neutral density for the ionising interaction at a given magnetic field, plasma velocity and density. On the other hand, the size of the sheath should not exceed ion gyro-radius. This condition will determine the lower limit on the neutral gas density. A straightforward calculation for the lower limit on the

neutral gas density needed to produce the non-thermal ions for establishing such an aforementioned sheath gives a value of 10^{13} m^{-3} for the parameters of our experiment. To verify this, an experiment would have to be performed with an effective interaction length of 10^{5} metre long kept under the base pressure of 10^{-9} Torr, which is beyond the scope of any laboratory experiment.

Chapter 4

PLASMA RETARDATION

In this chapter, we describe results of plasma retardation obtained in a limited parameter range of plasma stream but in a wide range of density of gas cloud (10^{17} - 10^{21} m^{-3}). Further, we have varied the mass ratio (ion/gas atom) in the experiment from 0.025 to 40. This data was obtained essentially to identify the role of atomic processes in the retardation of plasma stream. It is found that while atomic processes may account for the observed plasma retardation at high gas densities, they are insufficient to explain the results obtained at low gas densities. In fact, the conclusion is that plasma streams retard in low

gas densities faster than expected from theories which relate plasma retardation to atomic processes.

4.1 Experimental set-up

The experimental arrangement used is same as described in Chapter 3. The opening of gas valve and the electric discharge in the gun are synchronised so that the gas cloud in the interaction region has the desired axial spread and average density. The average gas density is varied between 10^{17} and 10^{21} m^{-3}. The density scale length (e-folding length) of the gas cloud varies from 2 cm at the average gas density of 10^{21} m^{-3} to 50 cm at 2×10^{17} m^{-3}. In the measurements reported here, the scale length of the gas cloud is ensured to be greater than the observed velocity retardation scale length. Since diffusion time of the neutral gas cloud is 100 μs, and transit time of the plasma stream through neutral gas cloud is only a few μs, the gas cloud appears stationary to the penetrating stream. The shot-to-shot variation in the density of the gas cloud is less than 10%. The plasma retardation is observed by measuring plasma velocity with V x B - probes placed at different points in the gas cloud; the distance between the probes varies from minimum of 0.8 cm to maximum of 8 cm. As mentioned in Section 2.3, the velocity measurements by these probes are

in good agreement with those obtained by measuring time-of-flight between two spaced Langmuir probes.

4.2 Scale lengths of plasma deceleration

The observations on plasma stream velocity are done just after plasma stream meets the neutral gas cloud. Typical velocity profiles obtained by V x B - probes placed 8 mm from each other along the plasma stream for hydrogen plasma interacting with argon neutral gas is shown in figure 4-1. The reduction in amplitude of signals shows that the plasma stream is decelerating. Figure 4-2 shows the variation of the velocity of hydrogen plasma as it streams through the argon neutral gas cloud at different gas densities. The velocity decreases, rapidly at high gas densities, as the plasma penetrates into the neutral gas. At the last V x B - probe, the velocity is lower by an order of magnitude in the dense clouds as compared to the same in the absence of neutral gas. Defining velocity retardation scale length as the e-folding distance, we have tabulated the observed retardation lengths at different gas densities in Table 4-1. This table also shows the observed retardation length for the cases where plasma stream ion mass is less than mass of gas cloud atoms. The numbers in brackets in this table are the computed values of the retardation length using equation

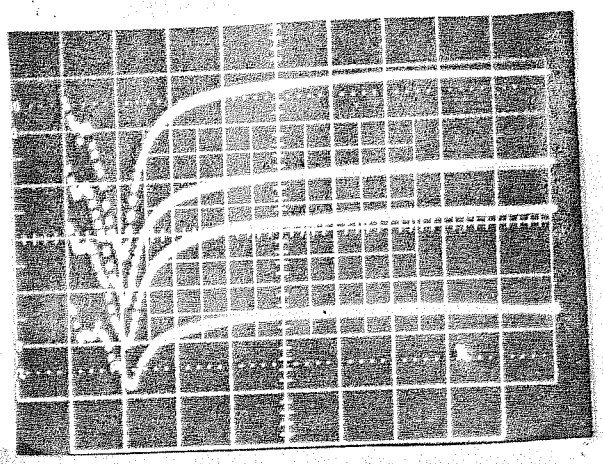


Figure 4-1. A typical record of hydrogen plasma stream velocity in the interaction region measured by four V x B - probes kept seperated by 8 mm from each other along the axis of the plasma stream. The measurements were made when hydrogen plasma stream was traversing through argon gas cloud density of 5×10^{19} m^{-3}.

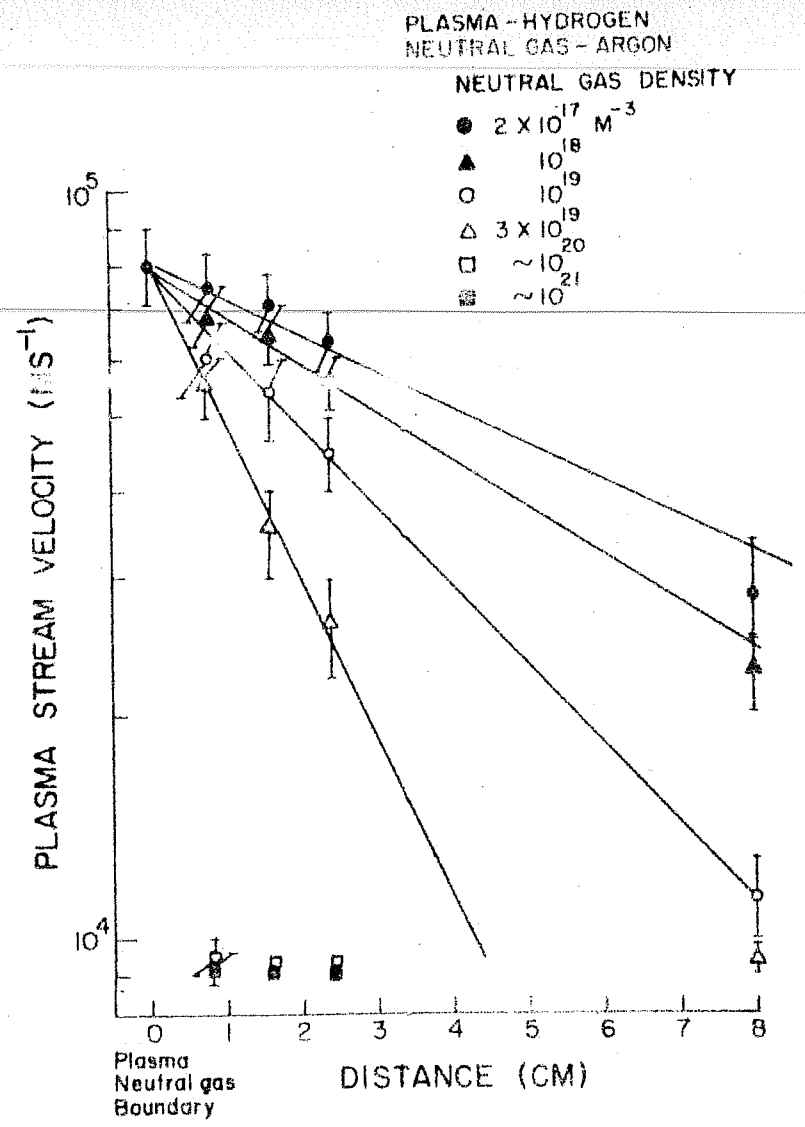


Figure 4-2. Hydrogen plasma velocity at different points in the argon gas cloud of indicated gas density. The plasma neutral gas boundary is the position in the experimental region upto which the plasma moves unretarded. The Alfven's critical velocity of argon is 8.7 km s^{-1}.

(1.9). These calculations assume that the plasma electrons are heated to a temperature of about 100 eV during the onset of the plasma-neutral gas interaction. This assumption is fairly valid in view of the measurement of electron temperature in the experiment of Danielsson (1970) and Danielsson and Brenning (1975). These experiments indicate that the heating of electrons takes place at the penetration of the plasma into the neutral gas cloud and that the electron temperature may be as high as 100 eV. It must be remarked here that, in our experiment, the assumed electron temperature may be too high in case of hydrogen plasma interacting with any neutral gas cloud. This is because the maximum initial ion energy is 50 eV which is less than the assumed electron temperature. It is for this reason that we have not given the computed values of L in Tables 4-1 and 4-3, for the interactions where plasma stream is of hydrogen.

The results summarised in Table 4-1 clearly indicate that the retardation scale length does not scale as (M_i/M_n). At any average neutral gas density, we do not observe the expected increase in scale length by a factor of 40 as the mass of plasma ion is varied from 1 for hydrogen to 40 for argon. The maximum increase is by a factor of 3.5 at 2×10^{17} m^{-3} gas density. This is verified further by

Table 4-1

RETARDATION SCALE LENGTHS OF INDICATED PLASMAS GOING THROUGH ARGON GAS CLOUD ($M_i \leq M_n$)

Plasma	Scale length (cm)			
	$N_g = 10^{20}$	10^{19}	10^{18}	2×10^{17} m^{-3}
Hydrogen	< 0.5	4.5	7.0	10.0
Nitrogen	< 0.5 (0.14)	2.5 (1.4)	4.0 (14.0)	7.0 (70.0)
Oxygen	< 0.5 (0.16)	2.5 (1.6)	3.0 (16.0)	10.0 (80.0)
Neon	< 0.5 (0.2)	2.0 (2.0)	10.0 (20.0)	30.0 (100.0)
Argon	< 0.5 (0.4)	4.0 (4.0)	7.0 (40.0)	35.0 (200.0)

Table 4-2

RETARDATION SCALE LENGTHS FOR ARGON PLASMA GOING THROUGH INDICATED NEUTRAL GASES ($M_i \gtrsim M_n$)

Gas	Scale length (cm)			
	$N_g = 10^{20}$	10^{19}	10^{18}	2×10^{17} m^{-3}
Hydrogen	4.0 (80)	19.0 (800)	24.0 (8000)	36.0 (40000)
Nitrogen	1.5 (1.4)	6.0 (14)	12.0 (140)	20.0 (700)
Oxygen	2.0 (22.5)	10.0 (225)	15.0 (2250)	40.0 (11250)
Neon	1.0 (3.6)	5.0 (36)	13.0 (360)	30.0 (1800)
Argon	0.5 (0.4)	4.0 (4)	7.0 (40)	35.0 (200)

Table 4-3

RETARDATION SCALE LENGTHS FOR SYMMETRIC PLASMA-NEUTRAL GAS INTERACTIONS ($M_i = M_n$)

Plasma/gas	Scale length (cm)			
	$N_g = 10^{20}$	10^{19}	10^{18}	2×10^{17} m^{-3}
Hydrgoen	1.6	4.0	9.0	20.0
Nitrogen	1.2 (0.5)	3.0 (5)	7.0 (50)	25.0 (250)
Oxygen	2.0 (9)	5.0 (90)	15.0 (900)	40.0 (4500)
Neon	1.0 (1.8)	4.5 (18)	12.0 (180)	26.0 (900)
Argon	0.5 (0.4)	4.0 (4)	7.0 (40)	35.0 (200)

studies in which mass ratios are inverted by interchanging the gases supplied to the plasma gun and the gas cloud region. These results are displayed in Table 4-2. A comparison between Tables 4-1 and 4-2 shows that although the observed plasma retardation length is always larger when $M_i > M_n$ than when $M_i < M_n$, the scale lengths for direct and inverted mass ratio are not related to each other by $(M_i/M_n)^2$. As a matter of fact, the ratio of scale length for $M_i > M_n$ to the same for the inverted mass ratio ranges between 3 and 5 and seems to be independent of mass ratio. Further, even after normalising the measured scale lengths for the ionisation function $\chi(E)$, they do not show the expected scaling.

The variation of scale length with the gas cloud density is such that it increases as the gas density (N_g) decreases. This variation is more pronounced for interactions which have $M_i > M_n$. The observed scale length, however, does not increase by an order of magnitude if the gas density is reduced by the same magnitude. An empirical fit shows that $L \propto N_g^{-\alpha}$, where α ranges from 0.15 for non-symmetrical $(M_i \neq M_n)$ to 0.5 for symmetrical $(M_i = M_n)$ plasma-neutral gas interactions.

We notice from Table 4-1 that there is a reasonably good agreement between the experimentally observed and the theoretically expected values of the plasma retardation scale

length at $N_g = 10^{19}$ m^{-3}. But this agreement is not seen at lower gas densities ($N_g < 10^{19}$ m^{-3}), and even at $N_g = 10^{19}$ m^{-3} for those interactions which have $M_i > M_n$ (see Table 4-2). In fact, the experimentally observed value of the retardation length is an order of magnitude less than the expected value for some of the interactions listed in Tables 4-1 and 4-2. In order to make sure that this result does not suffer from any ambiguity due to the dependence of retardation length on M_i/M_n, we have studied interactions in which mass ratio $M_i/M_n = 1$. In these interactions the same gas was used for the formation of the plasma stream and the gas cloud. The results are displayed in Table 4-3. It again shows that computed scale length is an order of magnitude greater than the observed value and confirms that the plasma retards faster than what is expected from equation (1.9).

The discrepancy between the observed and the expected retardation scale lengths can be reduced, at the most, by a factor of 2 if the value of V in equation (1.9) corresponds to the average velocity of the plasma during the interaction time rather than the initial velocity. The agreement can be made excellent if only the value of V were just about the critical velocity of the neutral gas. But, at this velocity, the rapid ionisation interaction, associated with the Alfven's critical velocity phenomenon, cannot

occur and the ionisation function $\chi(E)$ has considerably small value. Thus, it cannot be conjectured that the presumption of equalling V to the initial plasma velocity is the cause of the discrepancy reported here. Further, it may be argued that the assumed electron temperature for the calculation of $\chi(E)$ is either too high or too low. This can be ruled out for two reasons. Firstly, the experimental observations of Danielsson and Brenning (1975) have established that electrons can get heated to 100 eV. Secondly, the ionisation function $\chi(E)$, has a broad maximum in the range of 70 - 1000 eV for all the gases used in the formation of the gas cloud in our experiment. Even if the electrons were heated to more than the presumed value, it would not have changed the value of $\chi(E)$ very much. Also, assuming electron temperature less than 100 eV would only accentuate the discrepancy further as the value of $\chi(E)$ is lower at such a value than that at 100 eV. Hence, the discrepancy cannot either be explained on the basis of the ionisation function.

A comparison between the measured and the calculated interaction times also leads to the same conclusion as derived from the measurements of the retardation scale length. We find that the observed deceleration time is less than the calculated ionisation time for 100 eV electrons at all the gas densities considered here; the difference

increases as N_g decreases.

4.3 Discussion

Our results clearly show that ionisation of the gas cloud alone cannot explain the observed fast plasma retardation. Hence there is a need to consider explanations in terms of various collisions between plasma ions and gas atoms, wall losses and deceleration by electrostatic fields. In the following we discuss these processes one by one.

4.3.1 Role of various atomic processes

To evaluate the contributions of collisions to the retardation of plasma stream, we have to take into account (i) binary collisions between plasma stream particles and stationary neutral gas atoms and (ii) those collisions which occur only after the onset of plasma-neutral gas interaction. For our convenience we call the first type of collision losses as 'direct' losses and the second type as 'indirect'.

(a) 'Direct' losses

Since the main portion of the momentum/energy is residing with plasma ions we consider here only those collisions which involve plasma ions. We have considered all the possible collisions that can occur between a plasma ion and a neutral gas atom. They are : (i) charge transfer

collisions; (ii) ion-neutral ionisation and (iii) ion-neutral elastic scattering collisions. For the sake of simplicity, we calculate the loss of energy suffered by plasma stream as a result of these collisions and extend conclusions drawn from it to the discussion of plasma retardation.

An expression for the energy lost, E_l, by the plasma stream due to the collisions listed above, can be written as

$$E_l = N_p \sum_k \left[N_g \langle \sigma V \rangle_k \right] \tau E_i \qquad .. \quad (4.1)$$

where

N_g is the neutral gas density;

τ is the duration of interaction;

E_i is the kinetic energy of each plasma stream ion and

$\langle \sigma V \rangle_k$ is the effective reaction rate for k^{th} type of interaction.

The summation is performed over all the three types of collisions. It must be noted that equation (4.1) assumes that the whole of E_i residing with plasma ion is lost during a collision. The above calculation thus will give the upper limit to the estimate of plasma stream energy lost due to direct collisional processes. Since the plasma stream retards during interaction, σ changes for each of the

collisions mentioned above. We calculate here the reaction rate σv averaged over initial plasma stream velocity value to plasma stream velocity at the end of the experimentally observed retardation length. An example of how .. σv is evaluated is given below.

consider an interaction between argon plasma stream and argon neutral gas. The velocity of head of plasma stream as a function of time during interaction with argon gas cloud is plotted in figure 4-3. The value of σ for charge exchange collisions between argon ion and argon atom is shown in figure 4-4 as a function of ion energy. Using figures 4-3 and 4-4, the average reaction rate for charge exchange process is evaluated using expression

$$\langle \sigma v \rangle_{chex} = \frac{1}{\tau} \int_0^{\tau} \sigma v(t)\, dt \qquad .. \quad (4.2)$$

where τ is the duration of interaction.

The procedure is repeated for ion-neutral ionisation and scattering collisions. The calculated average reaction rates are tabulated in Table 4-4 and used in equation (4.1) to estimate the average energy loss per ion of plasma stream. Similarly, calculations are repeated for all the other plasma-neutral gas interactions studied here.

It was found that the energy lost through these

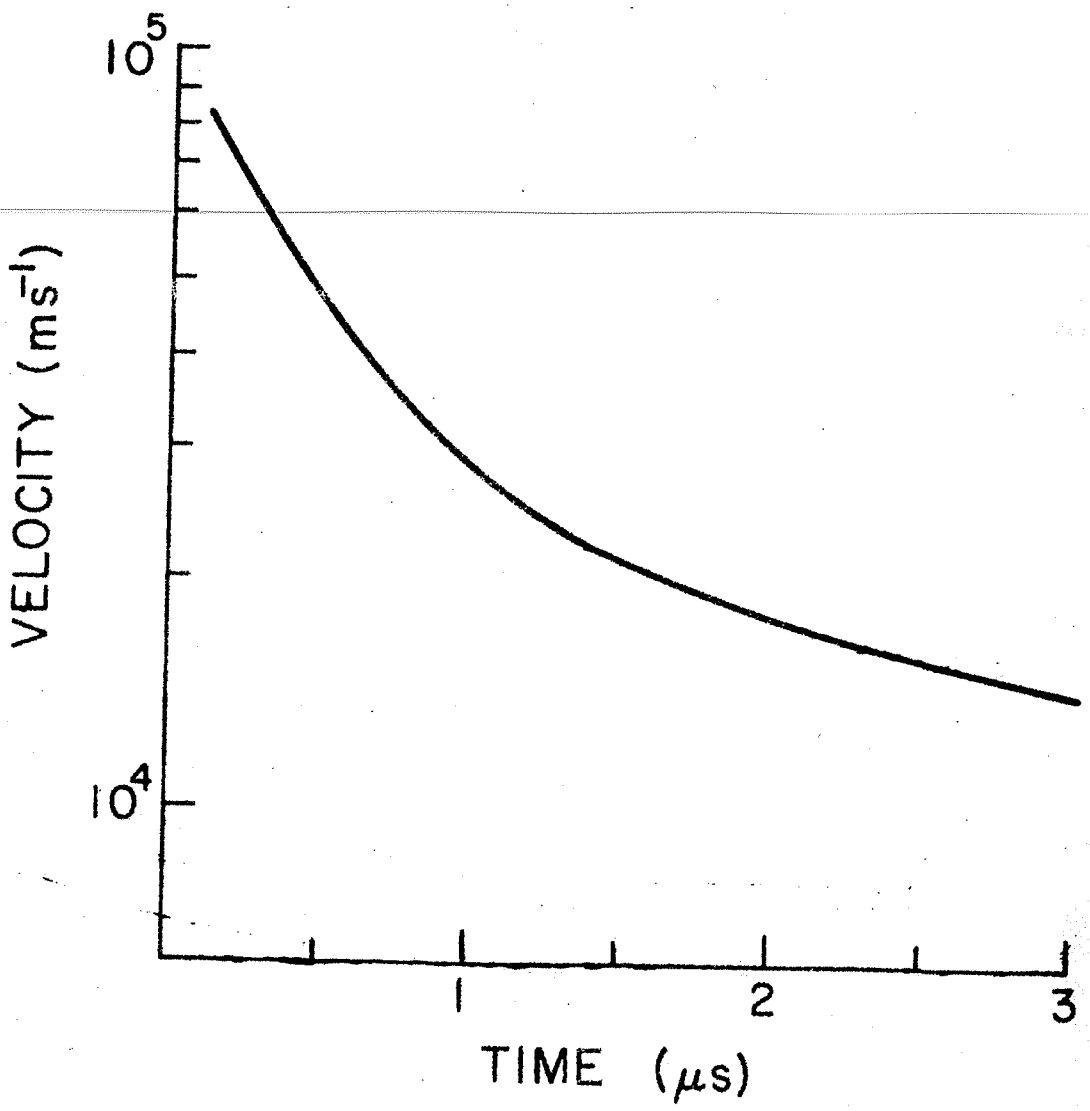


Figure 4-3. Plot of velocity of argon plasma stream front as a function of time when it penetrates through argon gas cloud of density 10^{19} m^{-3}.

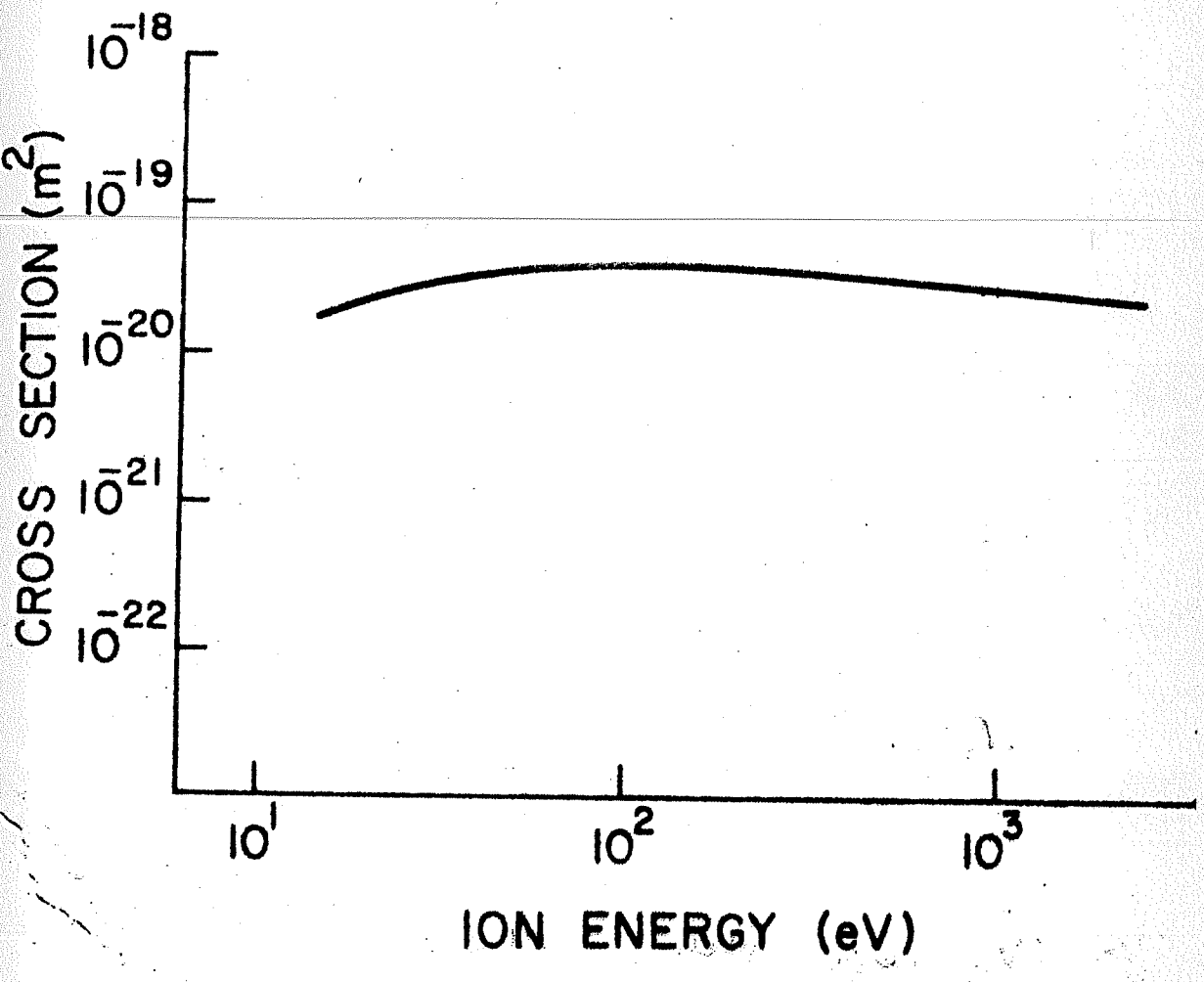


Figure 4-4. Cross section curve for resonant charge exchange process for argon ions with argon gas atoms.

Table 4-4

TOTAL REACTION RATES FOR DIRECT COLLISIONAL PROCESSES - CHARGE TRANSFER, IONISATION & SCATTERING COLLISIONS BETWEEN PLASMA STREAM IONS AND NEUTRAL GAS ATOMS FOR (a) SYMMETRIC AND (b) ASYMMETRIC PLASMA- NEUTRAL GAS INTERACTIONS

Plasma-neutral gas	$\langle \sigma v \rangle^*$
	$m^3\ s^{-1}$
(a) Symmetric	
H - H	3.1×10^{-14}
N - N	0.82 "
O - O	4.01 "
Ne- Ne	0.9 "
Ar- Ar	0.75 "
(b) Asymmetric	
H - Ar	0.22×10^{-15}
N - Ar	0.3 "
O - Ar	0.48 "
Ne- Ar	1.02 "
Ar- H	0.75 "
Ar- N	0.72 "
Ar- O	0.97 "
Ar- Ne	0.85 "

* averaged over initial velocity to Alfven's critical velocity.

collisions in symmetric interactions ($M_i/M_n = 1$) is more than the same in case of asymmetric interactions ($M_i/M_n \neq 1$). This is because of high resonant charge exchange collision cross section value in the former case. The total energy loss is about 15% at 10^{19} m^{-3} for $M_i = M_n$ and about 1.5% for $M_i/M_n \neq 1$. However, at $N_g = 10^{17}$ m^{-3}, the energy loss due to collisions drops down to about 1%. Hence these collisions are not sufficient to explain the observed plasma retardation.

(b) Indirect losses

After plasma-neutral gas interaction is switched on, there are two important processes by which energy of plasma stream can be lost. The first refers to energisation of electrons in the sheath at the interface and subsequently loss of this energy through ionisation processes. Secondly, there can be symmetric charge exchange collisions, for which cross section is very high, between the accelerated newly created ions and parent gas atom. Other collisions like ion-ion and ion-electron coulomb scatterings are neglected as they have small cross sections.

For calculating the energy loss by ionisation process, a value for electron energy is to be assumed. From discussions, in section 4.2, it is clear that a value of 100 eV for the electron energy is reasonable for making an estimate of

ionisation produced in neutral gas atom. The values for this process at electron energy of 100 eV are shown in Table 4-5, for plasma-neutral gas interactions corresponding to various neutral gases. Using this value the number of ionisations produced in gas cloud by plasma stream electrons is calculated using equation

$$N_i = N_p N_g \sigma_e v \tau \qquad .. (4.3)$$

where N_p is the stream density;

N_g is the neutral gas cloud density;

σ_e is the value of electron impact ionisation cross section at electron energy corresponding to 100 eV;

v is the electron velocity at 100 eV and

τ is the duration of interaction.

Once new electrons are produced during ionisation, they can quickly get energised and ionise the gas atoms. Danielsson and Brenning (1975) observed a seven-fold increase in plasma density. For our estimation, we have used the value 10 as multipliticity factor. Thus the total ionisation produced per original plasma electron is (including multiplicity factor)

$$\bar{N}_i \sim 10\, N_i \qquad .. (4.4)$$

Table 4-5

CROSS SECTION VALUES FOR ELECTRON IMPACT IONISATION COLLISIONS WITH VARIOUS GAS ATOMS (E = 100 eV)

Neutral gas	σ_e (m^2)
Hydrogen	0.68×10^{-20}
Nitrogen	2.8 "
Oxygen	0.17 "
Neon	0.77 "
Argon	3.65 "

and that on the average the energy lost by ionisation from plasma stream is

$$E_2 = \bar{N}_i E_{ion} \quad .. \quad (4.5)$$

where E_{ion} is the ionisation energy of each neutral gas atom.

Now we evaluate the energy lost by symmetric charge exchange collisions between newly produced ions and neutral gas atoms. We have assumed that all the newly formed ions are accelerated to Alfvén's critical velocity in a single step before they undergo charge exchange collisions. The resonant charge exchange reacting rates for various interactions are listed in Table 4-6. The energy loss due to resonant charge exchange is evaluated using expression

$$E_3 = \bar{N}_i N_g \left[\sigma_{chex} V_{cr} \right] E_{ion} \quad .. \quad (4.6)$$

It is found that at neutral gas density of 10^{19} m^{-3}, energy loss due to resonant charge exchange collisions occurring after the interaction has set in is about 25% of the initial plasma stream energy. At $N_g = 2 \times 10^{17}$ m^{-3}, it is less than 1%. Since the resonant charge exchange cross section is quite large, it may be argued that if newly formed ions are decelerated by resonant charge exchange with the

Table 4-6

REACTION RATES FOR SYMMETRIC CHARGE EXCHANGE PROCESS BETWEEN NEWLY PRODUCED ION AND PARENT GAS ATOMS

Neutral gas	(σV_{cr})
	$m^3 s^{-1}$
Hydrogen	2.45×10^{-14}
Nitrogen	0.57 "
Oxygen	1.02 "
Neon	0.43 "
Argon	0.22 "

neutral gas, they must be reaccelerated by the plasma in the same way as newly formed ions. Such a process would add to further braking of the plasma motion. It should be borne in mind, however, that the plasma deceleration length and correspondingly the acceleration length for the newly formed ions is much smaller than resonant charge exchange path. This will allow only a small fraction (10%) of the newly formed ions to undergo the processes of reacceleration. Hence the net effect of reacceleration is not so much to decelerate the plasma as to give a spread in the velocity component of the newly formed ions along the direction of the stream.

The average energy loss of the plasma stream taking into account all the collisions discussed above is given by

$$E = E_1 + E_2 + E_3 \qquad .. \quad (4.7)$$

Table 4-7 summarises the total energy loss for various plasma-neutral gas interactions at gas densities 10^{19} m^{-3} and 2×10^{17} m^{-3}, by all the atomic collisional processes. It seems that binary collisions can partially account for the observed plasma retardation at high gas densities and therefore may explain the difference between the observed and expected retardation scale lengths in some interactions studied in our experiment. However, the role of

Table 4-7

TOTAL ENERGY LOSS OF PLASMA STREAM BY VARIOUS DIRECT AND INDIRECT ATOMIC PROCESSES

Interaction	Percentage energy loss	
	$N_g = 10^{19}$	2×10^{17} m^{-3}
H - H	60	~3
N - N	40	~2
O - O	50	~2
Ne- Ne	45	~2
Ar - Ar	40	~2
H - Ar	50	~2
N - Ar	25	~1
O - Ar	25	~1
Ne- Ar	25	~1
Ar- H	10	~1
Ar- N	15	~1
Ar - O	15	~1
Ar- Ne	20	~1

these collisions cannot even partially explain the observed fast plasma retardation.

4.3.2 Wall losses

The boundaries present in the experimental set-up can act as sink for particles and their energy. This section discusses the effect of walls and estimates the amount of energy that can be lost to walls during plasma-neutral gas interaction.

Let us consider the motion of ions in the presence of polarisation electric field resulting from the applied transverse magnetic field. If the ions are able to reach the negative charge layer, the ions get lost, reducing the polarisation electric field. The time taken, τ_{loss}, for an ion to reach the negative charge layer is given by

$$\tau_{loss} = \left[\frac{2 M_i d}{e E_{pol}} \right]^{\frac{1}{2}} \quad .. \quad (4.8)$$

where

M_i is the mass of plasma ions

d is the distance of plasma boundary from the axis of plasma stream and

E_{pol} is the polarisation electric field value.

The value of τ_{loss} varies from 0.5 μs for hydrogen and 3.5 μs for argon. The gyrotime for hydrogen ion at B = 1 kG

is of the order of a few μs and hence the hydrogen ion makes its gyromotion and drifts along plasma stream direction rather than losing to the walls. On the other hand, for a heavy ion like argon, it may give an impression that the ions will get lost to the walls as the gyrotime for argon ion at 1 kG is 30 μs. But it must be noted that the interaction time is lesser than 5 μs for argon and hence even argon ions will not get lost to the walls appreciably.

Further, we also have experimental evidences to show that the wall losses are negligibly small to merit any serious considerations. Firstly, the plasma retardation in the interaction where plasma ion gyroradius (r_i) is greater than the diameter of the device (D), is not observed to be faster than those for which $r_i < D$. Secondly, α seems to have the same value (~ 0.5) for all symmetric interactions such as argon - argon, nitrogen - nitrogen, oxygen - oxygen, neon - neon and hydrogen - hydrogen. If the momentum losses to the walls were of any importance, for argon - argon interaction, α should have been very much different from that for hydrogen - hydrogen.

4.3.3 Deceleration by electrostatic fields

Using the space charge model of Varma (1978) described in Chapter 1, an expression for plasma deceleration length

is given (Varma, private communication) by

$$L = V_o \left[\frac{3}{2}\right]^{2/3} \left[1 + \frac{n_e m_e}{\epsilon_o B^2}\right]^{1/3} (\omega_{pn}^2 Q)^{-1/3} \quad .. (4.9)$$

where

V_o is the plasma stream velocity;

ω_{pn} is the ion plasma frequency;

Q is the ionisation rate and

$\frac{n_e m_e}{\epsilon_o B^2}$ is the term arising in the dielectric constant value due to the polarisation drift of electrons.

Table 4-8 lists the evaluated deceleration lengths for various symmetric plasma-neutral gas interactions using the above expression. Due to the reasons discussed in Section 4.2, the value Q in the above evaluations corresponds to an electron energy of 100 eV except in the case of hydrogen where it corresponds to 50 eV. A comparison between Tables 4-8 and 4-3 shows that the predicted values by Varma's model are very close to the observed decelerating lengths. However, such a fit is not observed in the case of asymmetric interactions.

Table 4-8

ESTIMATED VALUES OF DECELERATION LENGTHS BY VARMA'S MODEL FOR VARIOUS SYMMETRIC PLASMA-NEUTRAL GAS INTERACTIONS

Plasma/gas	Scale lengths (cm)			
	$N_g =$ 10^{20}	10^{19}	10^{18}	2×10^{17} m^{-3}
Hydrogen	0.45	.97	3.75	10.4
Nitrogen	0.53	1.2	4.6	12.4
Oxygen	1.4	3.1	12.2	33.0
Neon	0.9	2.0	7.9	21.5
Argon	0.7	1.5	5.9	16.2

Chapter 5

SHEATH AND CURRENT STRUCTURE

In chapters 3 and 4, we have shown that if the relative velocity between the plasma and gas is high enough, the interaction leads to a fast retardation of plasma stream until a critical velocity determined by equation (1.1) is reached. In Chapter 1, we have discussed that the formation of the sheath may be providing a causal connection between the ionisation and braking of plasma motion. In this chapter, we present the investigations on the space charge sheath structure.

5.1 The experimental set-up

The experimental set-up used is as described in Chapter 4. A schematic of the set-up showing the locations of diagnostics deployed in the interaction region is given in figure 5-1. The diagnostics for measuring space charge sheath consists of a floating Langmuir cylindrical probe of 2 mm length and 0.2 mm diameter. The long side of the probe is aligned along the magnetic field and perpendicular to the plasma streaming direction. A discussion of the use of floating Langmuir probes for the measurement of space charge potential in drifting plasma in magnetic field is given in Appendix 'B'.

The current structures are detected by a self-integrated Rogowski coil at low gas densities and by a shielded three-axis magnetic probe at high gas densities. We had to use magnetic probe at high gas densities because the dimension of closed current structure is 5 mm and its presence could not be detected by Rogowski coil with major radius of 2 cm. The current in Rogowski coil is measured inductively so as to avoid any direct electrical connection with the probes. The magnetic probe is housed in a quartz casing whose inner surface is coated with 5 micron silver and the electrical connections are taken through shielded

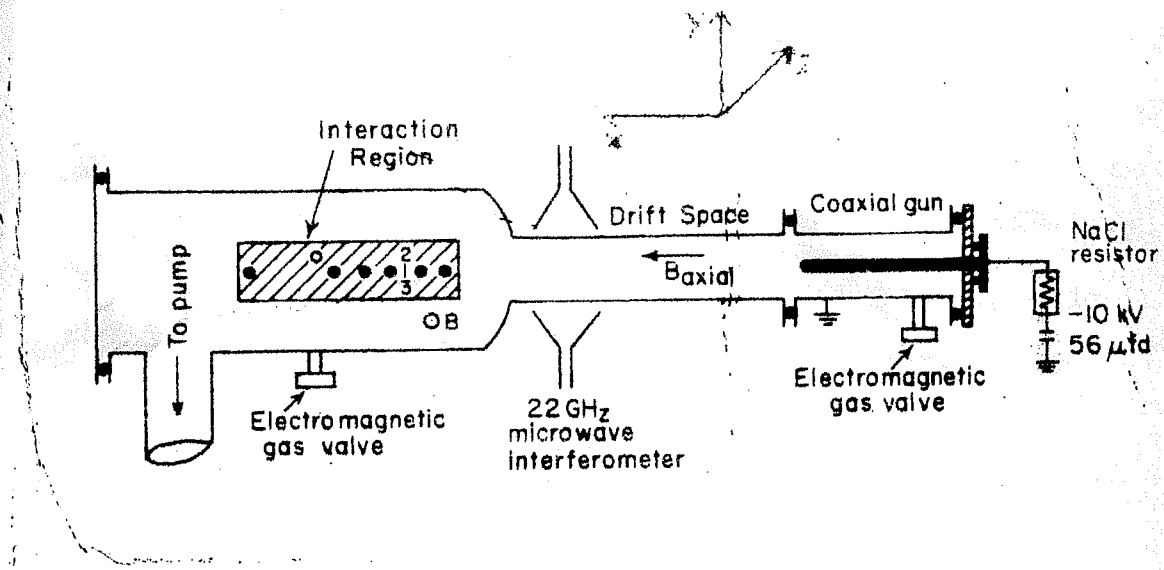


Figure 5-1. A schematic of the set-up for measuring sheath characteristics and currents. 1, 2 & 3 represent the locations of Rogowski coils. Closed circles represent the locations of floating Langmuir probes for the measurements of sheath potential and electric field. The open circle represents the position of shielded three-axis magnetic probe.

cables.

For the results reported here we have used hydrogen, nitrogen, oxygen, neon and argon for the formation of plasma streams and gas clouds. Most of the results reported here, however, are based on the studies of argon plasma - argon gas interaction. At typical operating plasma velocity of 100 km s^{-1}, the kinetic energy of plasma ion varies from 50 eV for hydrogen to 2 keV for argon. The average gas density is varied between 10^{17} m^{-3} and 10^{21} m^{-3}. The transverse magnetic field is normally maintained at 1 kG. For investigations of determining the lower limit of the magnetic field for plasma-neutral gas interaction to occur, the magnetic field is varied in the range of 0 - 1000 G.

5.2 Observations on space charge sheath

The velocity of argon plasma stream traversing the interaction region without gas cloud is measured by a V x B - probe and is shown in figure 5-2. A similar profile is obtained for the plasma density. For this stream, the peak density is $\sim$ 5 x 10^{18} m^{-3}, peak velocity is 100 km s^{-1} and the total duration of the plasma streams is $\sim$ 50 μs. For the same stream, floating potential of a Langmuir probe is measured. This is shown in figure 5-2(b). Although plasma velocity and density vary over the pulse width, the

floating potential seems to remain nearly constant and negative at about 30 V.

The effect of introducing a gas cloud in the interaction region is shown in figure 5-3. For this case, argon gas cloud of 10^{19} m^{-3} density is introduced and velocity profile of the plasma stream and floating potential of a Langmuir probe are simultaneously measured. A comparison between figure 5-2(a) and figure 5-3(a) shows that the plasma velocity has reduced as a result of interaction with the gas cloud. The floating potential of the Langmuir probe registers a positive spike of greater than 50 V followed by a negative plateau. This is shown in figure 5-3(b). The plateau after the spike is similar to that observed in case of the plasma stream traversing the interaction region without a gas cloud (as seen in figure 5-2(b)). On an expanded time scale, shown in figure 5-3(c), we see that floating potential rises to about + 145 V in about 2 μs. The potential remains steady for 1 μs and then decays to negative plateau of 30 V in about 2 μs.

5.2.1 Detection of sheath

As discussed later, the observed changes in floating potential are due to variation of the plasma potential in

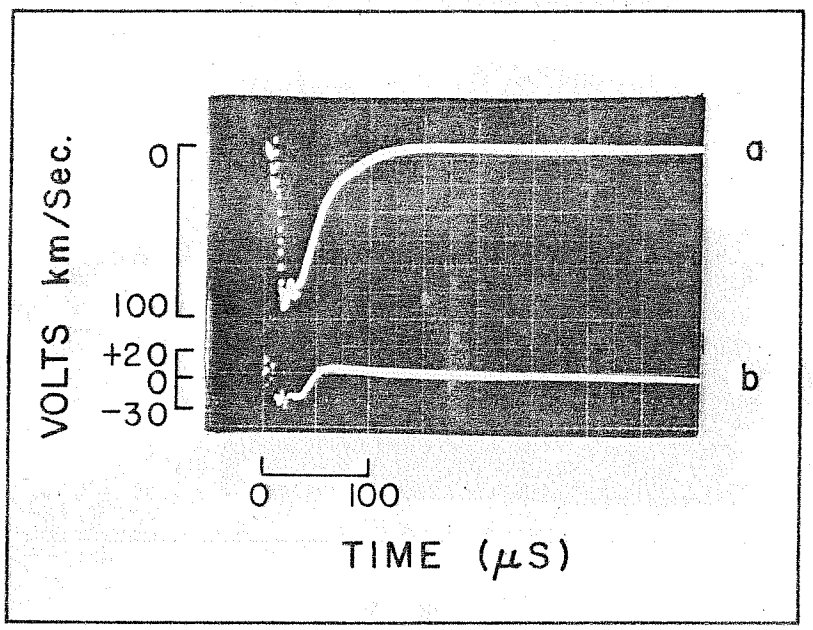


Figure 5-2. (a) Velocity and (b) floating potential profiles obtained by V x B - probe and floating Langmuir probe respectively for hydrogen plasma stream going through a back-ground neutral gas at 10^{-6} Torr.

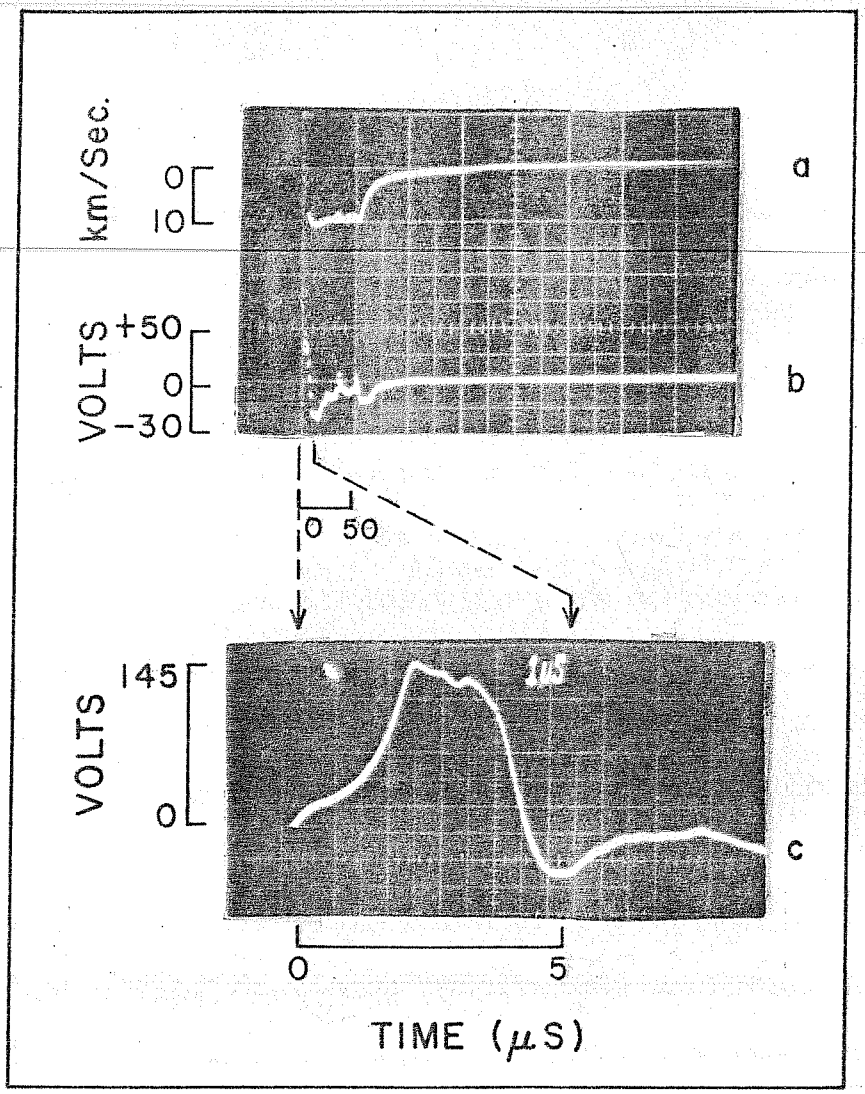


Figure 5-3. (a) Velocity and (b) potential profiles obtained by V x B - probe and floating Langmuir probe respectively for argon plasma stream going through argon gas cloud of density 10^{19} m^{-3}. The profiles are obtained at the centre of interaction region. B = 1 kG. (c) The potential profile of positive peak observed in (b) at shorter time scale.

the plasma as it traverses the floating probe. We identify the initial increase in floating potential with the presence of a sheath. That this sheath is a result of the interaction of the plasma stream with the gas cloud is further confirmed by measurements of the electric field in the streaming direction. The electric field is measured by a double probe. A differential amplifier with high common mode rejection is used to discriminate between the signal and any stray pick-up. Figure 5-4 shows that as the plasma stream penetrates a gas cloud, an electric field in the streaming direction is established. The electric field vanishes just before it reverses, at the termination of the sheath region. After the reversal, we do not observe any appreciable electric field in the stream. When the stream traverses the interaction region kept at 10^{-6} Torr, no electric field in the direction of the stream is detected. Another test for the existence of the sheath pertains to absence of the sheath when the transverse magnetic field is reduced to zero but the stream is allowed to penetrate through a gas cloud.

Although velocity of the plasma stream remains above the critical velocity for argon for about 30 μs, the sheath extent is limited to 5 μs only. This shows that thickness of the sheath is much smaller than the extent of the plasma column interacting with the gas cloud and that the sheath

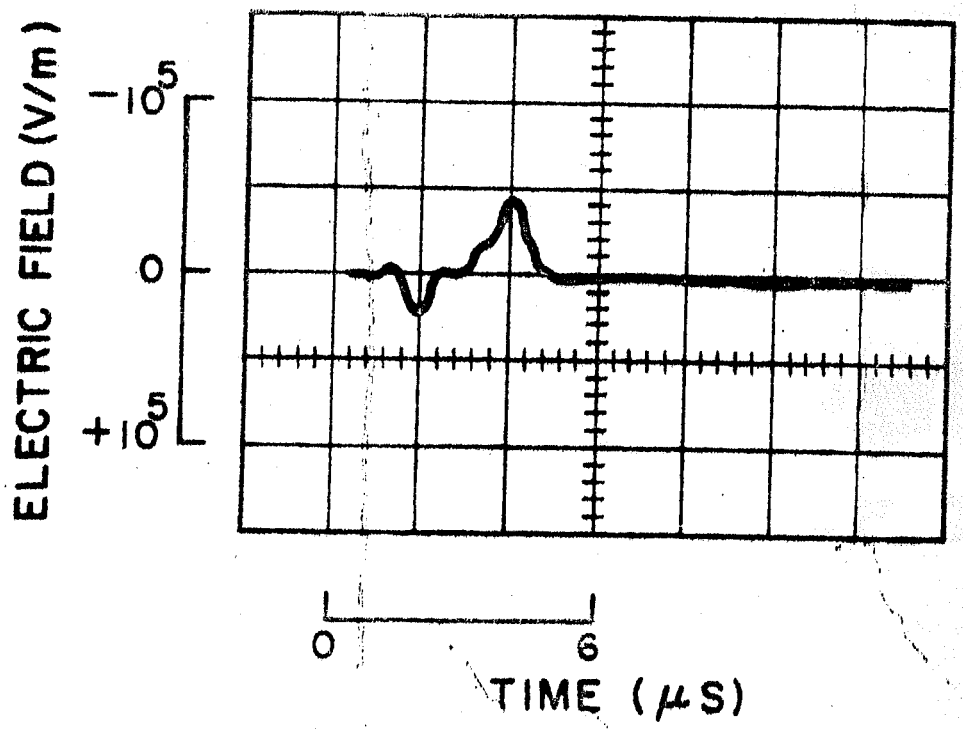


Figure 5-4. Typical sheath electric field measured by a double probe for argon plasma interacting with argon neutral gas. N_g = 10^{18} m^{-3}. Note the reversal of electric field direction.

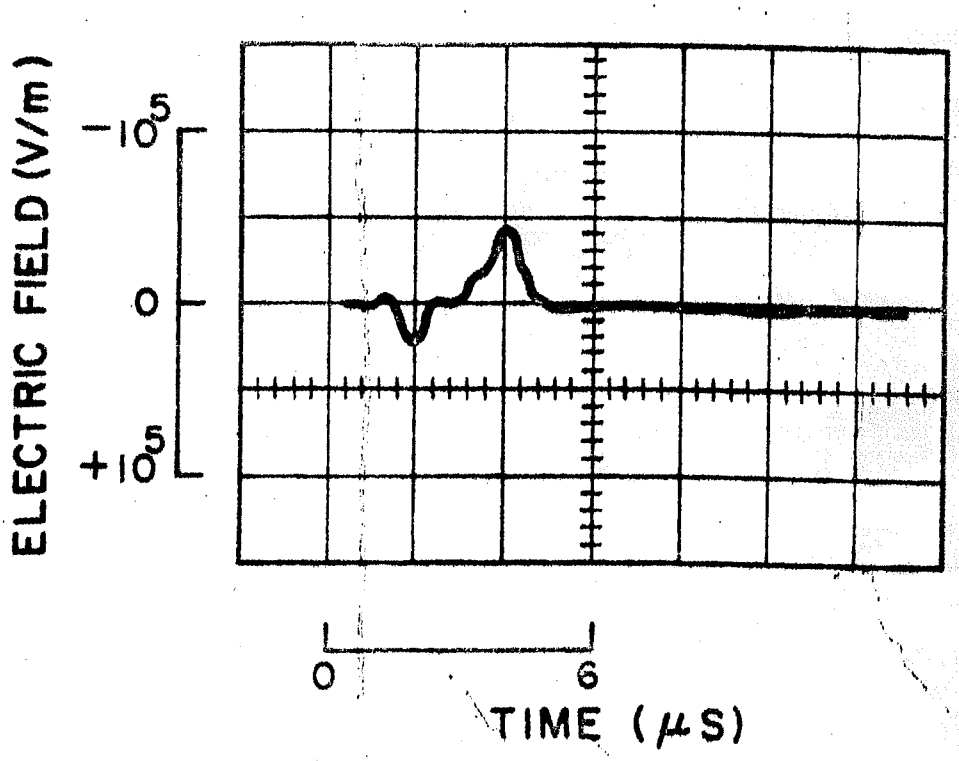


Figure 5-4. Typical sheath electric field measured by a double probe for argon plasma interacting with argon neutral gas. N_g = 10^{18} m^{-3}. Note the reversal of electric field direction.

is located at the head of the plasma stream. We calculated the sheath thickness by multiplying the observed sheath velocity by the observed duration of sheath. At $N_g = 10^{19}$ m^{-3}, the thickness of the sheath is 5 cm. This is much smaller than the length D of the plasma stream which is 150 cm. We also note that the portion of the plasma stream trailing behind the sheath region does not result in formation of a new sheath as it interacts with the gas cloud. Nor do we observe any increase in the sheath thickness or plasma potential as more and more of the plasma stream interacts with the gas cloud.

5.2.2 Sheath Velocity

The sheath region is not stationary. It moves and remains at the front of the plasma stream. This is indicated in figure 5-5. The average velocity of the sheath region is the same as the local plasma velocity in the retarding region. Its velocity decreases as the front of the plasma stream retards to Alfven's critical velocity. From measurements of different V x B - probes at different positions in the gas cloud, we note that plasma trailing behind the sheath is at a velocity greater than the sheath velocity and this situation continues to be so till the whole plasma stream is retarded to the critical velocity.

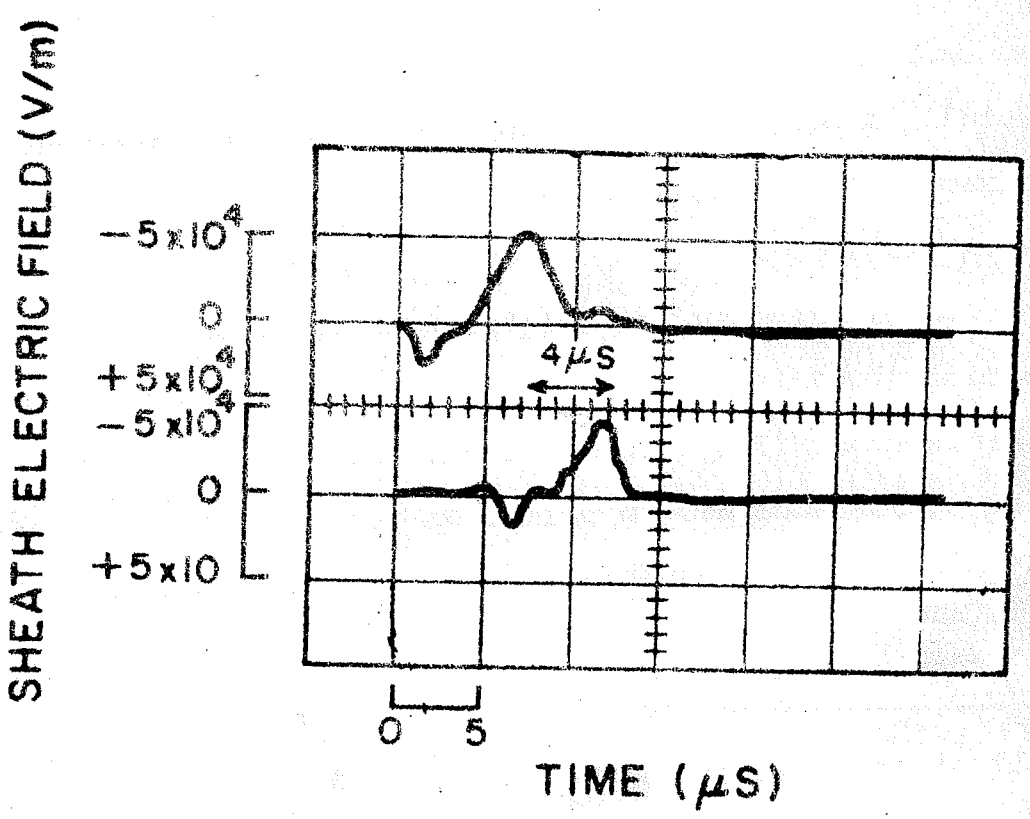


Figure 5-5. Velocity measurement of sheath. Sheath electric fields measured at two points, separated by 8 cm, in the interaction region, for argon plasma traversing through argon gas cloud of density 10^{18} m^{-3}. The average velocity corresponds to 2×10^4 m s^{-1}.

5.2.3 Sheath Potential

Simultaneous with the decrease of the sheath velocity, we note that the maximum potential of the sheath also decreases as the sheath moves at the head of plasma stream. This is shown in figure 5-6. Figure 5-7 is a plot of the maximum potential of the sheath against the velocity of the plasma stream as it retards from its initial velocity to Alfven's critical velocity. It may be noted that although initial kinetic energy of argon ion is about 2 keV, the maximum sheath potential at the beginning of the interaction is not more than 150 V but is certainly far more than the ionisation potential of argon. At the beginning of the interaction, the shot-to-shot variation in the maximum sheath potential is considerable as indicated by the vertical bars in figure 5-6. As the plasma stream retards to slightly greater than Alfvén's critical velocity, the potential falls to about 20 V. At Alfvén's critical velocity, the sheath potential falls either to a low value of 10 - 15 V or vanishes altogether after the stream passes through the gas cloud.

Effect of initial plasma stream energy on the formation of the sheath was further studied by varying the composition of the plasma stream. The plasma streams were

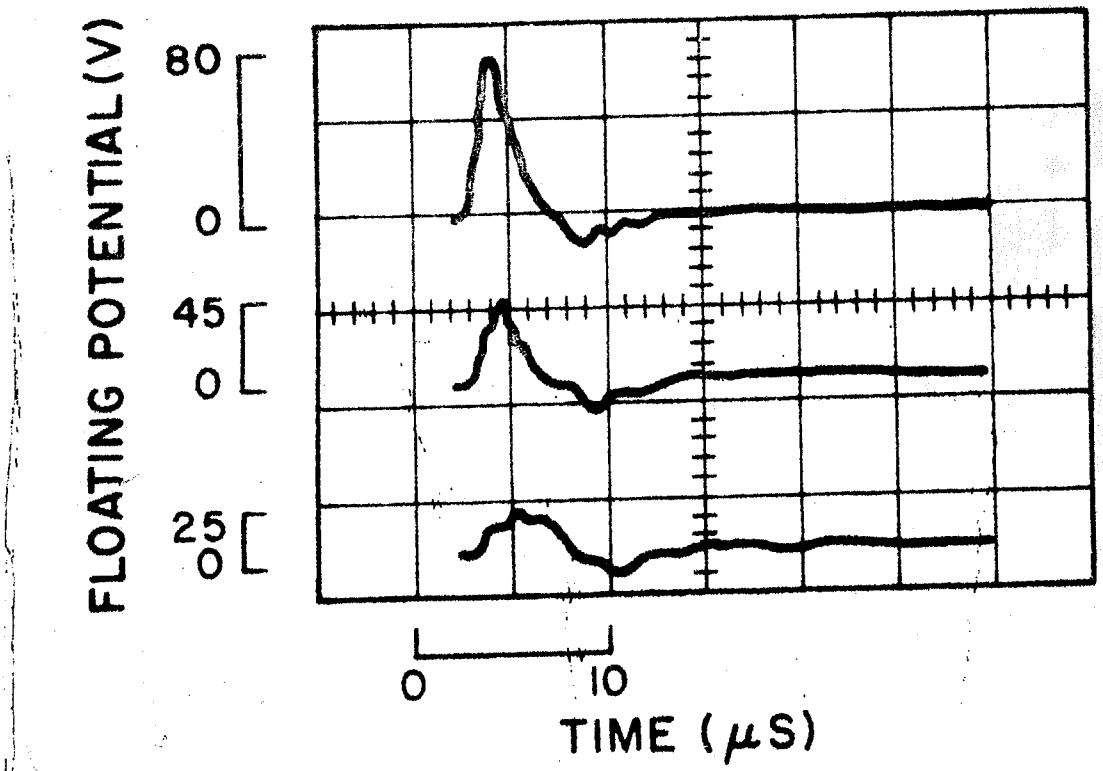


Figure 5-6. Potential profiles measured by three floating Langmuir probes placed at 3 axial points kept separated by 2 cm in the interaction region. Argon plasma retards in argon gas cloud of 10^{19} m-3. Note the decrease in plasma potential with distance.

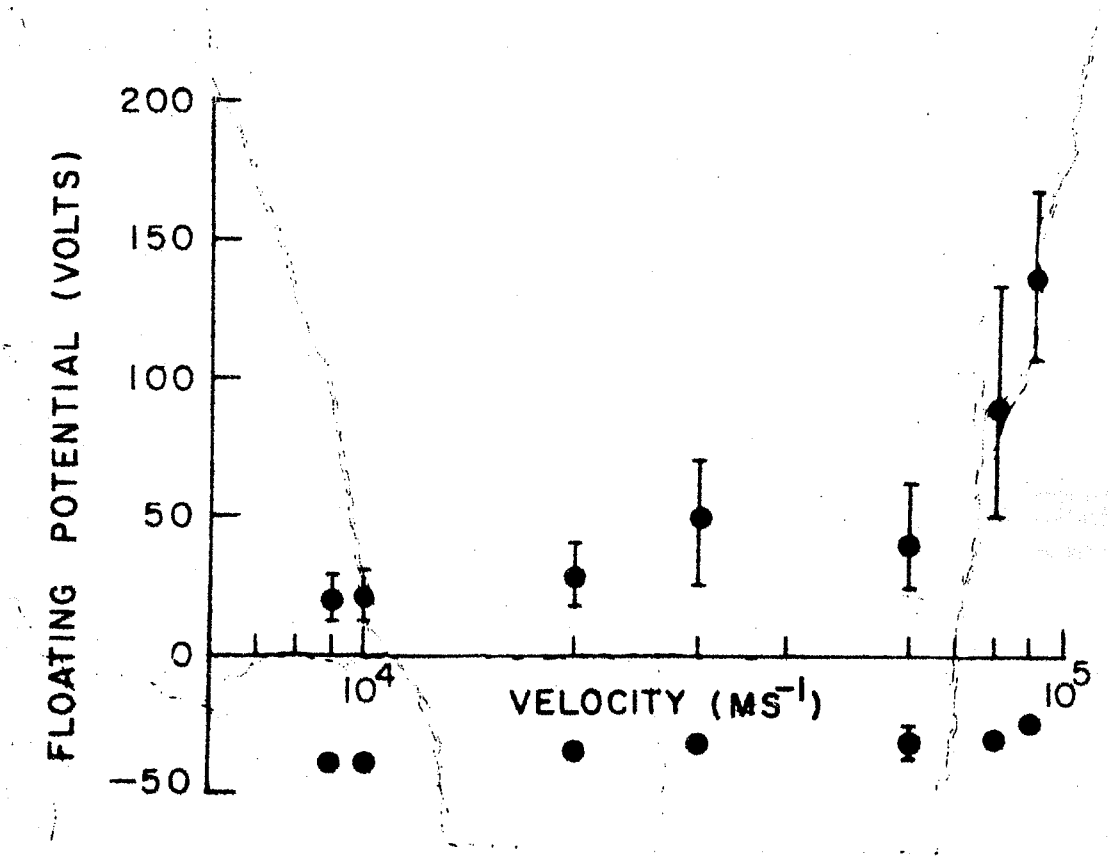


Figure 5-7. Peak positive and negative values of floating potential at a fixed point in the interaction region plotted against the initial velocity of argon plasma stream penetrating argon gas cloud.

made out of hydrogen, argon, neon and nitrogen so that initial kinetic energy of the plasma ion could be varied over a broad spectrum of 50 eV to 2 keV. In case of hydrogen, which has very low initial kinetic energy of 50 eV, the maximum sheath potential is about 50 V. On the other hand, for nitrogen, oxygen, neon and argon, the maximum sheath potential varied between 100 and 200 V. Limited by the performance of the plasma gun, we could not investigate whether sheath potential rises to 100 V or more if the initial kinetic energy of hydrogen ion were increased to about 1 keV. The conclusion of these studies seems to be that maximum sheath potential ranges between 50 - 200 V and that the variation is neither related to the initial kinetic energy of plasma ion nor to the ionisation potential of the gas atom.

The radial structure of the sheath region was investigated by deploying three floating Langmuir probes at three radial positions with a maximum separation of 5 cm between the probes. We found that there is very little variation of either maximum sheath potential or general structure of the sheath region with radius. This indicates that constant sheath potential contours lie in a plane perpendicular to the streaming direction and that there is no radial electric field established in the sheath region.

5.2.4 Effect of gas density

Figure 5-8 displays the effect of varying gas density on the formation of space charge sheath in argon-argon interaction. Similar trends were observed for other interactions. It is seen that the sheath thickness increases as the gas density is reduced. It is about 11 cm at $N_g = 10^{17}$ m^{-3} and 5 cm at $N_g = 10^{19}$ m^{-3} in case of argon-argon interaction. The sheath thickness varies as $N_g^{1/3}$ as expected from equation (1.7). While the sheath thickness varies with the gas density, the maximum sheath potential remains constant. The resulting decrease in electric field with the gas density is thus solely due to increase in the thickness of the sheath region. The average values of electric fields at different gas densities are summarised in Table 5.1 for argon plasma-argon gas and hydrogen plasma-argon gas interactions. We note that the value of electric field ranges between 10^4 - 10^5 V/m. The variation of electric field with the gas density is as predicted by equation (1.8) in the interactions mentioned in Table 4-1 and other interactions studied in our experiment.

5.2.5 Role of atomic processes

The role of atomic processes in the formation of the sheath region is displayed in Table 5-2. The table

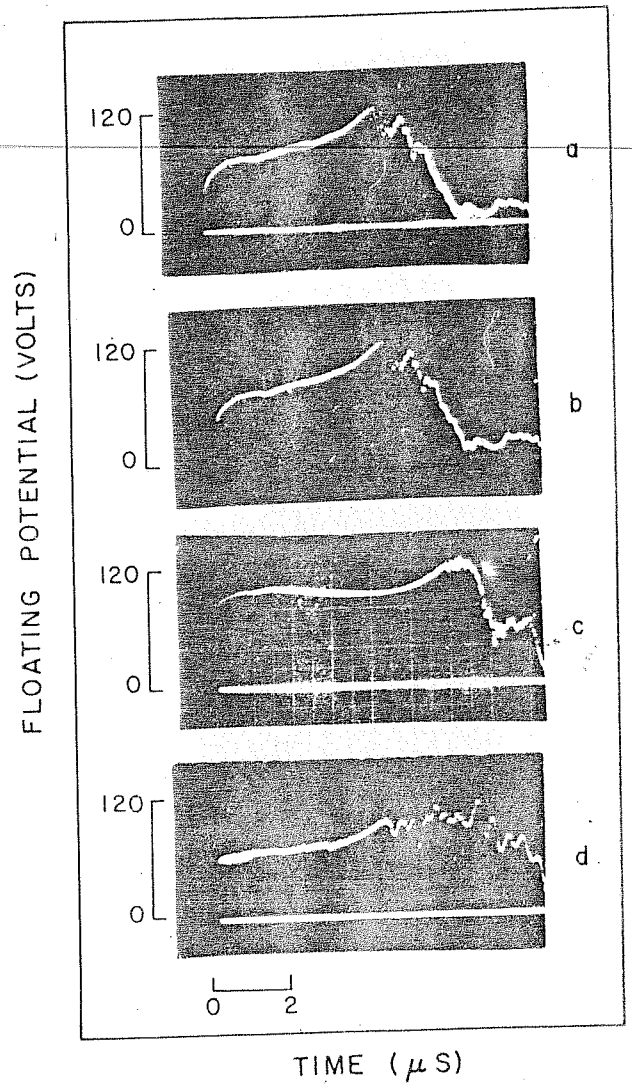


Figure 5-8. Potential profiles measured by floating Langmuir probe for argon plasma stream penetrating argon gas cloud at various densities (a) 10^{19} m^{-3}; (b) 6×10^{18} m^{-3}; (c) 10^{18} m^{-3} and (d) 2×10^{17} m^{-3}.

Table 5-1

OBSERVED SHEATH ELECTRIC FIELDS AT VARIOUS GAS CLOUD DENSITIES FOR (i) HYDROGEN - ARGON & (ii) ARGON - ARGON INTERACTIONS. E_l AND E_t ARE THE AVERAGE ELECTRIC FIELDS AT THE LEADING AND TRAILING EDGES OF SHEATH.

Density	E_l		E_t	
	H-Ar	Ar-Ar	H-Ar	Ar-Ar
m^{-3}	V/m	V/m	V/m	V/m
10^{19}	3.3×10^3	8.25×10^3	5.0×10^3	10.0×10^3
5×10^{18}	2.5 "	6.0 "	2.0 "	7.0 "
10^{18}	1.6 "	4.0 "	1.2 "	3.0 "
10^{17}	0.8 "	2.0 "	1.0 "	1.0 "

displays the observed electric field in the sheath region for symmetric ($M_i = M_n$) and asymmetric ($M_i \neq M_n$) interactions separately. The charge exchange cross section in symmetric interactions is atleast two orders of magnitude more than the same for asymmetric interactions. Table 5-2 shows that this is not reflected in the value of the electric field in the sheath region. Also tabulated is the cross section of electron impact ionisation collisions at electron temperature of 5 eV. In asymmetric interactions, ionisation collisions seem to have a more dominating role than charge exchange collisions in the formation of the sheath. This may be the reason as to why there is a lack of correlation between charge exchange cross section and sheath characteristics. Another reason for lack of correlation may be the overwhelming dominance of symmetric charge exchange collisions between accelerated secondary ions and the gas atoms in case of asymmetric interactions. For these charge exchange collisions to play a role, the requirement is that, acceleration time of the secondary ions be of the order of sheath formation time.

Perhaps more appropriate would be to seek a correlation between charge exchange cross section and the formation time of the sheath region. Even though a floating

Table 5-2

CHARGE TRANSFER AND ELECTRON IMPACT IONISATION REACTION RATES COMPARED WITH THE OBSERVED RISE TIME AND ELECTRIC FIELDS OF SHEATH

Interaction	$\langle \sigma v \rangle^{*}_{chex}$	$\langle \sigma v \rangle^{**}_{elec\ imp}$	Rise time $\left[\frac{E_l + E_t}{2}\right]^{***}$
	$m^3\ s^{-1}$	$m^3\ s^{-1}$	μs	V/m
H - Ar	0.2×10^{-15}	5.0×10^{-16}	1.5	4.0×10^3
Ar- H	0.74 "	3.0 "	2.5	3.0 "
H - H	3.1×10^{-14}	3.0×10^{-16}	1.6	4.1×10^3
N - N	0.82 "	2.0 "	1.8	5.0 "
O - O	4.0 "	2.0 "	1.4	6.8 "
Ar-Ar	0.75 "	5.0 "	1.2	6.75 "

* evaluated as an average over the velocity range from initial plasma velocity to Alfven's critical velocity

** evaluated assuming 5 eV maxwellian temperature for plasma stream electrons.

*** E_l & E_t are the average electric fields at the leading and trailing edges of sheath respectively.

probe is placed very close to where the plasma stream just impacts the gas cloud, we were not able to trace out the evolutionary phase of the sheath region because of difficulty in exactly locating the beginning of sheath formation. Apparently, sheath formation takes place within less than 1 μs, after the plasma stream starts penetrating the gas cloud. If the sheath formation time is taken to be the same as the observed rise time, we do not find any correlation of this parameter with the charge exchange cross section. This is indicated in Table 5-2, where rise times for various plasma-neutral gas interactions are listed for the gas density 10^{19} m^{-3}. Note that the rise times are obtained from observations such as displayed in figure 5-3(c) and is defined as the time required for the floating potential to rise to the maximum positive value as the sheath region passes through the floating Langmuir probe. The lack of correlation may be due to the fact that the defined rise time may have no relationship with the sheath formation time. Thus the role of atomic processes in the formation of sheath is not clearly brought out by our studies.

5.3 Interaction at low magnetic fields

In order to understand what role magnetic field plays on the formation of sheath, the interaction was

studied without this field and with varying field. Without the magnetic field, the velocity was monitored by time-of-flight method and we found that there was no sheath formed and there was no plasma retardation. However, as the magnetic field was increased, we began to observe the formation of sheath and retardation of the plasma velocity only when magnetic field was more than 50 G. Also, results at such low magnetic fields were irreproducible. The reproducibility was observed only when the magnetic field was about 300 G or more. These results can be treated as an evidence for the necessity of transverse magnetic field for the formation of the sheath and Alfvén's critical velocity phenomenon to occur. As discussed later, the lower limit on the magnetic field may be arising due to the conditions on modified two-stream instability for giving rise to electron heating parallel to the magnetic field.

5.4 Currents in sheath

In order to verify whether the sheath carries any current, magnetic probes and a Rogowski coil were placed in the interaction region. Firstly measurements were carried out without plasma stream interacting with a gas cloud. This observation was made to check whether there is any

current flow from the central electrode of the gun through plasma stream to the grounded end section of the device. We had expected such a current flow to the ground as plasma pulse width (50 μs) happens to be larger than the transit time (10 μs) of the stream through the drift tube. From various checks we made, the conclusion is that such a current flow, if present, is less than 15 A, which is the limit of sensitivity of magnetic and Rogowski coil probes.

During the interaction the change in the magnetic field as seen a three-axis magnetic probe is shown in figure 5-9, for the case of a 100 km s^{-1} argon stream penetrating through argon gas cloud of 10^{19} m^{-3} density. A change in the magnetic field, $\Delta B \sim 10$ G, is observed. Further, the current flow seems to be in a single closed loop. This fact is revealed by the two reversal in the observed magnetic field and is confirmed by the observations made with a Rogowski coil.

To obtain the direction and magnitude of currents we utilised the data obtained by Rogowski coil. Typical current profile is shown in figure 5-10. A passage of single current loop is indicated by one reversal in the signal output of the Rogowski coil. From various interactions studied on our experiment, the following characteristics of the current structures may be noted:

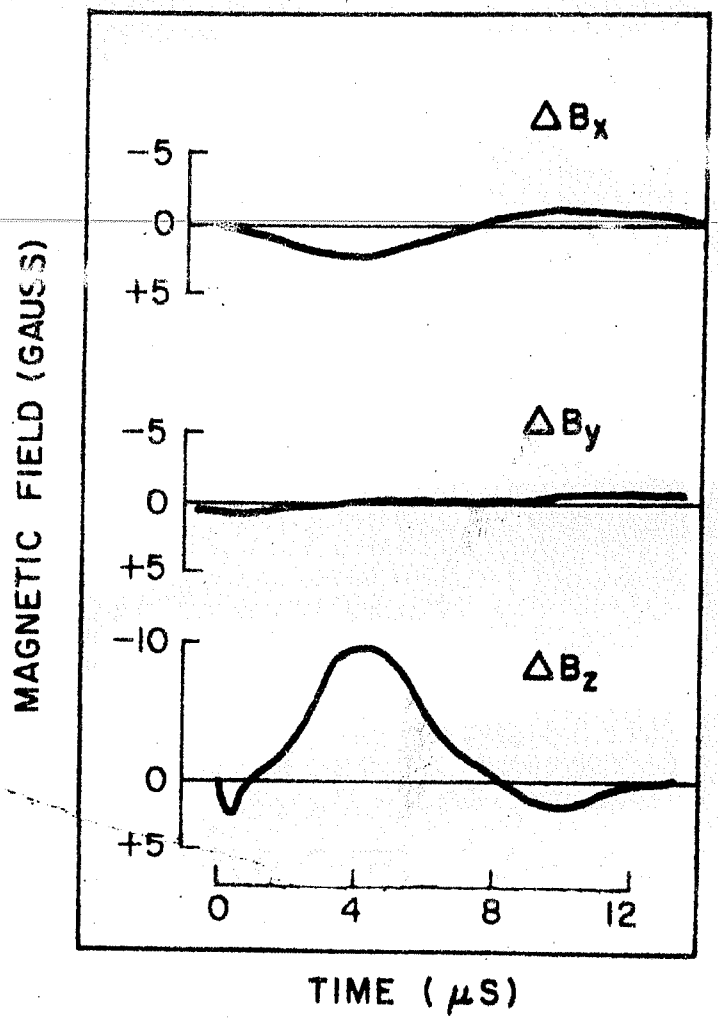


Figure 5-9. Traces of graphically integrated outputs of three-axis magnetic probe. The obtained traces correspond to argon-argon interaction at 10^{19} m^{-3} gas density; B = 1 kG.

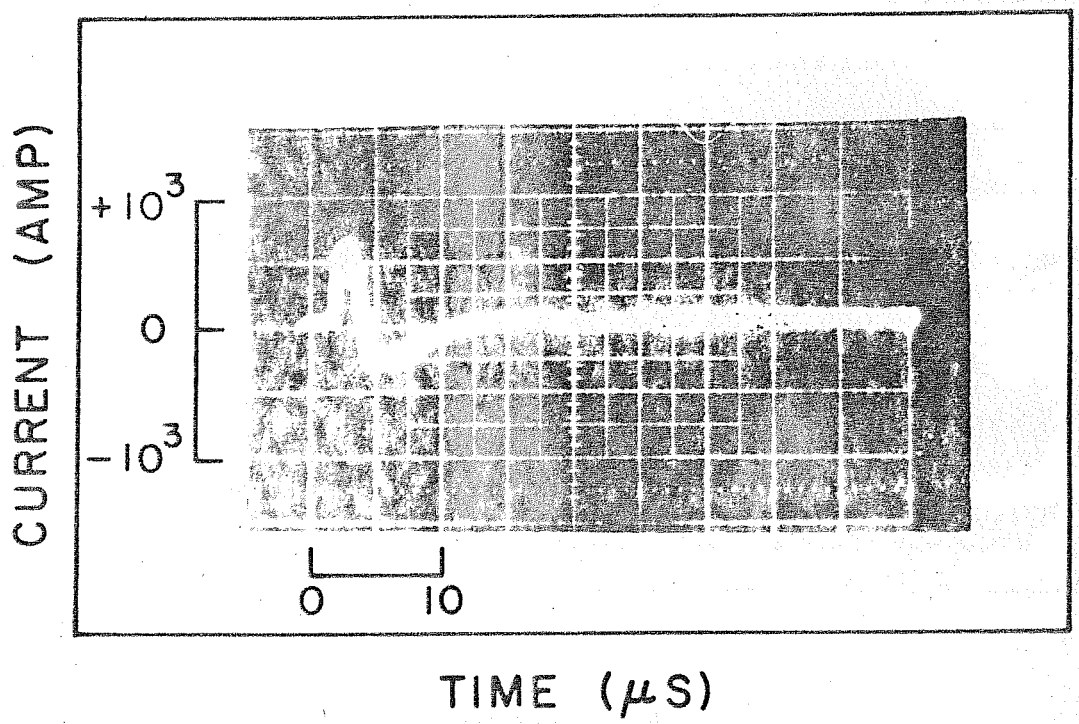


Figure 5-10. Current profile measured by a self-integrating Rogowski coil placed at the centre of interaction region for argon-argon interaction at 2×10^{17} m^{-3}.

(i) the total current flow is $\sim$ 170 A giving rise to current density of 10^5 A/m^2 for $N_g \sim 10^{19}$ m^{-3}. At higher gas densities we have not been successful in measuring currents in the interaction region. (ii) The orientation and direction of the current structure is diamagnetic. (iii) The current density decreases marginally by a factor of 2 when the gas density is decreased by 3 orders of magnitude. (iv) the extent of the current structure is confined and limited to the sheath region. (v) the direction of current flow at the front and rear portions of of the sheath region corresponds to the secondary electronic drift derived from sheath potential. (vi) the current loop closes at the boundary of the plasma column and not through the body of the plasma. This result is summarised in table 5-3 which displays the results of Rogowski coil placed at different positions in the interaction region. (vii) The magnitude and topology of the current loop does not seem to depend on, whether interaction is symmetric or asymmetric. This is indicated in Table 5-4.

5.5 Discussion

5.5.1 Formation and characteristics of sheath structure

The plasma-neutral gas interaction leads to formation of a space charge sheath. The existence of the space charge

Table 5-3

MAGNITUDE OF CURRENT DENSITIES FOR ARGON – ARGON INTERACTION. I_l & I_t CORRESPOND TO THE CURRENT DENSITIES AT THE LEADING AND TRAILING EDGES RESPECTIVELY.

Position of Rogowski coil*	Component	I_l	I_t
		A/m^2	A/m^2
1	x	$\lesssim 10^4$	$\lesssim 10^4$
	y	$\sim 10^5$	$\sim 10^5$
	z	$\lesssim 10^4$	$\lesssim 10^4$
2	x	$\sim 10^5$	
	y	$\lesssim 10^4$	
	z	$\lesssim 10^4$	
3	x	$\sim 10^5$	
	y	$\lesssim 10^4$	
	z	$\lesssim 10^4$	

* Positions 1, 2 and 3 of Rogowski coils and x, y and z coordinates are indicated in figure 5-1. At positions 2 and 3, the current is almost unidirectional.

Table 5-4

OBSERVED CURRENT DENSITIES ($I_{l,y}$ & $I_{t,y}$) MEASURED AT POSITION 1 FOR VARIOUS PLASMA-NEUTRAL GAS INTERACTIONS. ($N_g = 2 \times 10^{17}$ m^{-3}; B = 750 G).

Plasma-gas	$I_{l,y}$	$I_{t,y}$
	A/m^2	A/m^2
H - Ar	4×10^4	3×10^4
H - H	3×10^4	6×10^4
Ar- Ar	10^5	5×10^4

sheath is established from the observations of potential variation in the floating Langmuir probe when a plasma stream penetrates through a gas cloud. An alternative interpretation can be that the measured variation in floating potential is due to a variation in the electron temperature. Such a variation in the electron temperature may arise from the plasma-neutral gas interaction and resulting heating of electrons as has been experimentally demonstrated by Danielsson and Brenning (1975). However, the hotter electrons would make floating potential more negative, as the difference between the plasma and floating potentials is related to temperature. This is contrary to our observations which reveal that the potential variation is characterised by a sharp positive potential pulse followed by a negative plateau.

A floating probe can assume a positive value if the ion flux exceeds electron thermal flux. At electron temperature ranging between 5 - 100 eV, the ion energy has to range between 10 - 200 keV for ion flux to exceed electron flux. Maximum ion energy in our experiments is 2 keV and this energy is too small to have caused probe to assume a positive floating potential. An experimental evidence against this possibility is the observation of lack of

correlation between the positive potential and the ion energy. Further, the probe does not assume a positive value throughout the duration of the plasma stream. These observations also rule out positive floating potential resulting from the emission of secondary electrons by bombardment of energetic ions and x-rays emitted from heated electrons. The effect of magnetic field on the probe potential is taken care of by aligning the long side of the probe along the direction of the magnetic field so as to allow unrestrained access of electrons to the probe.

The characteristics of the sheath are: (i) The maximum sheath potential is 50 - 200 V. The value of the potential does not depend upon the initial plasma ion kinetic energy so long as the plasma drift velocity is well above the Alfvén's critical velocity. (ii) The electric field in the sheath is along the direction of the stream at the beginning of the sheath region and opposite to it at the termination of the sheath. There is no electric field along the direction of the magnetic field. (iii) The sheath thickness is much smaller than the length of the plasma stream and the sheath is always located at the head of the stream. (iv) While velocity of the sheath quickly reduces to the Alfvén's critical velocity, the plasma trailing behind it remains at higher velocity until the

whole plasma column is retarded to the critical velocity.

(v) The sheaths are accompanied by a singl current loop. The direction of the current is the same as the secondary electronic drift that can result from the sheath electric field and transverse magnetic field.

We now compare the characteristics of the sheath with predictions of various theories on the formation of a space charge sheath. According to Varma's model, some slow ions are implanted in the plasma due to their production by initial charge exchange and electron impact collisions. Over the time scale greater than the electron gyroperiod but much less than the ion gyroperiod, these slow ions accumulate to develop into a positive charge sheath while electrons quickly acquire E x B - drift velocity due to the presence of polarisation electric field. The sheath thus consists of a negative charge layer followed by a positive charge layer. The sheath is stationary over the time scale less than the ion gyroperiod. Additionally, the sheath has a component along the magnetic field. This electric field is large enough to give rise to electron energisation to about 100 eV. The observed sheath cahracteristics do not correspond to this model specifically because we neither see double charge sheaths nor any radial electric field. Furthermore, the sheath moves with a velocity of V_{cr} or more right from the

beginning of the interaction contrary to the prediction of the model. We have no direct evidence to suggest that initial formation of the sheath may be according to this model and that physical processes such as the ionisation of the gas cloud by hot electrons modify the sheath structure at a later stage of the interaction.

Another model is given by Lehnert. He has considered a steady-state potential structure resulting from inhomogeneities in non-thermal ions (Lehnert, 1967). Due to different densities more ions from the high density region spend part of their orbit in the low density region than vice versa. Therefore, a positive net charge should be built up in the low density region, and the electric field vector should point towards higher density. In our situation, the very few charge exchange and other ionisation collisions at the initial stage of the interaction may lead to the source of secondary ions. These secondary ions will form a group of non-thermal ions in the frame of reference in which polarisation electric field vanishes. The non-uniformity may be imposed either due to non-uniformity in the density of the gas cloud or by the very fact that, over the time scale of the sheath formation, the collisions take place in a localised region.

Lehnert's model also does not seem to be applicable

to our situation. First, whereas this model predicts an oscillating potential structure with monoatomic increase of the average potential over an ion gyroperiod, we observe only a positive charge sheath located at the head of the stream. Secondly, the sheath thickness is much less than the gyroradius of secondary ions. Finally the maximum potential of the sheath is much less than the initial kinetic energy of the ion even at the beginning of the interaction whereas in Lehnert's model the potential step amounts to 80% of the ion kinetic energy.

Piel et al. (1978) consider the formation of a sheath by Lehnert's mechanism but include the effects of destruction of gyro-orbits of the secondary ions by collisions and turbulent friction. They have not advanced any detailed theory for the formation of sheath but have given a descriptive model explaining their sheath observations. Their model differs from Lehnert's model (Lehnert, 1967) only in the direction of the electric field in the sheath region; the high density side is at high potential. The model is shown in figure 5-11(a). Our sheath observations cannot be described by this model because of observation of a reversal of the electric field at the termination of the sheath region.

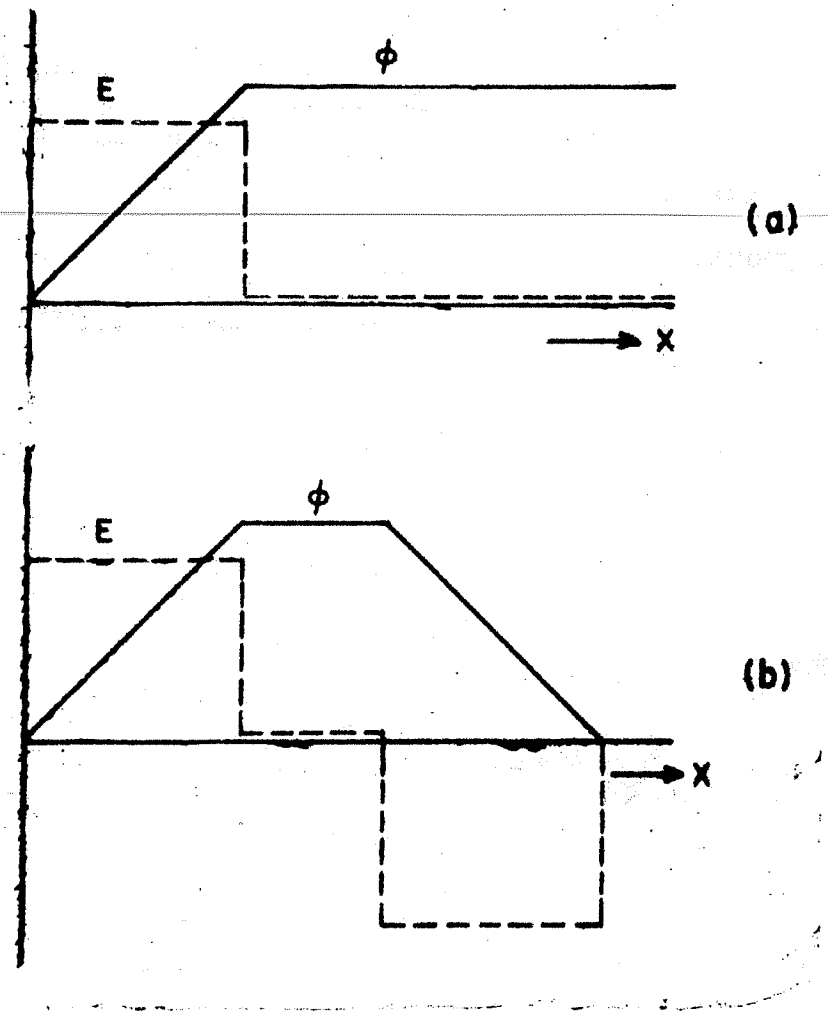


Figure 5-11. (a) Sheath model of Piel et al. (1980). (b) Our model.

Therefore, the sheath problem in direct collision experiments has to be considered in the light of our observations. A schematic of our sheath observations is displayed in figure 5-11(b). Initially the sheath may be formed according to description of Varma's or Lehnert's model. But soon after the interaction is initiated, the electrons gain enough energy to ionise the gas cloud. A copious amount of non-thermal ions are produced and in turn alter the potential structure in the sheath region. In order to charge the sheath region to a net positive charge, a mechanism of rapid loss of electrons has to be initiated. Figure 5-11(b) also shows that in the frame of reference of the sheath both the neutral gas and plasma trailing behind the sheath are approaching sheath region. This means that in the case of interaction of any extended plasma stream, the interaction is always carried out at the front of the plasma stream, i.e. in the region where the sheath is located. We wish to emphasize that this aspect of the interaction in case of extended streams is absent in the interactions where plasma stream pulse width is of the order of interaction time. The theoretical analysis of the schematic model prescribed here would need consideration of all the physical processes like initiation of the sheath, heating of electrons, ionisation of gas cloud and modifications of the

initially formed sheath region by the production and losses of newly generated electrons and ions in the sheath region.

5.5.2 Role of sheath in excitation of modified two-stream Instability

As noted earlier, the sheath electric field ranges between 10^3 - 10^4 V/m and does not depend upon the initial kinetic energy of the plasma ion. This field can give rise to secondary drift of electrons in the presence of transverse magnetic field. At magnetic field of 1 kG, the electrons, acquire a drift velocity ranging between 10^4 - 10^5 m s^{-1}. From the currents detected in the sheath region, the drift velocity of electrons is 10^5 m s^{-1}, if it is assumed that all the plasma electrons carry the current. The drift velocity can be lower in the case of the interactions at gas density 10^{18} m^{-3} if the newly generated electrons also take part in setting up the current loop in the sheath region. It seems that there is a good agreement between the drift velocity calculated from the sheath field and the same calculated from the measured current density.

At electron temperature of 5 eV, the ion sound speed varies from 2 x 10^3 m s^{-1} for hydrogen plasma to 3 x 10^2 m s^{-1} for argon plasma. Noting that the electron drift velocity is perpendicular to the magnetic field, the threshold conditions for excitation of modified two-stream instability

are satisfied. It is thus very likely that the electrons are getting heated during the interaction by modified two-stream instability or by its limiting variants in the presence of weak inhomogeneities. It is known that for this instability the electrons behave as if they had an effective mass much larger than their actual mass. This effective mass can in fact be comparable to the ion mass for the fastest growing mode (Buneman, 1962; Krall and Liewer, 1971; Ott et al., 1978; McBride et al., 1972; Raadu, 1975; 1977; 1978). This results in an efficient transfer of initial drift energy to the electrons. It can be easily shown that, at relative drift velocity of $10^4 - 10^5$ m s^{-1}, the electrons can be heated up to 40 eV in case of hydrogen plasma and upto 200 eV in case of argon plasma. At these electron thermal energies, the cross section for electron impact ionisation is maximum. Thus, the formation of the sheath seems to be controlled by the processes of rapid ionisation of the gas cloud. It appears that the sheath electric field builds up just enough to give rise to efficient ionisation of the gas.

Another evidence for modified two-stream instability relates to the observation of lower limit on the magnetic field for Alfvén's critical velocity phenomenon to occur. We have shown that for the occurrence of Alfvén's critical

velocity phenomenon in our device, a minimum magnetic field of about 50 G is required and that results become reproducible only for fields greater than 300 G. This observation has an interesting connection with the modified two-stream instability. Raadu (1975) has shown that if $f_{pe} < f_{ce}$, where f_{pe} and f_{ce} are the electron plasma frequency and electron cyclotron frequency respectively, the electrons are energised mainly parallel to the magnetic field by the modified two-stream instability. This situation is realised in our device at magnetic fields greater than 50 G. Under the condition $f_{ce} < f_{pe}$, i.e., for magnetic fields less than 50 G or so, electron heating parallel to the field by modified two-stream instability is not expected. The non-occurrence of the critical velocity phenomenon at fields less than 50 G, thus may be related to the fact that unless parallel electron heating takes place, the interaction is prevented from occurring.

5.5.3 Role of currents in plasma retardation

In an earlier paper, we reported that plasma retardation at low gas densities cannot be explained by collisional processes (Venkataramani and Mattoo, 1980b). It was concluded that a far more efficient momentum loss mechanism is needed to explain the observed fast retardation. One

may think that momentum is transferred from the plasma to the ionised component of the gas via interactions with the magnetic field. The observed current structure may give rise to a j x B - force on the plasma while an essentially equal and opposite force on the ionised gas (Danielsson, 1970). Table 5-5 gives the required current density to retard the argon plasma stream at various argon gas densities in the observed retardation lengths (Venkataramani and Mattoo, 1980b). These values are compared with the experimentally measured current densities in the sheath region. We note a fairly good agreement at $N_g \sim 10^{17}$ m^{-3}.

From our earlier studies (Venkataramani and Mattoo, 1980b), we had concluded that there is a need for invoking a momentum loss mechanism other than binary collisions (see sections 4.3.1 and 4.3.2) for gas densities less than 10^{19} m^{-3}. The present investigations show that while j x B - force can account for plasma retardation at $N_g \sim 10^{17}$ m^{-3}, a combination of retardation forces due to currents and binary collisions is needed to explain the plasma retardation in the interactions at gas density ranging between 10^{18} - 10^{19} m^{-3}.

Table 5-5

ROLE OF CURRENT IN PLASMA RETARDATION: COMPARISON OF OBSERVED CURRENT DENSITIES WITH THE ESTIMATED VALUES FOR ARGON-ARGON INTERACTION.

Gas density	Retardation scale length	Observed current density	Estimated * current density
m^{-3}	cm	A/m^2	A/m^2
10^{19}	4	3×10^5	2×10^6
10^{18}	7	2×10^5	1.1×10^6
10^{17}	35	10^5	2.6×10^5

* obtained by calculating the j x B - force acting on the plasma to retard it in the observed deceleration lengths.

Chapter 6

CONCLUSION

In this thesis, studies on the interaction between a moving magnetised plasma and a stationary neutral gas cloud have been presented for a wide range of plasma and neutral gas cloud parameters. Experimental observations on the mechanisms for the occurrence of Alfvén's critical velocity phenomenon, its cause and effects, have been reported and discussed. The conclusions drawn from the results of our experiments and a model for plasma-neutral gas interaction are presented below.

6.1 Summary of the experimental results

(i) Though the kinetic energy is contained in the

plasma stream ion, the threshold condition on the relative velocity for the plasma-neutral gas interaction to get initiated does not depend on the mass of plasma stream ion. On the other hand, experiments have confirmed the definition in terms of the mass of neutral gas atom (vide equation 1.1). In other words, it was found that in certain cases the plasma-neutral gas interaction occurred even when the initial kinetic energy of a plasma stream ion is less than the ionisation energy of a neutral gas atom. This means that, during plasma-neutral gas interaction, an electron, on the average, acquires more than the kinetic energy of a single plasma stream ion. (ii) The Alfvén's critical velocity phenomenon is observed over a wide range of neutral gas densities ranging from 10^{17} - 10^{21} m^{-3} and it is found that only the integrated value of gas density is important and not the absolute value of it for decelerating the plasma stream to Alfvén's critical velocity. (iii) The detailed study of plasma retardation for various plasma streams and neutral gas clouds formed out of hydrogen, nitrogen, oxygen, neon and argon have shown that the classical collisional processes play only a partial role in the plasma retardation. The plasma retardation scale length is found to vary as $N_g^{-\alpha}$, where α varies from 0.15 for non-symmetric to 0.5 for symmetric

plasma-neutral gas interaction. The experiments do not show the variation of scale length over mass ratio in the range of 0.025 to 40. (iv) The cause and role of a space charge sheath that gets formed whenever the plasma stream penetrates the neutral gas cloud have been discussed. The observations on sheath indicate that it can lead to a secondary drift which can excite modified two-stream instability and consequently to strong electron heating and rapid ionisation of gas cloud. (v) The sheath is always accompanied by a single closed current loop with current density $\sim 10^5$ A/m^2. The observed currents are found sufficient to account for plasma retardation at the gas density of 10^{17} m^{-3}. However, at high gas densities ($N_g \sim 10^{19}$ m^{-3}), a combination of $\underline{j} \times \underline{B}$ forces and atomic processes can only explain the observed retardation. (vi) We have observed a strong evidence for the operation of modified two-stream instability in critical velocity interaction. At low magnetic fields, i.e. $f_{ce} \ll f_{pe}$, we did not observe the retardation of plasma stream to Alfvén's critical velocity. The non-occurrence of Alfvén's critical velocity phenomenon at these magnetic fields indicates the necessity of electron energisation parallel to magnetic field direction by modified two-stream instability for efficient transfer of plasma ion energy

to electrons and consequently to ionisation of gas atoms.

6.2 Model for plasma-neutral gas interaction

Basing on our observations, we put forth a model for plasma-neutral gas interaction that the following circular process is operative in the critical velocity experiments.

Firstly, when the plasma stream meets the neutral gas cloud, a fraction of the neutral gas cloud atoms charge exchange with the plasma stream ions or get ionised by electron impact ionisation or photoionisation processes. This leads to the presence of non-thermal ions in the plasma-neutral gas interface. Secondly, these non-thermal ions establish a space charge sheath. In this crossed electric and magnetic field region, there arises a relative drift between plasma electrons and ions, mainly because of ion inertia. Thirdly, this drift excites modified two-stream instability and energises electrons resulting in rapid ionisation of gas cloud, which increases the production of non-thermal ions. This process gives a positive feedback to the interaction. Then the composite plasma moves and the original plasma loses partially its momentum by binary collisions (at high gas densities). There are current structures formed at this time in the sheath which give rise to $\underline{j} \times \underline{B}$ - forces retarding the plasma stream

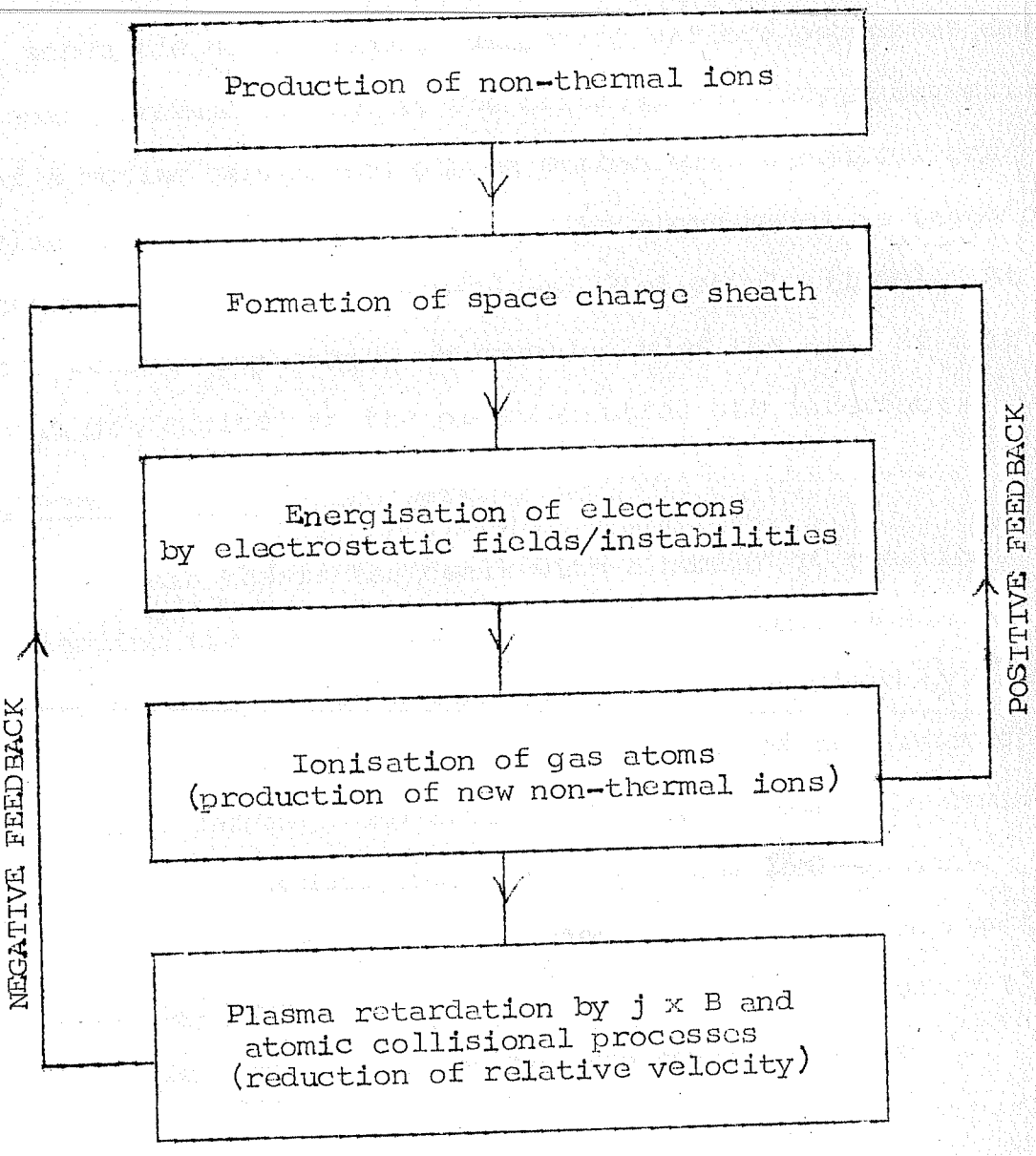


Figure 6-1. Model for plasma-neutral gas interaction.

particles and correspondingly accelerating neutral gas. This process offers a negative feed-back to the interaction. A schematic of the model, depicting various processes and their circular nature in the critical velocity interaction of a moving magnetised plasma stream with a neutral gas cloud is given in figure 6-1. The above model is based on the models of Sherman (1969) and Piel et al. (1980). At the retardation stage, we have included the role of currents that get excited in the plasma-neutral gas interface.

6.3 Scope for future work

This thesis has dealt with a number of questions regarding the plasma-neutral gas interaction. While an issue of whether the interaction is characterised by Varma's threshold has been settled, many aspects of the interaction are still far from understood. The major obstacle coming in the way of understanding has been the lack of non-perturbing diagnostics. Additionally, there are a number of physical processes simultaneously occurring during the interaction, that theories have to often resort to simplifications. Making a comparison between the experimental results and the theories has thus become a difficult task. We now list below the problems which require further elucidation. The investigations of these problems will certainly

narrow down the existing gap between the experiment and theory of the Alfven's critical velocity phenomenon.

6.3.1 Momentum/energy sharing between the original and newly produced ions

Although sharing of momentum between the original and newly produced ions has been identified as the most important agent which causally connects the plasma retardation with electron heating, very little has been said about the energy/momentum carried away by the newly produced ions. The modified two-stream instability, if operating during the interaction, would lead to ion heating. How much energy will go into the heating of ions, however, would depend upon the modes excited. On the other hand, in electrostatic acceleration model, it is envisaged that the newly produced ions would get accelerated to the Alfvén's critical velocity during the interaction. Another point which deserves a mention here is that it is not clear whether Alfvén's critical velocity phenomenon leads to a composite plasma whose mean velocity is the Alfvén's critical velocity or a composite plasma in which both the original and newly produced ions are moving with the Alfvén's critical velocity. Further, if the newly produced ions are accelerated in the sheath field, the charge

exchange collisions between the newly produced ions and parent gas atoms will considerably alter the energy spectrum of the accelerated ions. It is very obvious that the ionised component of the gas will have dispersion in its velocity component along the direction of plasma stream if one considers the effect due to reaccelerations of stationary ions resulting from successive resonant charge exchange collisions between the accelerated newly formed ions and the neutral gas atoms. Thus, the ionised component may appear to have been anisotropically heated. This apparent heating is different from the heating by modified two-stream instability invoked by Sherman (1969), Raadu (1975) and Piel et al. (1978). Thus, we do not have adequate understanding of how freshly produced ions behave during the interaction. This aspect, if experimentally investigated, would considerably facilitate in building theoretical model of the Alfvén's critical velocity phenomenon.

6.3.2 Instabilities

Basically, we have two kinds of theoretical models. One which invokes instabilities and the other which depends on electrostatic fields and does not make use of any instability for energisation of electrons. An experimental confirmation would once for all settle the issue of whether instabilities have a role to play or not. Although

indirect evidences exist (Brenning, 1980 ; Venkataramani and Mattoo, 1981c) for the operation of modified two-stream instability during the interaction, there does not exist a direct confirmation till now. The analysis of dispersion characteristics of instability becomes difficult mainly due to two reasons. Firstly the frame of reference is moving with plasma stream velocity which in actual experimental situations, varies with time. Secondly, the expected growth rates have time scales of the order of a few ns and the expected frequency of fluctuations is very high. Thus, we need a fast diagnostics in addition to a comprehensive understanding of interpreting the experimental results. The diagnostics should be non-perturbing type as the presence of a physical object like Langmuir probe is likely to result in an error in judgement and a considerable loss of particles. The particle beam probe may be of some help in resolving this issue.

6.3.3 Space charge

Our observations on space charge sheath are based on floating Langmuir probe. Although we have justified the usage of such a probe in our experiment, its use cannot certainly be extended to the whole parameter regime of plasma-neutral gas interaction. A detection of space

charge sheath by a diagnostic different from a perturbing one would serve as a useful confirmation of the results of our experiments. Again, we think that low energy particle beams (~150 eV) would be ideal as a diagnostic tool. Work in this direction is under progress in our laboratory.

6.3.4 Currents

It is evident from our evaluations described in Chapter 4 that a part of plasma momentum has to be lost by non-collisional means in plasma-neutral gas interaction. Although we have shown that the observed currents can account for plasma retardation at low gas densities, it is not fully clear whether the observed currents are a consequence of or cause for plasma retardation.

Thus, there is a clear need of theoretical model which can explain our observations of the plasma retardation.

6.3.5 Minimum critical density

Chapter 3 explains that critical velocity phenomenon is operative over a wide regime of neutral gas density. Theoretical considerations indicate that there may exist a lower limit on the neutral gas density for Alfvén's critical velocity phenomenon to occur. As this is a consequence of the model, an experimental verification is desirable.

6.3.6 Alfvén's cosmogonic theory

Alfvén's cosmogonic theory requires an interaction between a moving mixture of gases and a stationary plasma. Recently, the experiments of Axnäs (1978) has raised an interesting question about the operation of the critical velocity phenomenon in mixture of gases. He found that the critical velocity for a given mixture of gases, depends upon the composition and the ionisation function of the component gases. However, this experiment did not investigate what happens when the initial plasma velocity is greater than the critical velocity of one of the components but lesser than the composite value. According to Raadu (1978), it seems that critical velocity interaction does not occur at a value lesser than the composite value. If it is so, cosmogonic theories based on Alfvén's hypothesis will have to be modified. Our present efforts are directed at verifying the predictions of Raadu's theory.

Appendix 'A'

SYSTEM OPERATION

The experimental set-up utilises four condenser banks. The energy stored in these banks is utilised to open two fast electromagnetic valves, one provided at the interaction region and another one to admit gas into the plasma gun, to set up longitudinal magnetic field in the drift tube and to provide energy for discharge of the gas and its subsequent acceleration in the plasma gun. Further these banks are to be discharged sequentially. The requirements are as follows:

(1) For opening the electromagnetic gas valve situated at the interaction region, a fast (25μs) high current

(100 kA) pulse is to be passed through the field coils of electromagnetic valve. A similar current pulse is needed for opening another electromagnetic valve situated at plasma gun to inject gas cloud but with an adjustable delay.

(2) A slow ($\sim$ 3 ms) high current (125 A) pulse is to be generated and passed through the 40 cm long 16 cm diameter solenoid coils for producing an uniform axial magnetic field of 5 kG in the drift space to guide the plasma stream from the muzzle of gun to the interaction region. The large pulse time ensures a slow time variation of magnetic field while the plasma stream passes through drift space and interaction region.

(3) These three discharges have to be sequentially obtained with definite controllable delays between them as shown in figure A-1. This scheme of discharging different capacitor banks is adopted so as to ensure that plasma moves through the drift space when the magnetic field is at its peak value and that the plasma stream meets neutral gas cloud in the interaction region at the required time of gas evolution.

(4) The bank connected to the plasma is discharged by

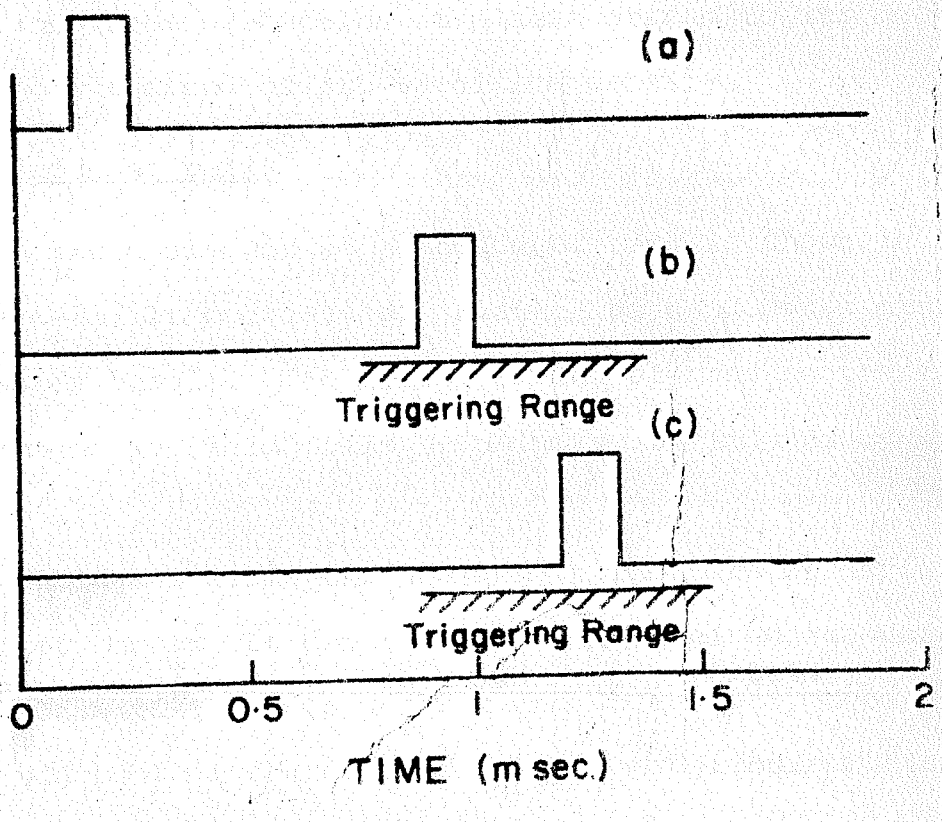


Figure A-1. The required triggering ranges. (a) trigger pulse for guide magnetic field. (b) trigger pulse for opening electromagnetic gas valve to feed gas to coaxial plasma gun. The triggering time is adjusted to ensure that plasma stream moves in the drift space when guide magnetic field is maximum. (c) trigger pulse for opening electromagnetic gas valve to inject a gas cloud in the interaction region. The indicated triggering range enables plasma stream to meet the gas cloud at various densities.

injection of the gas through the valve.

This Appendix describes condenser banks, thyratron switches for transfer of energy and sequencing of the different operations from production of plasma stream to its meeting with the gas cloud of pre-specified density.

A.1 Condenser banks

A basic circuit of a condenser bank is shown in figure A-2. It consists of a stack of condensers charged by a power supply. The energy is transferred to the field coils/magnetic field coils by using a low inductance spark gap.

Table A-1 lists the designed parameters of different capacitor banks. It can be seen that requirements vary from 100 kA to 125 A in current and 25 μs to 3 ms on the pulse width of discharge currents. These requirements are met by optimising impedances of capacitor banks and peak charging voltages. The transfer of energy is executed in the following way in all condenser banks except the one used with the plasma gun. The condenser bank is charged initially to a specified value of voltage. The spark gap is fired by a high voltage pulse (6 kV, 5 μs) derived from a thyratron. The discharge path is provided through field coils/solenoids (for obtaining magnetic fields).

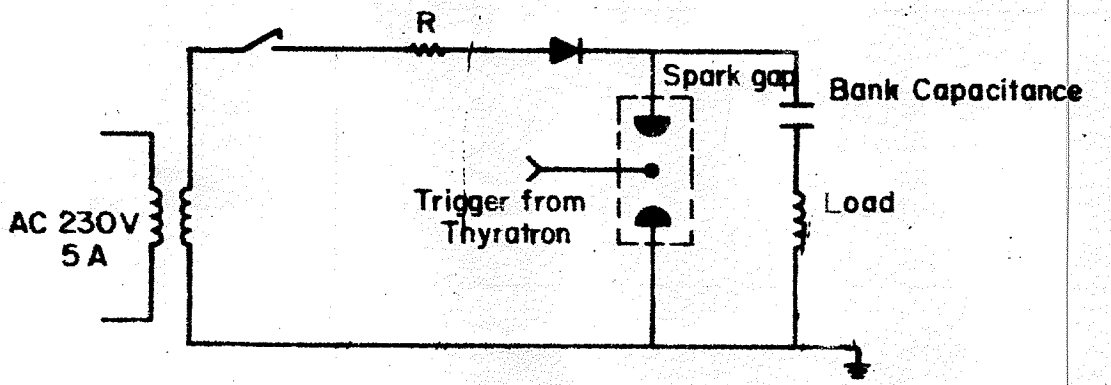


Figure A-2. A typical discharge circuit fired by a spark gap.

Table A-1

RELEVANT PARAMETERS OF VARIOUS DISCHARGE CIRCUITS

Parameter	Guide magnetic field	Gas valve for feeding gas to plasma gun	Gas valve for injecting gas cloud at interaction region	Coaxial plasma gun
Bank capacitance	20 μfd	14 μfd	14 μfd	56 μfd
Bank voltage	5 kV	10 - 12 kV	8 - 12 kV	6 - 10 kV
Load	solenoid coil	field coil for opening electromagnetic valve	field coil for opening electromagnetic valve	plasma gun discharge
Inductance	16 mH	1 μH	1 μH	.1 - 5 μH
Capacitance	-	-	-	50 nfd
Line inductance	negligible	negligible	negligible	0.2 μH
Pulse period	2 ms	25 μs	25 μs	25 - 30 μs
Peak discharge current	100 - 125 A	100 kA	100 kA	0.25 - 5 kA

Note that the condenser bank connected to the plasma gun is not connected to any spark gap. It is discharged when sufficient gas pressure builds up inside the coaxial gun after the electromagnetic valve is opened to admit the gas.

A.2 Triggering system

A.2.1 Master trigger

Master trigger unit is one which gives a monoshot pulse on the mechanical pressing of a push button, which triggers the whole sequence of discharges. The circuit diagram for obtaining this pulse is shown in dotted section of figure A-3.

A.2.2 Pulse generators

The master trigger pulse generates six different pulses which are used for triggering SCRs and for locking SCRs till the triggering time is reached. The circuit is shown in figure A-3. Figure A-4 explains the nature of these pulses and their sequence.

A.2.3 SCR trigger generators

The three triggering pulses derived from the circuit shown in figure A-4 are fed to three SCRs in parallel which generate correspondingly three trigger pulses for thyratrons. The circuit diagram is shown in figure A-5.

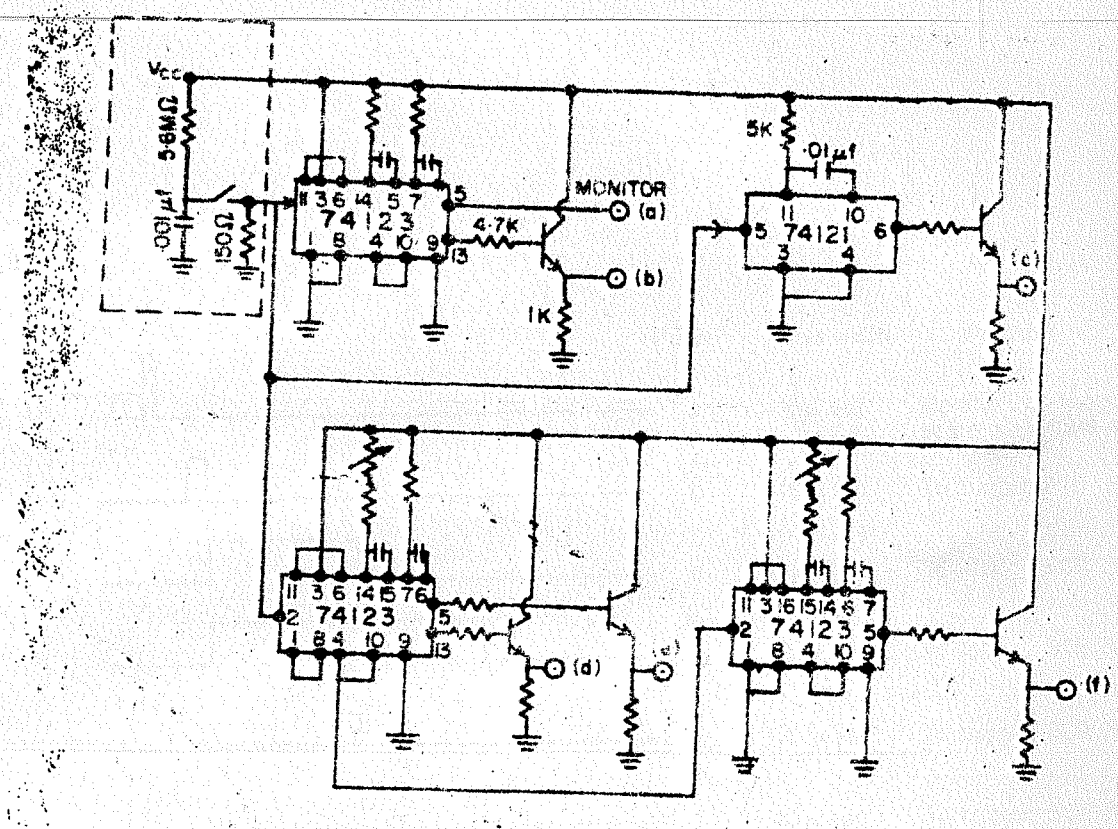


Figure A-3. Circuit diagram for producing monitor and delayed trigger pulses.

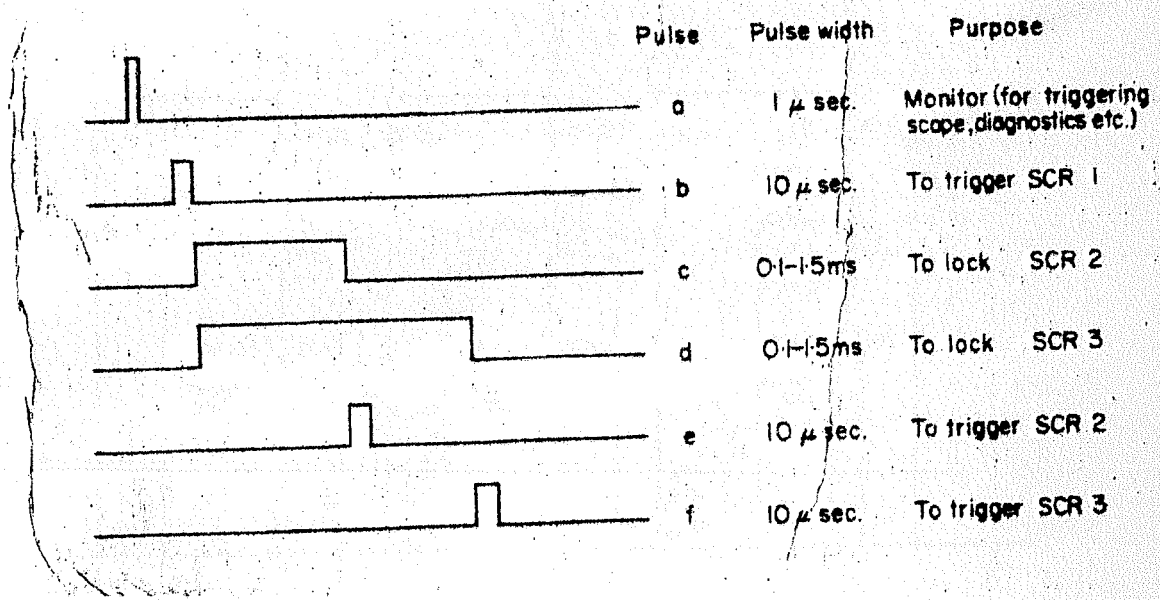


Figure A-4. Sequence of various pulses obtained from circuit shown in figure A-3.

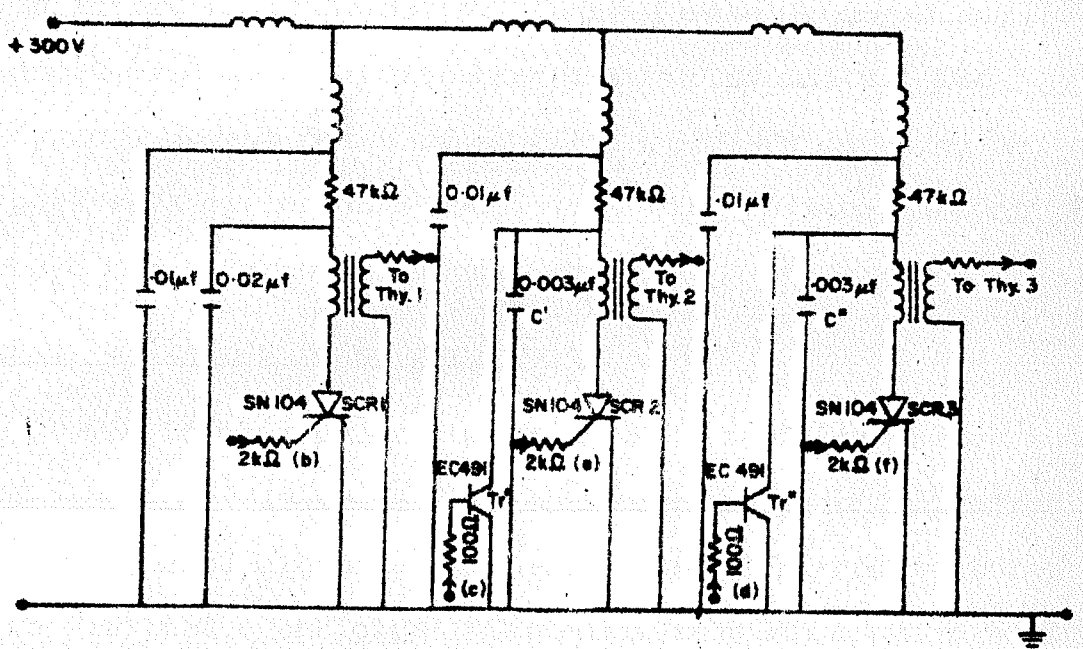


Figure A-5. Circuit for triggering SCRs.

During the triggering of first thyratron, the other two thyratrons normally get triggered owing to stray pulses. To avoid this, the cpacitances C' and C" are not allowed to get charged by keeping the transistors Tr' and Tr" conducting till the required time of triggering. This is achieved with the help of long pulses c and d indicated in figure A-4. A good shielding further reduces any cross-talk between different triggering units. The typical output pulse of an SCR is of 2 μs duration and the peak voltage is 175 - 300 Volts. The maximum current that can be drawn is 1 amp.

A.2.4 Thyratron trigger circuit.

The trigger pulse output at SCR is of low energy and cannot directly be used to activate the spark gap situated in discharge circuits. We have used thyratron switches to fire the spark gaps. The minimum voltage pulse needed to trigger the thyratron used is 175 Volts and minimum pulse width is 2 μs. This is easily matched by the SCR output. A typical thyratron circuit is shown in figure A-6. The output pulse is obtained across a resistor. Its peak voltage can be varied from 0.3 to 6 kV. The pulse width is about 5 μs. The maximum I^2t value allowed for the thyratron used in our triggering unit is 0.1 A s.

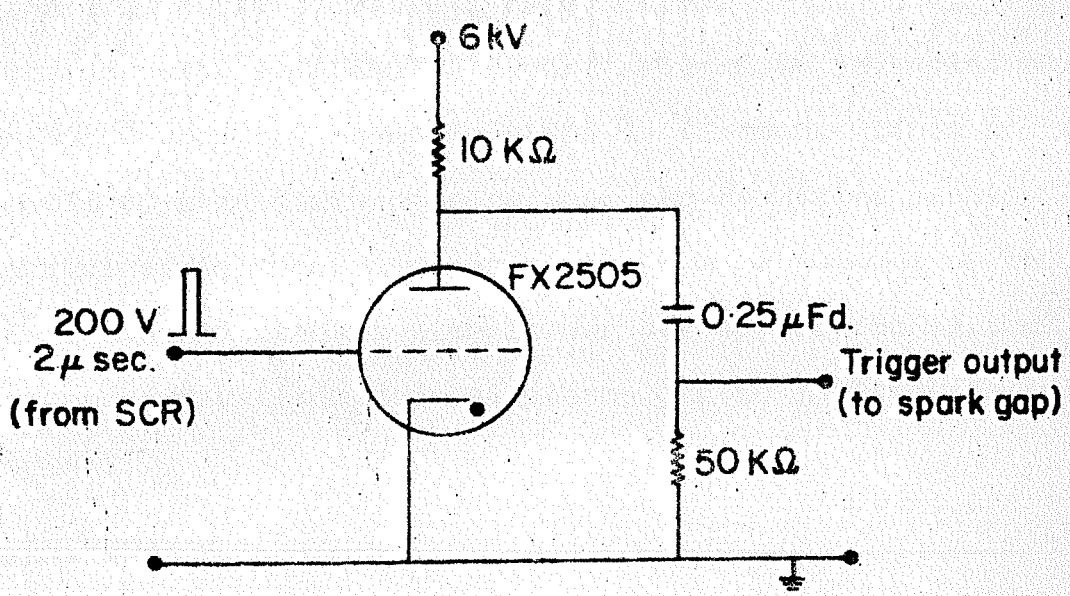


Figure A-6. A typical circuit for triggering a thyratron unit.

A.3 Synchronisation

The delay between the discharges of three condenser banks can be controlled externally by adjusting the triggering time of three SCRs. This is done by adjusting the delays in the outputs of pulse generator. The observed plasma discharge current, valve opening pulse, and magnetic field current pulse is shown in figure A-7. Note that plasma is produced when the magnetic field is maximum. It is to be mentioned that difference between the two valve opening current signals corresponds to the sum of generation time of plasma and transit time in our set-up for the plasma stream to move from coaxial plasma gun to interaction region.

A.4 Summary

A block diagram of the whole set-up is shown in figure A-8. The set-up enables us to study the interaction between moving plasma and neutral gas clouds of densities in a wide range (10^{17} -10^{21} m^{-3}). In our set-up, the varying density of gas cloud is obtained by varying the condenser bank voltages in the discharge circuit for valve opening. The finer changes in densities are obtained by triggering the second and third SCRs with proper delays,

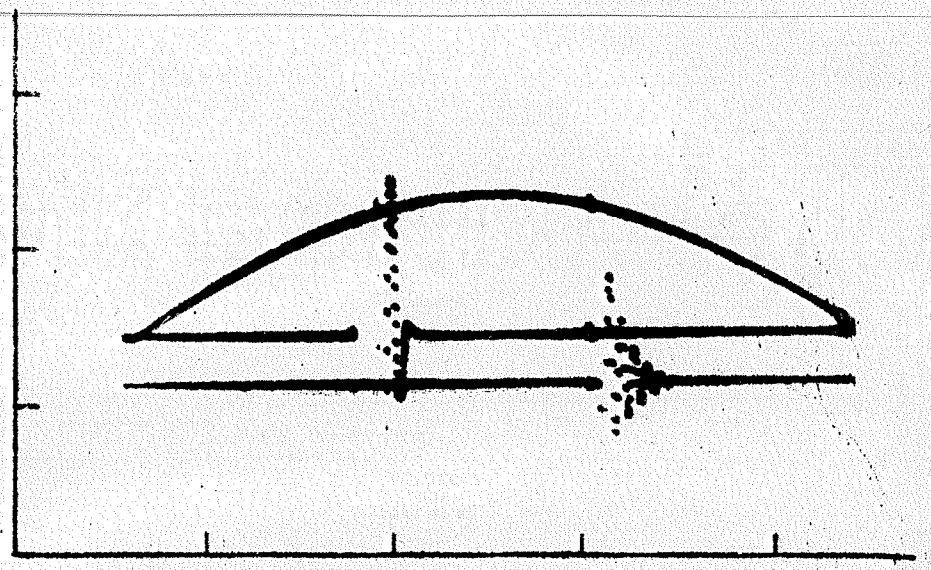


Figure A-7. Signals obtained from current probes showing the synchronisation of opening of the valve and the discharge of the plasma gun with respect to peak value of the half-sine guide magnetic field. The first pulse indicates the opening of the gas valve and the second the discharge current. Scale:- X-axis: 250 μs/div., Y-axis: 2.5 kG/div. for the guide magnetic field; 1 kA/div. for the current in the field coil of the valve and the discharge.

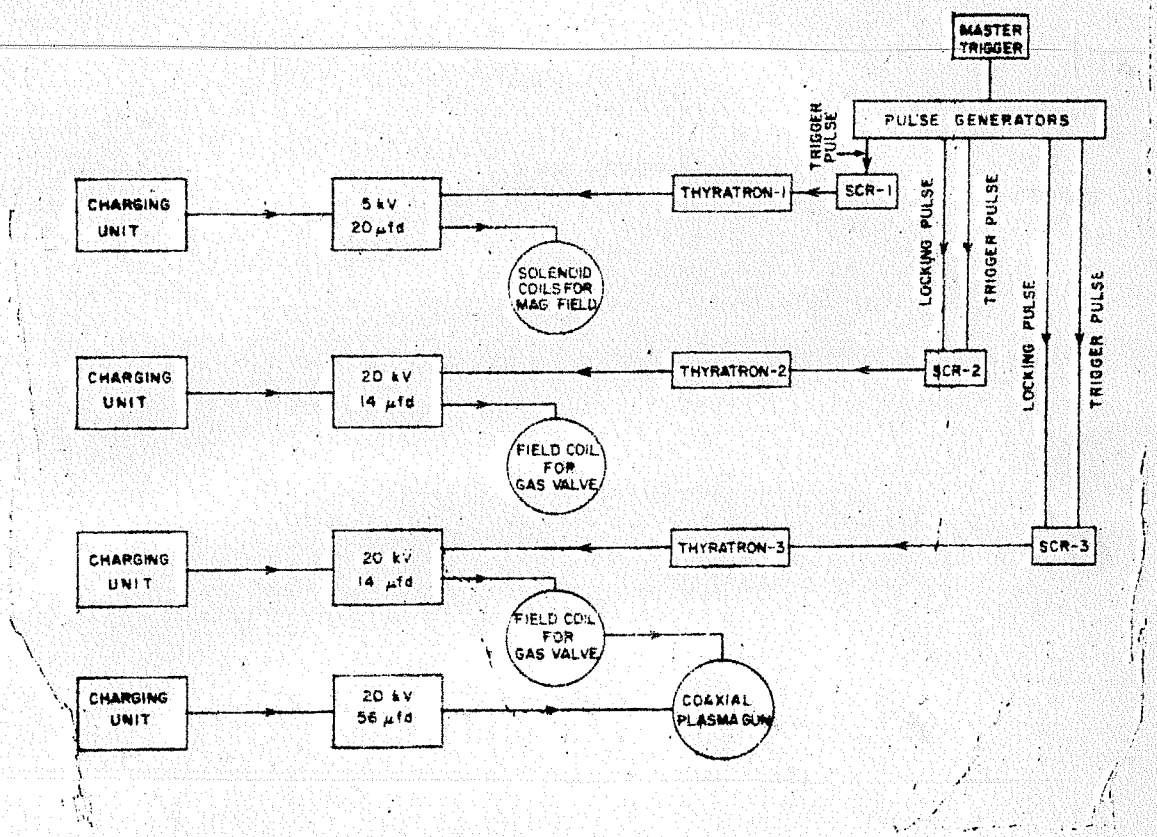


Figure A-8. Block diagram of the experimental set-up.

so that the plasma stream meets the neutral gas cloud at the required density while the injected gas cloud evolves in time.

Appendix 'B'

SHEATH POTENTIAL MEASUREMENT USING FLOATING LANGMUIR PROBE

Analysis of signal from Langmuir probe placed in a high density flowing plasma is not simple due to a variety of effects which can occur on the probe surface like outgasing, electron emission, photo-emission etc. The analysis is more complicated if magnetic field, collisions and oscillations in plasma density are also present in the probe region (Huddlestone and Leonard, 1965; Chung et al., 1975). Although the application of a Langmuir probe does not find easy justification over a wide regime of plasma parameters, it has been extensively used mainly due to its simplicity for measuring flowing plasma parameters

(Chung et al., 1975; Lindberg and Kristofferson, 1969; 1970; Danielsson, 1970; Lehnert et al., 1974; Markovic and Scott, 1971; Himmel et al., 1976). We have used floating Langmuir probes to study the characteristics of sheath that gets formed when a plasma stream penetrates a neutral gas cloud in the presence of magnetic field. The effects of ion sputtering, heated electrons etc. on the measurement of the plasma potential have been already discussed in Chapter 5 (see Section 5.4). In this Appendix, we discuss the effects due to orientation of the probe surface relative to the streaming direction and the magnetic field on the measurement of plasma potentials.

The "end effect" becomes important in measurements of flowing plasma with Langmuir probe (Bettinger and Chen, 1968; Hester and Sonin, 1970). This arises essentially when sheath radius becomes significantly greater than the probe radius. It depends on the parameter

$$\tau_l = \frac{l}{\lambda_D} \left[\frac{k T_e}{m_i}\right]^{\frac{1}{2}} \frac{1}{U} \qquad .. \quad (B.1)$$

where

l is the probe length;

λ_D is the Debye length;

T_e is the electron temperature;

m_i is the ion mass and

U is plasma velocity.

For $\tau_1 \gg 1$, the "end effect" is negligible. In our case, $\tau_1 \sim 10^2$ and hence this effect does not play any role. It should be mentioned that this effect becomes significant only when probe is kept aligned to plasma stream direction.

An important consideration arises from the currents that flow in the plasma column. When significant currents flow, non-uniformities in H are established. The magnetic Reynold's number R_m is a measure of this effect. When $R_m > 1$, even small currents will lead to large non-uniformities and these non-uniformities exist in a magnetic "boundary layer" of dimension $R_m^{-\frac{1}{2}}$ adjacent to the surface of probe. In such a case, Ampere's law modifies the flow of particles to probe.

The magnetic Reynold's number R_m is given by

$$R_m = \mu_o \sigma_c U L \qquad .. \qquad (B.2)$$

where

μ_o is permeability;

σ_c is electrical condictivity;

U is reference velocity and

L is length of probe.

For our case, $R_m \sim 10^{-3}$. Hence the potential measurements by Langmuir probe hold good even in the pr sence of currents in our experiment.

REFERENCES

Alfvén H (1954) On the origin of the solar system, Oxford University Press, Oxford.

Angerth B, Block L, Fahleson U and Soop K (1962) Nuc. Fusion Supplement Pt.1, 39

Axnäs I (1972) Royal Institute Technology Report 72-31

Axnäs I (1978) Astrophys. Space Sci. 55, 139

Beard D B (1966) Planet. Space Sci. 14, 303

Bettinger R T and Chen A A (1968) J. Geophys. Res. 73, 2513

Brenning N (1980) Royal Institute Technology Report, TRITA-EPP- 80-10

Buneman O (1962) Plasma Phys. 4, 111

Burlaga L F, Rahe J, Donn B and Neugebauer M (1973) Solar Phys. 30, 211

Chung P M, Talbot R and Touryan K J (1975) Electric probes in stationary and flowing plasmas, Springer Verlag, New York.

Colgate S A (1961) University of California, Lawrence Radiation Laboratory Report UCRL-6176

Colgate S A (1962) Electrodynamics and fluid dynamics of gaseous plasmas, Polytechnic press Inc. Brooklyn, New York.

Danielsson L (1973) Astrophys. Space Sci. 24, 459

Danielsson L and Brenning N (1975) Phys. Fluids 18, 661

Danielsson L and Kasai G H (1968) J. Geophys. Res. 73, 259

Eninger J (1965) Proc. 7th Int. Conf. on Ioniz. Phenomena in Gases, Belgrade 1, 520

Fahleson U V (1961) Phys. Fluids 4, 123

Hester S D and Sonin A A (1970) Phys. Fluids 13, 1265

Himmel G, Möbius E and Piel A (1976) Z. Naturforsch. 31a, 934

Huddlestone R H and Leonard S L (1965) Plasma diagnostic Techniques, Academic press, New York

Kanal M (1964) J. Appl. Phys. 35, 1697

Krall N A and Liewer P C (1971) Phys. Rev. A 4, 2094

Lehnert B (1967) Phys. Fluids 10, 2216

Lehnert B (1978) Astrophys. Space Sci. 55, 25

Lehnert B, Bergström J and Holmberg S (1966) Nuc. Fus. 6, 231

Lehnert B, Hellsten T and Raggi R (1974) Physica Scripta 9, 53

Lindberg L and Kristofferson L (1969) Royal Institute Tech. Report EPP-69-16

Lindberg L and Kristofferson L (1970) Plasma Physics 12, 831

Marshall J (1958) Proc. II Int. Conf. Peaceful Uses Atomic Energy (Geneva) 31, 341

Mattoo S K and Venkataramani N (1980) Phys. Lett. A 76, 257

Mc Bride J B, Ott E, Boris J P and Orens H (1972) Phys. Fluids 15, 2367

Mendis D A and Ip W H (1977) Space Sci. Rev. 20, 145

Möbius E, Boswell R W, Piel A and Henry D (1979a) Geophys. Res. Lett. 6, 29

Möbius E, Piel A and Himmel G (1979b) Z. Naturforsch. 34a, 405

Morkovic P D and Scott F R (1971) Phys. Fluids 14, 1742

Ott E, Mc Bride J B, Orens H and Boris J P (1972) Phys. Rev. Lett. 28, 88

Petelski E F, Brenning N, Ripken H W, Fahr H J and Axnas I (1979) Royal Inst. Report TRITA-EPP-79-19

Piel A and Möbius E (1978) SFB Plasma Physik Bochum/Julich Report 78-M2-040

Piel A, Möbius E and Himmel G (1978) S. B Plasma Physik Bochum/Julich Report 78-M2-037

Piel A, Möbius E and Himmel G (1980) Astrophys. Space Sci. 72, 211

Raadu M A (1975) Royal Institute Tech. Report TRITA-75-28

Raadu M A (1977) Royal Institute Techn Report TRITA-77-18

Raadu M A (1978) Astrophys. Space Sci. 55, 125

Raadu M A (1979) Royal Institute Tech. Report TRITA-79-14

Raadu M A (1980) Royal Institute Tech. Report TRITA-80-05

Segall S B and Koopman D W (1973) Phys. Fluids 16, 1149

Sherman J C (1969) Royal Institute Tech. Report 69-29

Sherman J C (1970) Royal Institute Tech. Report 70-15

Sherman J C (1972) Nobel Symposium No. 21, p.315 Ed. by Aina Elvius, Almquist & Wiksell, Stockholm.

Sherman J C (1973) Astrophys. Space Science 24, 487

Tan W P S (1973) J. Phys. D - App. Phys. 6, 1188

Varma R K (1978) Astrophys. Space Sci. 55, 113

Venkataramani N and Mattoo S K (1980a) Pramana 15, 117

Venkataramani N and Mattoo S K (1980b) Phys. Lett. A 79, 393

Venkataramani N and Mattoo S K (1980c) Proc. Ind. Acad. Sci. EPS 89, 431

Venkataramani N and Mattoo S K (1981a) Indian Journal of Pure and Applied Physics 19, 56

Venkataramani N and Mattoo S K (1981b) Indian Journal of Pure and Applied Physics (in press)

Venkataramani N and Mattoo S K (1981c) sent for publication

Venkataramani N and Mattoo S K (1981d) sent for publication

Venkataramani N and Mattoo S K (1981e) sent for publication

Wallis M K (1972) Royal Institute of Technology Report TRITA-72-02

Wurm (1963) The Physics of comets, The solar system, Ed. by Middle Hurst B M and Kuiper G P Vol. 4, University Press, Chicago.